Synthesis and Characterization of Novel Magnetite Nanoparticle Block Copolymer Complexes

Qian Zhang

Dissertation submitted to the faculty of Virginia Polytechnic Institute and State University in partial fulfillment of the requirements for the degree of

DOCTOR OF PHILOSOPHY

in

CHEMISTRY

Submitted to:

Judy S. Riffle (chair)

Richey M. Davis (co-chair)

James E. McGrath

Larry T. Taylor

Thomas C. Ward

April 3rd 2007
Blacksburg, Virginia

Keywords: magnetite, nanoparticle, stability, poly(ethylene oxide), stabilization, DLVO

Synthesis and Characterization of Novel Magnetite Nanoparticle Block Copolymer Complexes

Qian Zhang

Abstract

Magnetite (Fe$_3$O$_4$) nanoparticles were synthesized and complexed with carboxylate-functionalized block copolymers, and aqueous dispersions of the complexes were investigated as functions of their chemical and morphological structures. The block copolymer dispersants possessed either poly(ethylene oxide), poly(ethylene oxide-*co*-propylene oxide), or poly(ethylene oxide-*b*-propylene oxide) outer blocks, and all contained a polyurethane center block with pendant carboxylate functional groups. The complexes were formed through interactions of the carboxylates with the surfaces of the magnetite nanoparticles. Initial efforts utilized an aqueous coprecipitation method for the synthesis of magnetite nanoparticles, which yielded polydisperse magnetite nanoparticles. The average diameter of the magnetite cores in the complexes was 10 nm and the particles were superparamagnetic. Complexes with mass ratios of polymer to magnetite varying from 50:50 to 85:15 were studied. The nanoparticle complexes were characterized with a range of solution- and solid-state techniques including TGA, XPS, TEM, VSM, DLS and zeta potential measurements.

DLVO calculation methods, which sum the contributions from van der Waals, steric, electrostatic and magnetic forces were utilized to examine the interparticle potentials in the presence and absence of external magnetic fields. Compositions were identified wherein a

shallow, attractive interparticle potential minimum appears once the magnetic term is applied. This suggested the possibility of tuning the structures of superparamagnetic nanoparticle shells to allow discrete dispersions without a field, yet permit weak flocculation upon exposure to a field. This property has important implications for biomedical applications where movement of particles with an external magnetic field is desirable.

In a second study, well-defined, narrow size dispersity magnetite nanoparticles were synthesized via the thermolysis of an iron (III) acetylacetonate (Fe(acac)$_3$) precursor in the presence of benzyl alcohol. The magnetite nanoparticles were coated with triblock and pentablock copolymers possessing poly(ethylene oxide) and poly(propylene oxide-b-ethylene oxide) tailblocks and the carboxylate-functional anchor block.

DLVO calculations were applied to the new magnetite particles and diagrams of potential energy versus interparticle distance indicated the predominant effect of steric and magnetic interactions on the particle stability. DLVO calculations on the nanoparticle complexes predicted the presence of a secondary energy minimum in the presence of an applied magnetic field, which was attributed to the attractive magnetic interaction. Exposure of the pentablock copolymer-magnetite complexes in phosphate buffered saline to a 1500 Oe magnetic field with concomitant DLS measurements indicated flocculation of the magnetic nanoparticles. DLS measurements showed increased hydrodynamic radii and scattering intensities with time. These results warrant much further work to investigate the ability to tune the structures of superparamagnetic nanoparticle shells to permit discrete dispersion in the absence of a magnetic field, yet weak flocculation upon exposure to a magnetic field.

Acknowledgements

First of all, I would like to thank my principal research advisors, Dr. Judy S. Riffle and Dr. Richey M. Davis. I cannot thank them enough for their guidance, patience and support both in research and life. Their belief in me made possible my success in graduate school. Dr. Riffle served as a role model for me as the ideal professional female researcher and Dr. Davis trained me to think as a scientist. They both led me into the world of polymer and colloid science and guided me in the journey that is research. What I learned from them will benefit me throughout my life. In addition, it was an honor to have Dr. James McGrath, Dr. Larry Taylor, and Dr. Thomas Ward serve on my committee. I especially will thank Dr. James McGrath for his wonderful class and advices and for his great knowledge and contribution to our polymer program. I also want to thank Dr. Timothy Long for his kind support and his consideration of me. You are very special to me.

My research at Virginia Tech was strengthened through collaborations with Dr. Tanya Bronich (University of Nebraska, Medical Center) and Dr. Rob Woodward (University of Western Australia). I also want to thank them for their input into our research collaborations and their help.

Special thanks goes to my labmates, Shane Thompson and Beth Caba, Nikorn Pothayee and Thompson Mefford for collaborative efforts on my research. Moreover, I would also like to thank all of the labmates, Dr. Yi-nian Lin, Ragy Ragheb, Will Miles, John Boyd, Phil Hefesteler, Mou Paul in the Riffle and Davis research groups for their friendship and support. I would also like to acknowledge all of the friends that I have made during my stay at

Table of Contents

List of Figures

List of Tables

Chapter 1 Scientific Motivation and Rationale

Magnetic nanoparticles that display high saturation magnetization and high magnetic susceptibility are of great interest for medical applications. For in vivo applications, well-defined organic coatings on the nanoparticles that form polymer-nanoparticle colloids are needed to prevent aggregation. Investigations of the coatings on the surfaces of nanoparticles are of great interest, because the coating can alter the charge, functionality, and reactivity of the surface and can enhance the stability and dispersibility of the nanoparticles.

Self-organization of amphiphilic diblock copolymers in solution can result in several possible morphologies including micelles, rods, lamellae, and vesicles. Micelles, which are the most common morphology, can serve as nano- or micro-reactors to facilitate formation of the magnetic nanoparticles.[12]

Particle size is crucial for biomedical applications. Nanoparticle drug delivery systems, due to their diminutive size, can penetrate across barriers, and pass through small capillaries into cells to allow efficient drug accumulation at the targeted locations in the body.[13] Diameters below 1 μm are required to avoid clogging of the capillaries, and to favor diffusion of the particles into organic tissues when they are intravenously injected into the body for drug delivery.[13] In order to quantitatively define the particles, particle size and shape homogeneity is important. The control over particle size and the absence of particle aggregation is desirable. Static light scattering (SLS) and dynamic light scattering (DLS) are the primary techniques for characterizing block copolymer solution properties.[14-17]

The hydrodynamic radius, polydispersity and aggregation number are essential for understanding micellization. Fluorescence spectroscopy and surface tension measurements

in addition to light scattering methods, are useful for characterizing polymer micelles. Atomic force microscopy (AFM), X-ray photoelectron spectroscopy (XPS) and transmission electron microscopy (TEM) can be used to characterize adsorption of micelles and nanoparticles on surfaces.

Chapter 2 Literature Review: Magnetite Nanoparticle Block Copolymer Complexes and DLVO Theory

2.1 Characterization of Solution Properties of Diblock Copolymer Magnetic Nanoparticle Complexes

2.1.1 Light Scattering

Scattering results from interactions of electrons in the molecules with the oscillating electric field of radiation. Dipoles are induced in the molecules that oscillate with the electric field. Since an oscillating dipole is a source of electromagnetic radiation, the molecules emit light, which is scattered in all directions. Almost all of the scattering is elastic (or Rayleigh) scattering.
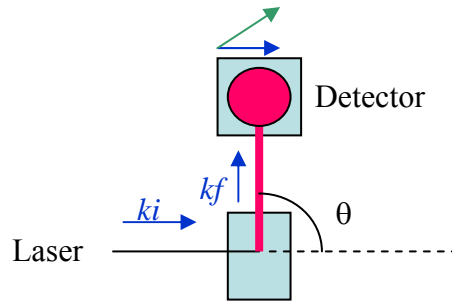
Figure 2.1 Schematic of a light scattering instrument.

A light scattering instrument is shown in Figure 2.1. Monochromatic light from a laser source is directed into a sample. The wave vector is ki, and the scattered light is shown as a wave vector kf. The vector difference is q,

$$q = kf - ki \qquad\qquad 2.1$$

$$q = \frac{4\pi n_0}{\lambda}\sin\left(\frac{\theta}{2}\right) \qquad\qquad 2.2$$

where λ is the wavelength of the incident light, and n_o is the refractive index of the medium.

2.1.1.1 Dynamic Light Scattering

Dynamic light scattering (also called Quasi Elastic Light Scattering [QELS] and Photon Correlation Spectroscopy [PCS]) is well-suited to determining small changes in mean particle diameter such as those due to adsorbed layers on a surface. DLS measures real-time scattering intensities $I(t)$, and these can be used to calculate the diffusion coefficient (D_T) and the hydrodynamic radius (R_h). The intensity time-correlation function (TCF) $G(\tau)$ is calculated from $I(t)$ as

$$G(\tau) = \lim_{T \to \infty} \left[\frac{1}{T} \int_0^T I(t)I(t+\tau)dt \right] \qquad 2.3$$

where τ is the lag-time, and T is the total time. The TCF is an inverse Laplace function transformed to obtain the distribution of relaxation times in the sample. TCFs can be analyzed in terms of cumulant or stretched-exponential fits. The normalized intensity autocorrelation function after baseline-subtraction can be described as

$$g(\tau) = \frac{G(\tau)}{G(0)} = \exp(-q^2 D_T \tau) \qquad 2.4$$

where q is the magnitude of the scattering vector. For non-interacting spheres, the Stokes-Einstein relationship applies and the diffusion coefficient can be related to the hydrodynamic radius by

$$D = \frac{k_b T}{6\pi\eta R_h} \qquad 2.5$$

Here k_b is the Boltzmann constant, T is the temperature, and η is the viscosity of the suspending liquid. The hydrodynamic radius, which includes effects of shape and solvation, is the radius of a hypothetical hard sphere that diffuses with the same speed as the particle under examination, and this relates to different species as depicted in Figure 2.2. For the

center-of-mass motion, an ellipsoid with a hydrodynamic radius R_h experiences the same friction as a sphere of radius R_h. A linear chain with a hydrodynamic radius R_h diffuses with the same diffusion coefficient as the sphere of radius R_h. So the hydrodynamic radius of a nonspherical particle is the radius of a sphere that has the same translational diffusion speed as the particle. DLS can generally measure sizes in the range of 1 to 1000 nm.
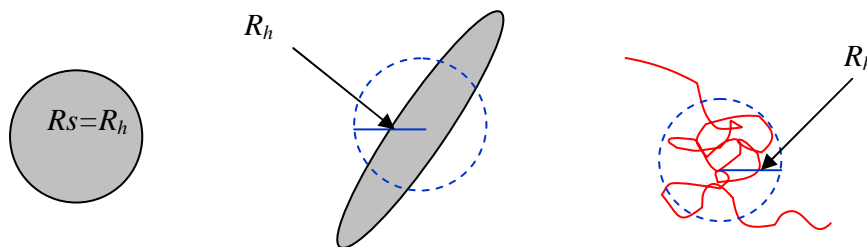
Figure 2.2 Relationship between hydrodynamic radius, R_h, and sizes for a sphere, an ellipsoid and a polymer coil.

Scattering can be described mainly in terms of two theories: Rayleigh scattering and Mie scattering. If the particles are small compared to the wavelength of the laser used (typically less than d = $\lambda/10$ or around 60nm for a He-Ne laser), Rayleigh scattering applies. The scattering from a particle illuminated by a vertically polarised laser will be essentially isotropic, i.e. equal in all directions. In the Rayleigh approximation, intensity I α d^6 and also that I α $1/\lambda^4$, where I = intensity of light scattered, d = particle diameter and λ = laser wavelength. The d^6 term tells us that a 50 nm particle will scatter 10^6 times as much light as a 5 nm particle. This d^6 factor also means it is difficult with DLS to measure, say, a mixture of

1000 nm and 10nm particles because the contribution to the total light scattered by the small particles will be extremely small. The inverse relationship to λ^4 means that a higher scattering intensity is obtained as the wavelength of the laser used decreases. For Mie scattering, when the size of the particles becomes roughly equivalent to the wavelength of the illuminating light, then a complex function of maxima and minima with respect to angle is observed.

2.1.1.2 Dynamic Light Scattering Data Analysis

Size is obtained from the correlation function by using various algorithms. There are two approaches that can be taken (1) fit a single exponential to the correlation function to obtain the mean size (z-average diameter) and an estimate of the width of the distribution (polydispersity index) (this is called the Cumulants analysis), or (2) fit a multiple exponential to the correlation function to obtain the distribution of particle sizes (such as Non-negative least squares (NNLS) or CONTIN. The size distribution obtained is a plot of the relative intensity of light scattered by particles in various size classes and is therefore known as an intensity size distribution. If the distribution by intensity is a single fairly smooth peak, then there is little point in doing the conversion to a volume distribution using the Mie theory. If the optical parameters are correct, this will just provide a slightly different shaped peak. However, if the plot shows a substantial tail, or more than one peak, then Mie theory can make use of the input parameter of sample refractive index to convert the intensity distribution to a volume distribution. This will then give a more realistic view of the importance of the tail or second peak present.

2.1.1.3 Static Light Scattering

Static light scattering measures time-averaged intensities (mean square fluctuations) as a function of angle. In Rayleigh regime the second virial coefficient can be obtained from measuring the intensity of light scattered for a given polymer concentration by the following equation:

$$\frac{KC}{R_\theta} = \frac{1}{M} + 2A_2C \qquad\qquad 2.6$$

C is weight concentration, R_θ is the Rayleigh ratio, M is the weight average molecular weight, A_2 is the 2nd virial coefficient, indicative of solute-solvent interactions, and K is the optical constant. Static light scattering data can provide information on the average molecular weights of micelles, M, and the second virial coefficients A_2. For an uncharged macromolecule, the second virial coefficient depends on the volume of the molecule and on the nature of the solvent-solute interaction.

K can be described as

$$K = \frac{4\pi^2 n_o^2 (dn/dc)^2}{N_A \lambda^4} \qquad\qquad 2.7$$

where n_o is the solvent refractive index, dn/dc is the refractive index increment of the micellar solution, and λ is the wavelength of the incident light.

2.1.2 X-Ray Photoelectron Spectroscopy (XPS)

X-ray photoelectron spectroscopy (XPS, also called electron spectroscopy for chemical analysis, ESCA) is a method that uses x-rays to eject electrons from inner-shell orbitals. A specimen is bombarded with x-rays. Then electrons, either from the valence or the inner-core, are emitted. The energy of incident x-rays, hv, and the kinetic energy, E_k of the emitted electrons are measured. The binding energy, E_b, of these photoelectrons is given by

$$E_k = h\nu - E_b - E_w \qquad\qquad 2.8$$

where E_w is the work function of the spectrometer. XPS instruments consist of a monochromatic x-ray source, an energy analyzer for the photoelectrons, and an electron detector. The analysis and detection of photoelectrons requires that the sample be analyzed in a high-vacuum chamber.

XPS can be used to determine the chemical composition of a solid flat surface semi-quantitatively. The sampling depth of the XPS experiments is approximately 5-10 nm for polymers, depending on the material studied. XPS can also provide information on the surface compositions of nanoparticles. The presence of a copolymer on a metal or metal oxide surface can be confirmed by analyzing the surface atomic compositions of the nanoparticles. Thus XPS can be utilized to determine qualitatively if the block copolymer covers the metal surface.

2.2 Magnetic Fluids

2.2.1 Principles of Magnetism

Magnetism arises from electron spin in orbitals of the constituent atoms of a material. Atoms with unpaired electrons possess a net spin which can result in magnetic dipole

moment. Magnetic effects result from the arrangement of these atoms in crystalline lattices and the alignment of the spins. Several categories of magnetic materials exist, depending on the response of the material to an external applied field. Magnetic materials are classified into five categories: diamagnetic, paramagnetic, ferromagnetic, ferrimagnetic, and antiferromagnetic.[18] Ferromagnetic materials sustain a magnetic field after an applied field is removed. The spins of each atom are thus aligned by exposure to the external magnetic field. Ferrimagnetic materials also sustain a magnetic field. However, due to the presence of different lattice sites in the crystalline network, certain atoms possess spins that oppose the applied magnetic field while other atoms at different positions within the lattice possess spins that align with the magnetic field. In order to be ferrimagnetic, the net spin must align with the applied field. Antiferromagnetic materials do not sustain a magnetic field due to alternating alignment of spins in the crystalline lattice. Superparamagnetic materials align their spins with an external applied field but then lose this orientation once the field is removed.

2.2.2 Magnetic Properties of Nanoparticles

Magnetic nanoparticles consist of nanometer scale particles composed of magnetic materials such as cobalt or magnetite. The magnetic properties of these nanoparticles differ from the bulk material due to the fact that the particle dimensions are generally smaller than the typical domain size within the bulk material. A domain is a region of the bulk material, typically several tens to hundreds of nanometers in size, in which the magnetic moments of the atoms are aligned. The domains in a bulk magnetic material can be aligned by applying

an external magnetic field, and if the domains remain aligned after the field is removed then the material is considered ferromagnetic. In the case of nanoparticles that are dispersed in a medium, the magnetic behavior depends on several factors. The behavior depends on the magnetic anisotropy in the material, which is related to the crystallographic orientation of the material and spin-orbit coupling.[19] The magnetic anisotropy constant K can be decreased by decreasing the particle size. If the nanoparticles have a size that is less than the typical domain size in the bulk material, then the nanoparticles will consist of a single domain.[20] If the nanoparticles are still above the superparamagnetic diameter (D_{sp}), then the relaxation time of the magnetic moment will be slow enough (~100 seconds) that they will not readily align in a magnetic field and are considered to be blocked.[19] If the diameter of the particles is less than this superparamagnetic diameter, then the particles' magnetic moment will move freely to align with an applied field and are considered superparamagnetic.[21] Increasing temperature can lead to superparamagnetic behavior since thermal energy can overcome the magnetic anisotropy of the particles at the blocking temperature.

2.2.3 Magnetic Hysteresis

Magnetic hysteresis measurements are conducted by applying an external magnetic field to a sample and observing the changes in magnetization within the sample at each point as the external field is increased, then decreased. A typical hysteresis loop plot was shown in Figure 2.3. The greatest magnetization reached in the sample is called the saturation magnetization. The magnetization obtained when there is zero applied field (descending from the saturation point) is called the remanence magnetization. As the field is applied in

the reverse direction, the magnetization decreases from the remanence value and reaches zero

at a point which is called the magnetic coercivity. Typically, superparamagnetic

nanoparticles will exhibit no hysteresis and thus have zero magnetic coercivities and no

remanence magnetization, whereas blocked nanoparticles will exhibit both. The saturation

magnetization of magnetic nanoparticles is typically lower than that of the corresponding

bulk magnetic material due in part to nonmagnetic surface layers and high magnetic

anisotropy.[22] The magnetization curves can be used to determine the size distribution of

magnetic nanoparticles.[23] This is due to the fact that different size nanoparticles have

different magnetic moments. The magnetization curve for a monodisperse sample of

magnetite is derived from the Langevin function. Dispersity in the sizes of the nanoparticles

leads to different magnetization behavior compared to monodisperse samples, leading to a

broadening of the magnetization curve.
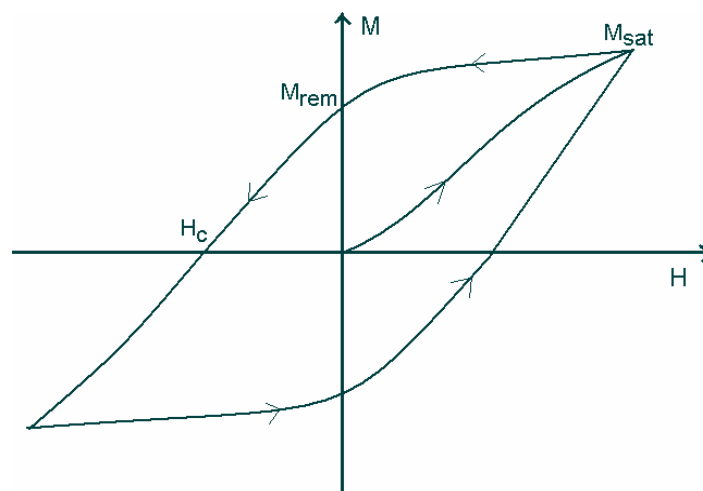
Figure 2.3 Typical magnetic hysteresis curves. H_c is the coercive strength, M_{sat} is the

saturation magnetization and M_{rem} is the remanence magnetization.

2.2.4 Synthesis of Magnetic Nanoparticles

Magnetic nanoparticles can be prepared by reducing an organometallic molecular precursor in solution in the presence or absence of a dispersion stabilizer such as a polymer. Cobalt nanoparticles can be prepared by thermolysis of dicobalt octacarbonyl ($Co_2(CO)_8$), or through the reduction of cobalt (II) formate.[24-26] A block copolymer which can form micelles to be utilized as small reactor sites can provide an ideal stabilizing protective layer for the nanoparticles. Such block copolymers possess a ligand-containing block which coordinates to the surface of the nanoparticles and a solubilizing block which establishes some of the solution properties of the nanoparticles. The synthetic method and stabilizer can strongly affect the properties of the nanoparticles.

2.2.5 Cobalt Nanoparticles

Cobalt nanoparticles typically exhibit a face-centered cubic crystalline lattice (FCC), which is not as desirable as the hexagonal closest packed structure (HCP) that has better magnetic properties. Korobov studied 4-nm cobalt nanoparticles dispersed in a polyethylene matrix, synthesized by the thermolysis of cobalt (II) formate at 290 °C.[27] They observed high magnetic anisotropy for the cobalt nanoparticles and high hysteresis which they attributed to surface effects. The particles possessed a high blocking temperature (600K) and high magnetic coercivity (590 Oe), which made them suitable for fabricating magnetic recording media.

Riffle et al. synthesized cobalt nanoparticles by thermolysis of dicobalt octacarbonyl ($Co_2(CO)_8$) in the presence of a micellar nitrile-containing central functionalized triblock

siloxane copolymer.[28, 29]   A ferrofluid was then created by adding a PDMS carrier fluid and removing solvent with vacuum. The particles exhibited superparamagnetic behavior, although low temperature (5 K) experiments showed some hysteresis ($H_c \neq 0$).   This indicated that the particles were below their blocking temperature. Oxidative degradation, which is a disadvantage of cobalt nanoparticles, was observed using magnetic hysteresis measurements.

Riffle et al. also synthesized diblock copolymers of poly(dimethylsiloxane-*b*-vinylmethylsiloxane) which were later modified via hydrosilation of the pendant vinyl groups to include trimethoxylsilyl functional groups.[29] These functional groups had the ability to covalently bind to the surface of cobalt, and these polymers were used to synthesize cobalt nanoparticles.

2.2.6 Iron Containing Nanoparticles

Magnetite (Fe_3O_4), a ferrimagnetic material, is one of the most common iron-containing compositions.   One advantage of magnetite nanoparticles is the higher oxidative stability compared to cobalt.[29] Furthermore, magnetite nanoparticles are less toxic and more biocompatible than cobalt nanoparticles.   Magnetite nanoparticles can be synthesized by adding a mixture of $FeCl_3$ and $FeCl_2$ to an aqueous ammonium hydroxide solution.[30] This method is often termed the solution coprecipitation method. Chu et al. synthesized magnetite nanoparticles through solution coprecipitation and then introduced them into a seeded precipitation polymerization of methacrylic acid, resulting in nanoparticles which exhibited a bimodal size distribution in dynamic light scattering measurements (peaks at $R_h = 3.1$ nm and 42 nm).[31]   The particles exhibited different stabilities in water depending on the nature of

small molecule stabilizer ligands such as tris(hydroxymethyl)aminomethane hydroxide (TRIZMA) and tetramethylammonium hydroxide. It was found that tetramethylammonium hydroxide yielded relatively poor stability compared to TRIZMA, a more hydrophilic stabilizer. Liu et al. synthesized 10-nm particles and stabilized them with poly(diallyldimethylammonium chloride) at a pH of 8.5.[32] Riffle et al. synthesized 8.8 nm magnetite nanoparticles also using the ferric chloride / ferrous chloride scheme.[33] However, a novel triblock copolymer consisting of a carboxylic acid functionalized center block designed to coordinate the magnetite and water-soluble polyethylene oxide end-blocks was used to create biocompatible nanoparticles.[33] The saturation magnetization of the magnetite particles was 65-70 emu/g and the particles displayed superparamagnetism. The solution co-precipitation method typically results in magnetite with high size and shape polydispersity as well as the presence of aggregates of particles. It may be advantageous to apply special agitation/mixing strategies to improve the size distributions. These features make the co-precipitation method disadvantageous for synthesis of magnetite nanoparticles where size homogeneity and reproducibility are important.

Sobal et al. obtained narrower size distribution magnetite nanoparticles through a solution co-precipitation method in which hydrochloric acid and sodium oleate were used to generate oleic acid in the aqueous reaction mixture containing dissolved Fe(II) and Fe(III) salts.[34] Sodium hydroxide was added to the mixture to form the magnetite. The particle size distribution was narrow with a mean size of Fe_3O_4 nanoparticles of 9.1 nm and a standard deviation of 2.3 nm by analysis of TEM images.[35]

Another method of synthesizing magnetite nanoparticles of narrow size distributions is

the high temperature thermolysis method pioneered by Sun et al.[1] This method involves

utilizing an organometallic precursor, Fe(acac)$_3$, as well as ligands such as oleic acid and

oleylamine in the presence of 1,2-hexadecanediol as a reductant. The resultant nanoparticles

had narrow size distributions and the size of the nanoparticles could be controlled by the

duration of the reaction and the use of seeded reactions. The nanoparticles synthesized using

this method possessed hydrophobic surfaces which required ligand exchange of the

hydrophobic oleic acid/oleylamine ligands in order to obtain stable aqueous dispersions. Sun

et al. synthesized 4-nm FePt nanoparticles by reducing FeCl$_2$ and Pt(acac)$_2$ with LiBEt$_3$H in

the presence of oleic acid, oleylamine, 1,2-hexadecanediol and phenyl ether as solvent.[36]

The oleic acid was needed to coordinate to Fe surface sites whereas the oleylamine was

reported to coordinate with Pt surface sites.   Due to the high magnetic anisotropy of FePt

($K_u = 10^8$ erg/cm^3), the nanoparticles have promise for ultrahigh density data storage. The

nanoparticles self-assembled on a silicon surface in the presence of polyethyleneimine to

produce long range hexagonal packing.   The crystalline structure of the nanoparticles was

FCC and they exhibited superparamagnetic behavior in the assemblies.   Annealing of the

assemblies at 500 ºC lead to a crystalline rearrangement to the face centered tetragonal (FCT)

phase, and also lead to ferromagnetic behavior.   The magnetic coercivity increased with

increasing annealing and the moment density of the nanoparticles increased by a factor of

about 20 to about 1000 emu/cm^3.   Recently, Sun et al. reported the synthesis of

nanocrystalline cube shaped nanoparticles with very narrow size dispersity.   Superlattices of

the cubic nanoparticles were created which had potential applications for data storage.[37]

A non-aqueous method (Figure 2.4) of synthesizing narrow dispersity, small (< 20 nm)

magnetite nanoparticles was disclosed by Sun et al.[1] The method is analogous to that used to synthesize the FePt nanoparticles which have very narrow size distribution with less than 5% standard deviation.[38] $Fe(acac)_3$ was reduced in the presence of oleic acid, oleylamine and 1,2-hexadecanediol in phenyl ether at 265 °C. The resultant nanoparticles self-assembled and could be transformed into γ-Fe_2O_3 (maghemite) or α-Fe. The magnetite nanoparticles were superparamagnetic and possessed saturation magnetizations of 82 emu/g. This method was also extended to the synthesis of mixed metal ($MnFe_2O_4$, $CoFe_2O_4$) nanoparticles.[39]
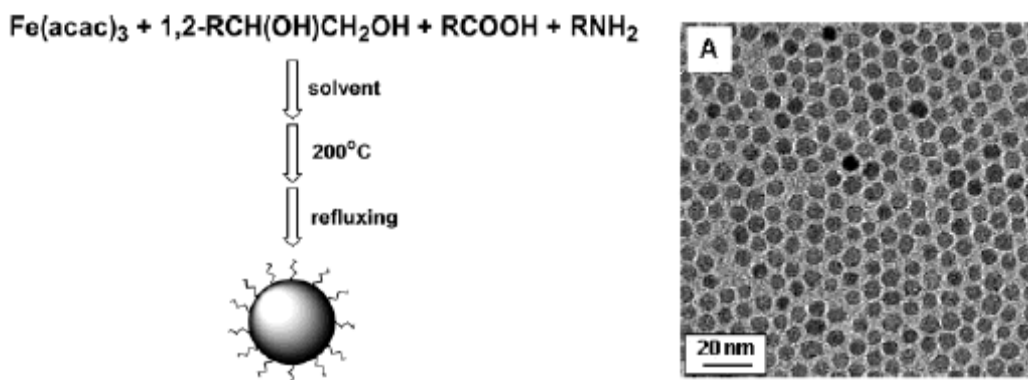
Figure 2.4 Organic phase magnetite nanoparticle synthesis and resulting HRTEM image of a monolayer of nanoparticles. Reprinted with permission from Sun et al. [1] Copyright 2002 American Chemical Society

Magnetite nanoparticles can also be synthesized by thermolysis of $Fe(CO)_5$ in the presence of oxygen. This has been shown to produce well-defined iron oxide nanoparticles, with smaller sizes (11 nm) being superparamagnetic and larger sizes (19 nm) being ferrimagnetic.[40] Sun also used the thermolysis techniques to synthesize metallic iron nanoparticles.[41]

Although Sun's thermolysis route has led to the synthesis of narrow size distribution

nanoparticles, there are some drawbacks to these methods. Primarily, the magnetite that is synthesized contains oleic acid and oleylamine ligands, which are often difficult to replace with polymeric ligands. Furthermore, there are several ligands as well as high temperature organic solvents required in the synthesis.

Recently, Pinna et al. synthesized narrow size distribution magnetite nanoparticles with a high temperature thermolysis using only benzyl alcohol as a ligand.[42] In this reaction, benzyl alcohol served as both the reductant and the solvent. It is reasoned that benzoic acid formed by oxidation of benzyl alcohol in these reactions may also function as a ligand for the magnetite.

Shapes other than simple spheres or nano-crystals of iron oxides have been synthesized. For instance, Zhang et al. synthesized hollow nanospheres of ferrite MFe_2O_4 (M = Mn, Co, Mg, Ni, Zn) through the adsorption of 15-nm ferrite nanoparticles onto the surface of carboxylic acid functionalized polystyrene nanoparticles (d = 230 nm).[43] These coated polystyrene particles were then calcined at high temperature, leaving behind a hollow sphere of ferrite. Yu et al. developed a novel method of creating hollow microcapsules (d = 200 nm) consisting of magnetite, through the solution phase precipitation of nanoparticles from aqueous solution in the presence of dodecylamine micellar templates.[44] The structures appeared to consist of shells of agglomerated magnetite nanoparticles (d~ 30nm). The shape of the microcapsules could be modulated from hollow spheres to hollow cubes by changing the amount of dodecylamine used in the synthesis.

One of the potential difficulties of magnetite nanoparticles is their tendency to oxidize and their sensitivity to oxygen. This results in a slow decrease of saturation magnetization

with time. A number of different approaches have been used to protect the magnetite from oxidation. One approach is the coating of magnetite nanoparticles with gold layers.[45] Unfortunately, this did not lead to great improvements in oxidative stability, likely due to incomplete coverage of the nanoparticle surface with gold.

Maghemite, γ-Fe$_2$O$_3$, is a close relative to magnetite.   It is also ferrimagnetic, although it has a lower saturation magnetization, 81 emu/g than magnetite 98 emu/g. [46]   Maghemite is an oxidation product of magnetite, and workers have reported conversion of magnetite to maghemite through annealing treatments.[47]

2.2.7 Methods for Binding Polymers to Magnetite Nanoparticles

Polymer stabilized dispersions of nanoparticles can be achieved utilizing complexes that have the polymer dispersants adsorbed onto the nanoparticle surfaces.   The polymer-magnetite complexes are often prepared through the adsorption of pre-synthesized polymers onto the surface of magnetite via functional groups such as phosphates, sulfates or carboxylates.[48]   Alternatively, surface-initiated polymerization may be used to synthesize polymer-grafted nanoparticles.   Takahara et al. synthesized polystyrene and poly(3-vinylpyridine) coated nanoparticles via surface-initiated polymerization using phosphoric acid functional alkoxyamine initiators.[49]   Thus, nitroxide mediated polymerization was utilized to create polymer grafted nanoparticles. The poly(3-vinylpyridine) coated nanoparticles were dispersible in water under acidic conditions. Such conditions resulted in protonation of the pyridine rings on the polymer backbone.

Another method used to create polymer-grafted nanoparticles is through the attachment

of a polymerizable group to the nanoparticle surface.   This was achieved by Shamim et al.,

who adsorbed thioglycolic acid onto magnetic nanoparticles and then reacted these

carboxylic acid functionalized particles with 4-aminostyrene.[50] The modified nanoparticles

were introduced into a radical precipitation polymerization of N-isopropylacrylamide

(NIPAM). The poly(NIPAM) functionalized particles exhibited unusual behavior due to the

temperature and pH-responsive properties of poly(NIPAM). Poly(NIPAM) exhibits an LCST

at 32 $^{\circ}$C where the amide groups lose hydration with water molecules and the polymer

undergoes a coil to globule transition.   Shamim et al. studied the adsorption of bovine serum

albumin protein onto these particles as a function of pH and temperature.[50]

Polymers may be used to control the sizes of nanoparticles, in addition to serving as

supports for maintaining colloidal stability in solution. In the case of maghemite synthesis

through thermolysis of $Fe(CO)_5$, the addition of Pluronic block copolymers into the synthesis

mixtures of the nanoparticles resulted in a particle size distribution with 13% standard

deviation.   The sizes of the particles were controlled between 5 and 22 nm by the ratio of

Pluronic block copolymer to solvent.[51] When the concentrations of Pluronic block copolymer

added to the reaction were increased, the sizes of the nanoparticles decreased.

Covalent attachment of polymers to nanoparticle surfaces has also been reported.

Aoyagi et al. modified the surfaces of magnetite nanoparticles with

3-aminopropyltriethoxysilane (APTES).[2] This resulted in amino groups at the magnetite

surface as well as Fe-O-Si bonds between the silane coupling agent and the magnetite. XPS

confirmed the presence of nitrogen on the surface of the magnetite. The amine groups at the

nanoparticle surface were then reacted with a random copolymer of 2-carboxyisopropyl

acrylamide and 2-(benzyloxycarbonyl)aminoisopropyl acrylamide. The presence of the

poly(NIPAM) derivative layer on the surface of the magnetite was confirmed with TEM

measurements after the polymer was stained. DLS was used to monitor the real-time

aggregation of the nanoparticles above the LCST of the NIPAM copolymers (~25 $^{\circ}$C). The

hydrodynamic radii increased with time upon heating above the LCST (Figure 2.5).

Additionally, the magnetite nanoparticles were found to aggregate in the presence of an

alternating magnetic field, and this was attributed to heating caused by this oscillating field.
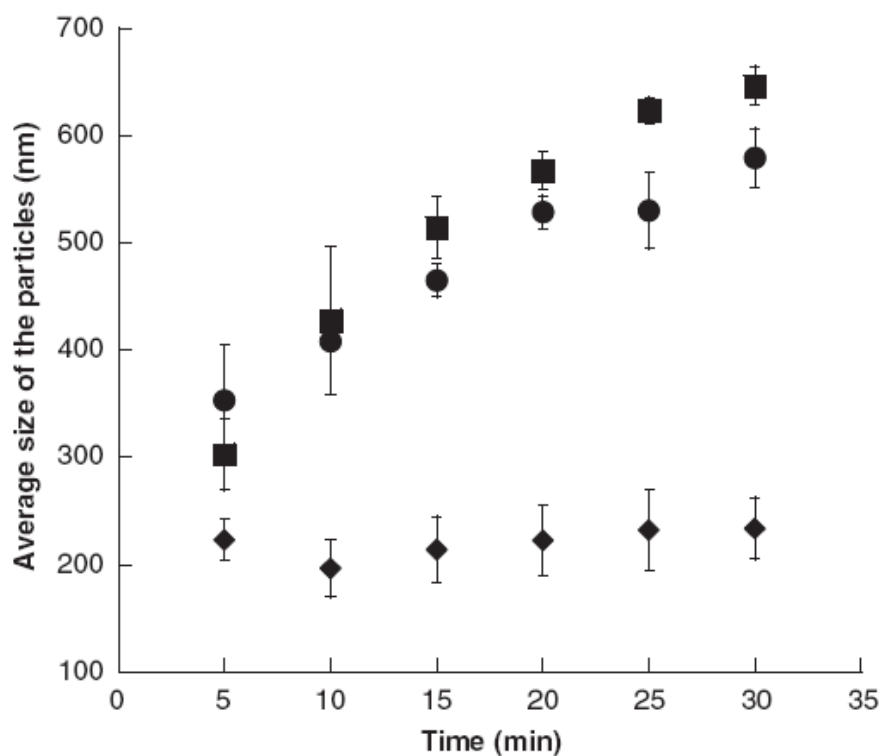
Figure 2.5 Increase in average particle size for poly(NIPAM) coated magnetite nanoparticles

for temperatures below (20 $^{\circ}$C, diamonds) and above (30 $^{\circ}$C, squares, 40 $^{\circ}$C, circles) the

LCST. Reprint from Wakamatsu et al.[2] Copyright 2006, with permission from Elsevier.

2.2.8 Binding Small Molecules to Magnetite Surfaces

Numerous small molecules have been used to modify magnetite surfaces. Lee et al.

coated magnetite nanoparticles with amino acids such as leucine, arginine and cysteine, through displacement of oxalate anions that had been introduced during the magnetite synthesis.[52]   The amino acid modification was confirmed with FTIR and TGA, and FTIR also suggested displacement of the oxalate anions.   The modified nanoparticles have potential applications in protein separation and protein delivery.

Oleic acid is probably the most common small molecule which is complexed with magnetite.[53, 54]   Oleic acid possesses a non-polar hydrocarbon tail and a polar, carboxylic acid head group. Carboxylate anions are known to coordinate to the surface of magnetite, presumably through a coordination of iron atoms with the both carboxylate oxygens.[55]   With the polar head group anchored on the magnetite surface, the non-polar tail extends into solution, causing the magnetite to be hydrophobic and dispersible in organic solvents. Korolev et al. studied the adsorption of oleic, linoleic and linolenic acids on magnetite surfaces and generated isotherms of these processes.[56]

Spherical aggregates were created from oleic acid and oleylamine coated magnetite nanoparticles through the introduction of β-Cyclodextrin into a high temperature magnetite thermolysis reaction in ethylene glycol.[55] β-Cyclodextrin is well known to form inclusion complexes with unsaturated fatty acids such as oleic acid.   The spherical aggregate sizes could be controlled roughly between 100 nm and 2 um through changing the *b*-cyclodextrin concentration and temperature of the reactions.

2.2.9 Magnetic Microspheres and Microcapsules

Much work has been devoted to the synthesis of magnetic microspheres.   These

typically have diameters from several hundreds of nanometers up to microns. Also of interest are microcapsules, which possess similar dimensions, but also contain a hollow core that can be filled with pharmaceutical agents or other materials. Magnetic microspheres have advantages over individual nanoparticles due to higher drug loading capacity,[57] and they also have potential for controlled release using biodegradable polymers. Furthermore, microspheres can be designed with a long retention time in the body, since they are too large to be excreted through the kidneys. However, microspheres do not possess the same ability to enter cells that individual nanoparticles possess. On the other hand, microspheres have greater magnetophoretic mobility because there is more magnetite in the microsphere compared to the single nanoparticle, resulting in a greater magnetic moment in the presence of a magnetic field.

Kang et al. demonstrated the synthesis of microcapsules containing cobalt nanoparticles (d = 13 nm) through the reduction of cobalt (II) ions in Pluronic block copolymer solutions in ethylene glycol.[58] The microcapsules had diameters from 1-5 microns and rough outer surfaces. Microspheres may also be synthesized via oil-in-water emulsion. Thus, Haam et al. synthesized drug-containing magnetic microspheres by mixing poly(ε-caprolactone) with hydrophobic oleic acid modified magnetite and a pharmaceutical agent in dichloromethane and emulsifying the mixture in water that contained a dissolved stabilizer.[57] This resulted in biodegradable magnetic microspheres that had potential applications in drug delivery. The microspheres exhibited movement in the presence of a gradient magnetic field using optical microscopy.

Horak and Chekina developed water-dispersible iron oxide nanoparticles through

precipitation of the nanoparticles in aqueous solutions of carboxymethyl-dextran.[59] The

modified iron oxide nanoparticles were introduced into emulsion polymerizations of glycidyl

methacrylate, resulting in incorporation of 5 wt% nanoparticles in 70-400 nm diameter

PGMA microspheres.   Liu et al. also reported the synthesis of magnetic microspheres

through incorporation of oleic acid-coated magnetite nanoparticles into emulsion

polymerizations of glycidyl methacrylate with methyl methacrylate and divinylbenzene as a

crosslinking reagent.[60]   The microspheres had diameters near 6 um and were covalently

coupled to glutaraldehyde-activated bovine serum albumin protein after exposure to ammonia

to introduce amino groups at the glycidyl residues.

Lindlar et al. synthesized magnetite containing microspheres with sizes ranging from

500-700 nm.[61] First, copolymers of glycidyl methacrylate with methyl methacrylate were

synthesized in an emulsion to create 500-700 nm colloidal particles.   Then ethylene diamine

was introduced to functionalize the particles with amine groups. Finally, iron salts were

introduced and the magnetite synthesis was carried out in the interior of the microspheres.

This resulted in a relatively homogeneous distribution of magnetite throughout the

microspheres as observed with TEM of cross-sections of the microspheres.   These

magnetite-containing microspheres organized into chain-like structures in solution in the

presence of a 125 mT magnetic field.

2.2.10 Applications of Magnetic Nanoparticles

The applications of magnetic nanoparticles range from magnetic recording media to

biomedical technologies where they can be used to provide localized heating or magnetic

resonance imaging (MRI) contrast agents.[62]   Magnetic nanoparticles have even been used as magnetically activated electrochemical switches.[63]   Aqueous suspensions of magnetite nanoparticles can be positioned in a specific area, allowing magnetic resonance imaging for medical diagnosis and AC magnetic field-assisted cancer therapy.[64]   For medical applications such as MRI contrast agents and cancer treatment, magnetite nanoparticles are generally superparamagnetic with sizes smaller than 20 nm in order to prevent removal from the bloodstream by the liver and spleen and to possibly allow entrance into cells.[1, 65]   Also, narrow size distributions are desired to create particles that have uniform behavior in the body.   Kinetic studies of uptake of MR contrast agents suggest that the particle's hydrodynamic size may play an important role.[66]   Larger polymer-coated magnetic particles (about 50 nm) were mainly trapped in the liver, while smaller sizes (about 30 nm) normally were useful for imaging the lymph node systems.   Magnetite has advantages over other MRI contrast agents due to the increased magnetic relaxivity compared to single paramagnetic complexes such as Gd^{3+} chelates.[67] Magnetite is particularly useful as a T_2 relaxation agent while gadolinium chelates are primarily T_1 agents.

For magnetic hyperthermia applications where an oscillating magnetic field is applied to induce local heating of magnetic nanoparticles, nanoparticles large enough to contain multiple domains can dissipate energy in an alternating magnetic field.[67] This is due to the fact that magnetic hyperthermia relies on magnetic hysteresis, which is not present in superparamagnetic nanoparticles (which are small enough to be comprised of only a single domain).   The mechanism of magnetic hyperthermia involves an increase in size of domains which are aligned with the externally applied magnetic field, resulting in movement of the

domain wall through the nanoparticle.[67]   When the field is reversed, the domain wall travels in the reverse direction as other domains in the particles grow in size. This movement of the domain wall causes magnetic hysteresis in ferro and ferromagnetic materials and results in heat generation. That being said, there is substantial evidence that smaller nanoparticles may also be able to heat the surrounding tissue upon application of a magnetic field.   The mechanism for this is not yet known.

Magnetic nanoparticle dispersions have potential applications in treating retinal detachment, a syndrome where the retina becomes separated from the choroid.[68] In order to treat this, a magnetic fluid which is immiscible with the aqueous vitreous humor has been proposed as a tamponade which gives 360° support to the retina and is held in place using an external magnetic scleral buckle.[68]

Magnetic separations of cells and biomolecules are rapidly gaining importance in biotechnology.   FePt nanoparticles have been used to separate 6-His tagged proteins through mutual coordination of nickel (II) cations between the 6-His units and nitrilotriacetic acid groups which were bound to the nanoparticles.[69]   Arylboronic acids were attached to magnetite nanoparticles in order to separate sugars.[70] This work involved polymerizing acrylic acid from surface-bound thiol functional groups using Ce^{4+} redox initiation followed by reaction of an amine functionalized boronic acid with the poly(acrylic acid). Polymerization from the surface of magnetite nanoparticles has also been investigated using a phosphoric acid functionalized TEMPO-based initiator (Figure 2.6).
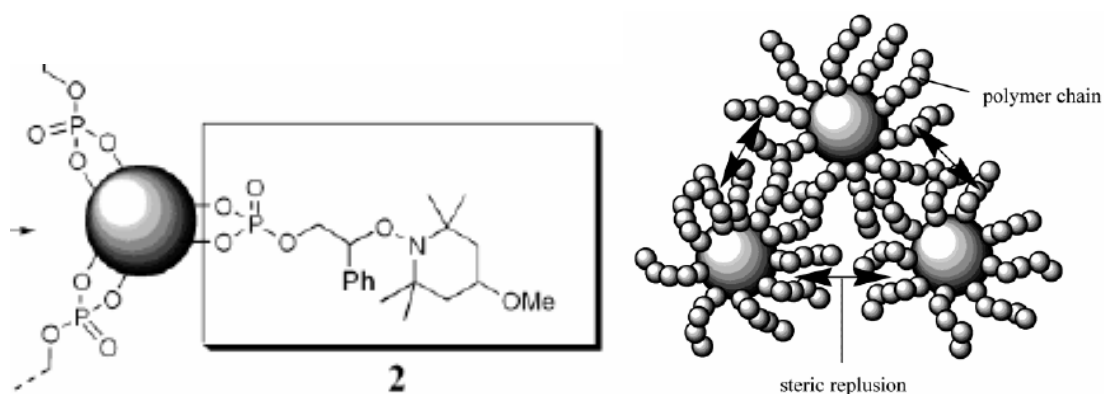
Figure 2.6 Surface initiated polymerization scheme involving nitroxide mediated polymerization. Reprinted with permission from Matsuno et al.[3]. Copyright 2004 American Chemical Society.

The applications of magnetic nanoparticles also extend to drug delivery. Delgado et al. studied poly(lactic acid) microspheres containing magnetite nanoparticles.[71] The microspheres were 1.7 um and were synthesized in a water/oil/water double emulsion where pharmaceutical drugs as well as magnetite nanoparticles could be carried in the inner aqueous phase. The use of poly(lactic acid) improves the biocompatibility of the nanoparticles. Stolnick et al. showed that the use of hydrophilic polymers increased blood circulation times and reduced accumulation of the polymer in the kidneys.[72] Gupta et al. showed that pullulan (a nonionic water soluble polysaccharide) could be used to reduce the toxicity of magnetite nanoparticles that were adsorbed into human dermal fibroblast cells.[73] Enzyme conjugation to magnetite nanoparticles has also been achieved.[74] It has been shown that nanoparticles coated with tetramethylammonium hydroxide groups can enter cells, as well as provide low toxicity in COS7 cells as determined from MTT assays.[75]

Riffle et al. studied the use of external magnetic fields to localize magnetic microspheres

in a flow-system which was designed to mimic blood vessels.[76]   The magnetic microspheres

consisted of oleic acid stabilized magnetite nanoparticles dispersed in a polyhydroxyether,

and these were fabricated into microspheres through high speed mixing with aqueous

solutions of poly(vinyl alcohol).   The results of the experiments demonstrated that magnetic

microspheres could be localized to specific regions of a flow system that mimicked the

circulatory system, using gradient magnetic fields of 0.9 T/m.   The fraction of microspheres

that were localized depended on the distance of the magnet from the flow system, the flow

rate employed and the loading of magnetite into the microspheres.

A further application of magnetic nanoparticles is removal of organic contaminants from

water.   Hatton, et al. studied poly(acrylic acid-g-PEO-g-PPO) stabilized magnetite

nanoparticles.[77]   In aqueous solution, the PPO segments resided close to the magnetic core

while the PEO chains extended into solution.   The PPO segments could collect organic

material from contaminated water, and the magnetic nanoparticles were separated from the

water by high gradient magnetic separation (HGMS).

Recently, Sun demonstrated the attachment of methoxyfunctional PEG derivatives to

magnetic nanoparticles through the use of 1,3,5-trichloro-s-triazines, which allowed coupling

of mono-hydroxyl PEG to an aminoalkylcatechol.[78]   These mPEG derivatives possessing

catechol ligands reportedly displaced the oleic acid surfactants, allowing dispersibility of the

otherwise hydrophobic nanoparticles in a range of buffer solutions which mimicked

physiological conditions.   The change in solubility and the increase in hydrodynamic radii

from 11.9 to 40.3 nm upon addition of the polymer provided indirect evidence of the

displacement of the oleic acid surfactants. However, the nanoparticles were stable only in

solutions with pH values greater than 7.   At lower pH, rapid flocculation was observed.

Recently, Mou et al. reported the synthesis of narrow size distribution magnetite nanoparticles coated with SiO_2, and these were incorporated in a mesoporous silica nanocomposite network.[4]   The size distributions of the particles appeared narrow from TEM images, but no quantitative analysis was provided of the size dispersity. These nanoparticle complexes were reported to have potential applications as MRI contrast agents, drug delivery carriers, and in cell sorting and labeling.   Preliminary experiments showed incorporation of the mesoporous silica structures into NIH 3T3 cells (Figure 2.7).
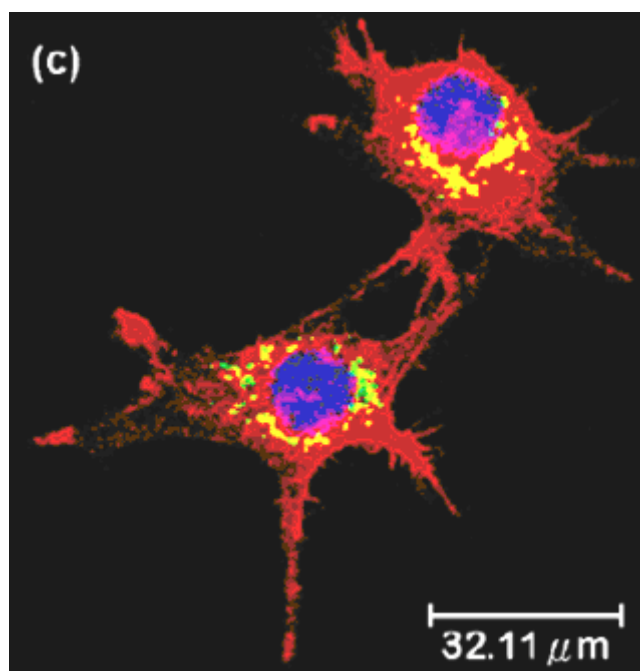
Figure 2.7 Merged confocal images of Mag-Dye@MSN in NIH 3T3 cells after 1 h of uptake time.   The cell skeleton was stained with rhodamine phalloidin (shown in red), and the cell nucleus was stained with DAPI (shown in blue). Reprinted with permission from Lin et al. [4]. Copyright 2006 American Chemical Society.

Magnetic composite nanoparticles were created by Mailander et al. who incorporated

10-12 nm magnetite nanoparticles into a 3-step miniemulsion polymerization of styrene and acrylic acid.[5]   This led to the formation of nanoparticles (d = 45-68 nm) which possessed iron oxide contents near 30 wt% and also possessed carboxylic acid groups at the particle surfaces.   These acrylic acid groups were thought to be important to facilitate passage of the nanoparticle complexes into cells. Cellular uptake was confirmed with fluorescence measurements, which revealed the presence of the nanoparticles in HeLa cells. Improvements in cell uptake were achieved through the grafting of L-lysine onto the surface of the particles through reaction with the acrylic acid residues.

In recent years, commercially available products based on magnetite nanoparticle complexes have been developed.   For instance, Ferumoxtran-10, a product consisting of 5 nm diameter magnetite nanoparticles supported by low molecular weight dextran are manufactured by Sinerem, resulting in a overall diameter of 30 nm (Guerret, France).[79] These nanoparticle complexes have been found to uptake selectively into human monocyte-macrophages which are present in atherosclerotic plaques in animal models. They are being applied as magnetic resonance imaging contrast (MRI) agents. The dextran coating on these nanoparticles helps prevent opsonization of the nanoparticles which results in uptake of the nanoparticles into the kidneys or spleen.   Furthermore, these complexes exhibit low cytotoxicity.

Superparamagnetic magnetite nanoparticle complexes have also been synthesized with lactobionic acid coatings, which cause specific uptake of the complexes into kidney cells (hepatocytes).[80]   These nanoparticle complexes have potential as magnetic contrast agents for diagnosing kidney diseases.   Experiments in mice have shown selective uptake of the

complexes into the kidneys.

Magnetic nanoparticles also have potential application in high density data storage. However, this relies on nanoparticles of large size which are ferromagnetic, or on collections of particles that also exhibit these characteristics. Buchanan et al. studied the rate of switching of a magnetic nanoparticle device based on iron nanoparticles embedded in SiO_2 and found ultrafast switching in response to a magnetic field, with switching times on the order of 26 ps.[81] In order to create a data storage system, regular arrays of nanoparticles, which can be addressed individually at specific locations are needed. Lei and Chim reported the use of an ultrathin porous alumina mask to deposit metallic (Ni) or semiconductor (CdSe) nanodots of ~20 nm in diameter.[82] The shape of the particles could be changed by using masks of different thicknesses and pore dimensions and changing the amount of material deposited. Yang et al. fabricated arrays of magnetite nanoparticle rings on gold surfaces.[83] The patterned magnetite was created by microcontact printing in which a hydrophilic SAM consisting of 16-mercaptohexadecanoic acid was patterned on a gold surface in the shape of discs. Then, the entire gold surface was exposed to a hydrophobic thiol (hexadecylmercaptan), which bonded to the areas not already patterned with the hydrophilic mercaptan. The gold surface was then allowed to condense water from humidified air, and this resulted in small droplets in the disc shaped areas patterned with the hydrophilic SAM. The entire surface, with the droplets, was then dipped in a solution of magnetite in chloroform and allowed to dry. The magnetic nanoparticles dried during evaporation stages in rings surrounding the water droplets.

Magnetite nanoparticles have been introduced into sub-micron poly(L-lactic acid) fibers

through electrospinning processes.[84]   An oleic acid coating on the magnetite surface was utilized to improve compatibility of the magnetite with the PLLA polymer. The biodegradable, biocompatible fibers were loaded with fluorescent proteins to study release rates.   These novel magnetic fibers have potential applications in drug delivery.[84] Magnetite nanoparticles have also been generated within the pores of mesoporous styrene-divinylbenzene networks, through successive introduction of ethanol, aqueous solutions of iron and aqueous base solutions.[85]   The networks retained their porosity after introducing the magnetite.   The presence of magnetite was confirmed with x-ray diffraction and Mossbauer spectroscopy.

Magnetic particles have also been used as probes to study the elasticity of surface grafted polymer brushes. Abdelghani-Jacquin et al. created gold-coated cobalt particles (d = 1.6 um) and used magnetic fields to direct the particles onto a hyaluronic acid grafted surface.[86]   This allowed the determination of viscoelastic parameters for the polymer grafted surfaces.

2.2.11 Ferrofluids

Ferrofluids consist of magnetic nanoparticles that are dispersed in a carrier fluid. The nanoparticles are typically coated with surfactants to enable stable dispersions. In order to form stable colloidal suspensions, magnetic nanoparticles must be small and superparamagnetic. If the particles are too large, then thermal energy cannot overcome their attractive forces and they will aggregate. Ferrofluids have applications in rotary shaft sealing, oscillation damping, and position sensing.[1] Buzmakov and Pshenichnikov studied rheological and diffusion properties of magnetite ferrofluids in kerosene with oleic acid stabilizers.[87] They suggested that the magnetite nanoparticles existed as small aggregates of several tens of particles and that these aggregates were stable to temperature changes. They attributed the formation of the aggregates to chemical reaction due to surface defects rather than to magnetic forces. Extensive modeling of Brownian motion of magnetic nanoparticles in ferrofluids has also been conducted.[88]

Ferrofluids are often used in making magnetic data storage devices. These are often composed of elongated cobalt modified α-Fe_2O_3 particles (d = 350 nm, aspect ratio = 6) suspended in organic solvents such as cyclohexanone containing a polymeric stabilizer, e.g. poly(vinyl chloride-*co*-vinyl acetate). Chae et al. studied the rheological properties of these systems, which are commercially used for printing on magnetic tape recording media.[89] Understanding the rheological properties of these magnetic inks is important due to the high speeds and high shear rates employed in commercial production lines. The authors observed non-Newtonian shear thinning properties and very little dependence of viscosities and fluid moduli on temperature. In contrast, the suspending medium possessed typical

Newtonian behavior with respect to shear and an Arrhenius dependence of viscosity on temperature. Since magnetic forces are independent of temperature (in the range of temperatures studied), the authors concluded that the rheological properties of the fluid were dominated by these interactions.

2.3 Colloidal stability

2.3.1 Introduction

A colloid is a particle, usually within the size range of 10^{-8} to 10^{-6} m which remains suspended in solvent due to Brownian motion. Colloidal particles collide with each other, and this can result in adhesion of the particles (aggregation). In a stable colloid, aggregation does not occur, whereas in an unstable colloid the growth of aggregates leads to flocculation and settling.

The stability of a colloidal suspension is determined by the surface forces acting between the particles as they approach. In the classical theory developed by Deryagin, Landau,[90] Verwey and Overbeek[91] known as DLVO theory, the total interparticle force is the sum of the repulsive electrostatic forces and attractive van der Waals (vdW) forces.

$$V_T = V_A + V_R \qquad\qquad 2.9$$

V_R denotes the component due to repulsive electrostatic forces and V_A denotes the attractive component due to vdW forces. The DLVO theory serves as the foundation for the description of interactions between colloidal particles and is applied to predict the stability of colloidal systems. It also describes the long-range interactions between particles and/or surfaces.
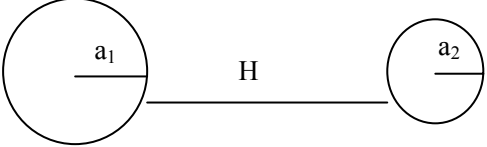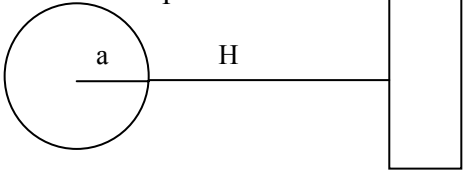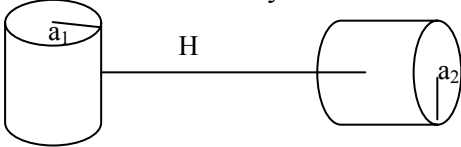
2.3.2 Classical Stability Theory: DLVO theory

2.3.2.1 van der Waals Contributions

In 1873, van der Waals proposed an improved gas law equation that included long-range attractive forces to explain the transitions from gas to liquid to solid as atomic separations were reduced.   London, Hamaker and others contributed to the calculation of vdW forces. The vdW interaction energy for a number of different geometries is provided in Table 2.1.

Table 2.1 Van der Waals interaction energies for different geometries

Geometry	Formula
two spheres	$V_a(H) = -A/6H \, (a_1a_2)/(a_1+a_2)$
sphere and wall	$V_a(H) = -Aa/6H$
Two crossed cylinders	$V_a(H) = -A(a_1a_2)^{0.5}/6H$

The attraction energy of the Gouy-Chapman-Stern double layer model [7] for two identical spheres, each with radius a, and surface separation H is given by

$$V_A = -\frac{A}{6}\left(\frac{2a^2}{H(4a+H)} + \frac{2a^2}{(2a+H)^2} + \ln\frac{H(4a+H)}{(2a+H)^2}\right)$$ 2.10

where A is the composite Hamaker constant, which is given by

$$A = A_{12} = \left(\sqrt{A_{11}} - \sqrt{A_{22}}\right)^2 \approx \sqrt{A_{11}A_{22}}$$ 2.11

A_{11} is the Hamaker constant of the particles and A_{22} is that of the liquid medium. For contact of two dissimilar materials in the presence of a third medium (A_{33}), the Hamaker constant can be calculated as

$$A_{132} = A_{12} + A_{33} - A_{13} - A_{23} \approx \left(\sqrt{A_{11}} - \sqrt{A_{33}}\right)\left(\sqrt{A_{22}} - \sqrt{A_{33}}\right)$$ 2.12

The Hamaker constant is related to the polarizability of the material by

$$A_{jj} = \frac{3}{4}\pi^2 h_p v_j \alpha_j q_j^2$$ 2.13

where h_p is Plank's constant, v_j is the dispersion frequency of the material, α_j is the polarizability, and q_j is the number of molecules per unit volume. Thus, the Hamaker constant is actually a function of particle separation at distances around 5-10 nm, however this effect is relatively small, and is usually ignored. This presents a first approach for calculating the vdW interaction between two bodies as a function of their separation distance (the so-called Hamaker approach). It determines the vdW interaction of two macroscopic bodies by carrying out a Hamaker-type integration of all the intermolecular interactions. Lifshitz developed a second approach,[92] which is more rigorous and provides the vdW interaction energy as a function of macroscopic properties of the interacting media, such as the dielectric permitivities and refractive indices. His interpretation did not acknowledge the molecular nature of matter but described it as a dielectric continuum interacting with the electromagnetic field. An advantage of the Lifshitz theory is that it implicitly incorporates all three molecular contributions to the dispersion interaction and thus does not depend on

additivity.   Instead it describes the system in terms of continuous media and uses only bulk properties.   The Hamaker approach is more popular, however, due to its greater simplicity and applicability, in spite of several shortcomings.   Lifshitz's method can be used to calculate the Hamaker constant from dielectric constants (ω) of the materials,

$$A_{132} = \frac{3}{4\pi} h \overline{\omega}_{132}$$
2.14

The Lifshitz and Hamaker theories are equivalent for media of non-polar molecules.[92]   The attractive force between colloid particles is directly proportional to the difference in the Hamaker constants between the dispersed particles and the dispersing medium.   For example, a colloid consisting of polystyrene in water is easy to stabilize because the Hamaker constants are similar, but for alumina, which has a much higher Hamaker constant than water, it is much more difficult to stabilize the suspension.

2.3.2.2 Electrostatic Contributions

Most charged colloidal particles possess electrical double layers at their surfaces, and these form the basis of repulsive interactions.   As shown in Figure 2.8, the arrangement of charges on the colloid surface and counter ions in the diffuse layer is known as the electrical double layer.   The liquid layer surrounding the particle exists in two parts; an inner region (Stern layer) where the ions are strongly bound and an outer (diffuse) region where they are less strongly associated.   In the diffuse layer, there is an artificial boundary within which the particle acts as a single entity (Figure 2.8).   The potential at this boundary is the zeta potential.

In DLVO theory, the attraction between two spheres, due to their polarizability (vdW

attraction), is compensated for by repulsive forces acting between the electrical double layers

of the two spheres. The electrostatic repulsion varies as r^{-1}, while the vdW attraction has a

r^{-3} dependence, where r is separation distance. Thus, the electrical double layer normally

prevents charged particles from approaching each other closely.
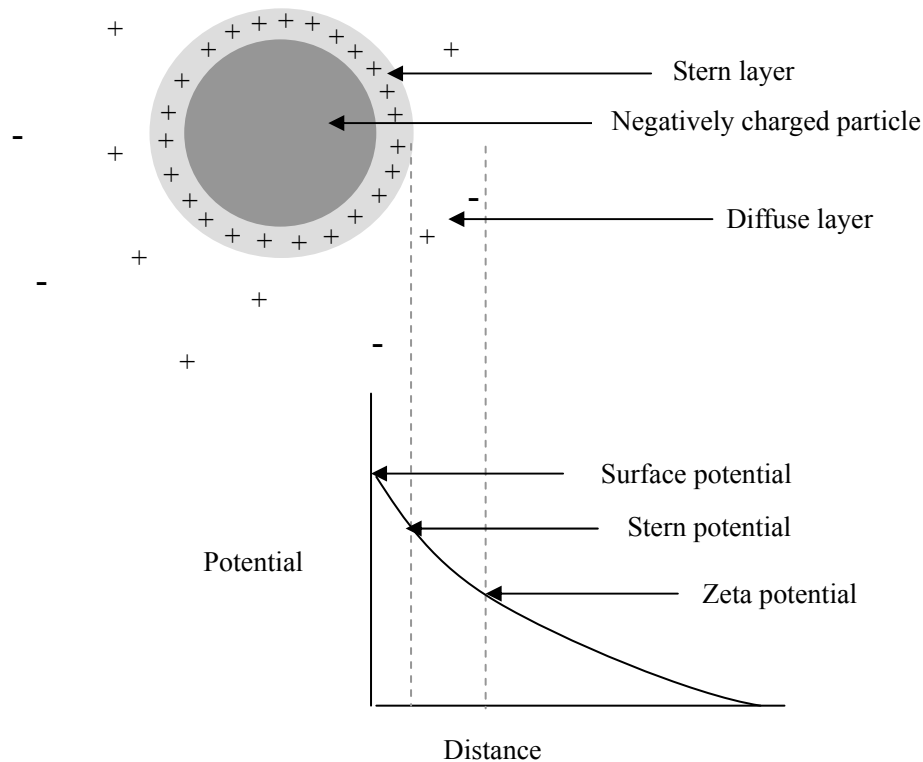
Figure 2.8 Diagrammatic representation of the Stern-Grahame electrical double layer model.

2.3.3 Extended DLVO theory

2.3.3.1. Steric Contribution

The classic and extended DLVO theories can explain the experimental results for bare and covered particles, respectively.   If there are polymer chains on the surface an additional repulsive potential has to be taken into account.   Stabilization of distance between particles can be caused by two different mechanisms.   When two particles covered with long chain molecules approach, the layers containing adsorbed or bound molecules overlap.   This overlap is equivalent to a local increase in the concentration of these molecules and, therefore, the free energy increases.   If the solvent is a good solvent, its molecules have a tendency to enter this zone and separate the particles.   This effect has been called the osmotic effect (Figure 2.9 a).
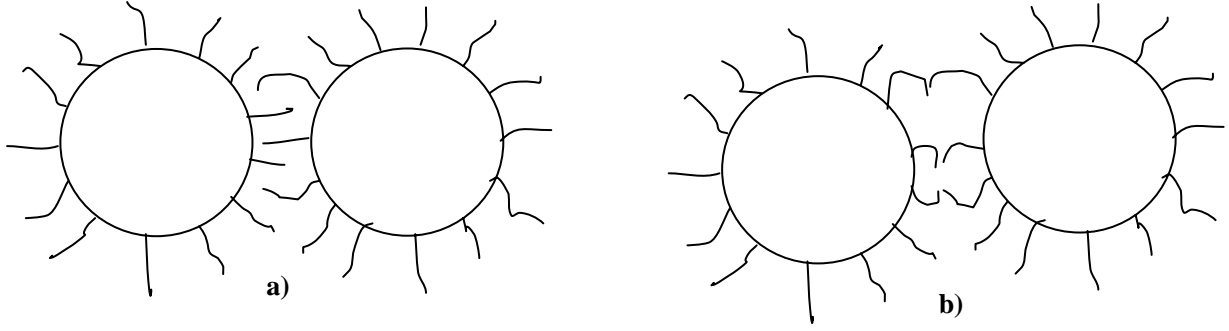
Figure 2.9 A schematic representation of the two steric effects **a.** osmotic effect **b.** elastic repulsion.

Another effect is due to the decreased entropy of polymeric chains restricted to the gap between adsorbed particles at very close distance, and this is called the "elastic effect" (Figure 2.9b).   Vincent et al. treated steric stabilization quantitatively. [6]   Two particles with an external covering of polymeric chains of thickness δ are influenced by the osmotic effect when they are nearer to one another than 2δ.[93]   The osmotic potential of repulsion (V_{osm}) is then given by

$$V_{osm} = \frac{4\pi a}{v_1}(\phi_2)^2(1/2-\chi)(\delta - H/2)^2 \qquad\qquad 2.15$$

where v_1 is the molecular volume of the solvent, ϕ_2 is the effective volume fraction of segments in the steric layer and χ is the Flory-Huggins interaction parameter.   H is the surface-surface separation between particles.   If both particles are closer than δ, an effect of the volume of restriction appears.   This can be expressed by a new potential of repulsion (V_{vr}, Eq. 20), so that at this distance the expression of the osmotic potential must be modified to[94]

$$V_{osm} = \frac{4\pi a}{v_1}(\phi_2)^2(1/2-\chi)\delta^2\left[\frac{H}{2\delta} - \frac{1}{4} - \ln\frac{H}{\delta}\right] \qquad\qquad 2.16$$

$$V_{vr} = \left(\frac{2\pi a}{MW} \phi_2 \delta^2 \rho_2 \right) \left(\frac{H}{\delta} \ln \left[\frac{h}{\delta} \left(\frac{3 - H/\delta}{2} \right)^2 \right] - 6 \ln \left[\frac{3 - H/\delta}{2} \right] + 3\left(1 + H/\delta\right) \right) \quad 2.17$$

where ρ_2 and MW are the density and molecular weight of the adsorbed polymer, respectively.

Due to the small radius of curvature for magnetic nanoparticles, polymer chains that extend from the surface may exhibit average extensions which differ from the expected values for flat surfaces.   This is clearly due to the reduced steric repulsion of the chains at greater distance from the core of the nanoparticle, effectively due to a decreased graft density per unit area at increasing distances from the core.

Nanoparticles coated with polymeric stabilizers may also be viewed as resembling star polymers.[95]   This may allow the application of models typically applied to star polymers to examine the size of complexes (hydrodynamic radius or radius of gyration) in solution. Another analogy may be drawn between magnetite nanoparticle complexes and block copolymer micelles, where steric crowding interactions play a large role in the extension of the polymer chain "brushes" from the surface.[96]   Additionally, magnetic nanoparticles may be related to dendrimers, which are similar to star polymers with the exception of having very well-defined molecular structures and typically possess fractal geometries resulting from repetitive branching.[97] A precautionary note however is that dendrimers will be much stiffer than the arms of a star polymer.

Likos et al. developed a model for starlike polymer molecules to predict the steric potentials V_s for colloidal particles with brushes comparable to the particle core size.[97, 98] The model is useful for describing potential energies of star polymers, micelles and sterically stabilized colloidal particles. This model is consistent with the Density Distribution model

employed for predicting brush dimensions in that both account for chain-chain interactions and curvature effects using the blob model of Daoud and Cotton.[99]

Moreover, this model can account for pair interactions ranging from soft- to hard-sphere like interactions as the number and length of corona chains are varied. We adapted the model essentially by replacing the star polymer core with the magnetite particle plus the inner polymer layer. The interparticle potential V_s is given by

$$V_s(r) = 5/18 f^{1.5} \frac{1}{1+\sqrt{f}/2} \frac{\sigma}{r} \exp[\frac{-\sqrt{f}(r-\sigma)}{2\sigma}]kT \qquad \text{for } r \geq \sigma$$

$$V_s(r) = 5/18 f^{1.5} [-\ln(\frac{\sigma}{r}) + \frac{1}{1+\sqrt{f}/2}]kT \qquad \text{for } r \leq \sigma$$

2.18

The length scale σ has been shown by Likos[97, 98] to be equal to $1.3*R_g$, where in our case, R_g is the radius of gyration of the magnetite-polymer complex. R_g is calculated[100]

$$\langle R_g^2 \rangle = \int_0^\infty n(r)r^4 dr / \int_0^\infty n(r)r^2 dr \qquad 2.19$$

where n(r) is defined in terms of the refractive indices of the core (n_c), inner layer (n_s), and solvent (n_0) and is given by

$$n(r) = n_c - n_o \qquad\qquad r < R_c$$

$$n(r) = (n_s - n_o)C(l/r)^3 (r/l)^{1/\nu} \qquad R_c < r < R_{eff}$$

$$n(r) = 0 \qquad\qquad R_{eff} < r. \qquad 2.20$$

The model allows for calculating the R_g accounting for the high graft density. So the particles consist of three regions: the core, the unswollen brush, and the swollen brush. The

part of the brush with the high graft density collapses and forms a melt-like layer which has a chain density close to the bulk density of the polymer. Therefore, the brush extension calculation should account for the melt-like layer, instead of a layer that is solvated and extended as a brush. The swollen brush can be calculated from the Density Distribution Model as shown in equation 14 where f is graft density, v is the excluded volume parameter and R_c is the radius of the core of the particle.

$$L_{shell} = \left[Nl^{1/v} \frac{8 f^{(1-v)/2v}}{3v4^{1/v}} + (R_c)^{1/v} \right]^{v} - R_c \qquad 2.21$$

Recent studies have quantified the contribution of steric stabilization to the stability of a system with adsorbed nonionic surfactants. Electrostatically stabilized dispersions are sensitive to the presence of electrolytes, while sterically stabilized dispersions are thermodynamically stable and, as such, much less influenced by electrolyte concentration. According to Einarson and Berg, a weak point in this interpretation appears if the steric and electrostatic stabilization are not independent.[8]
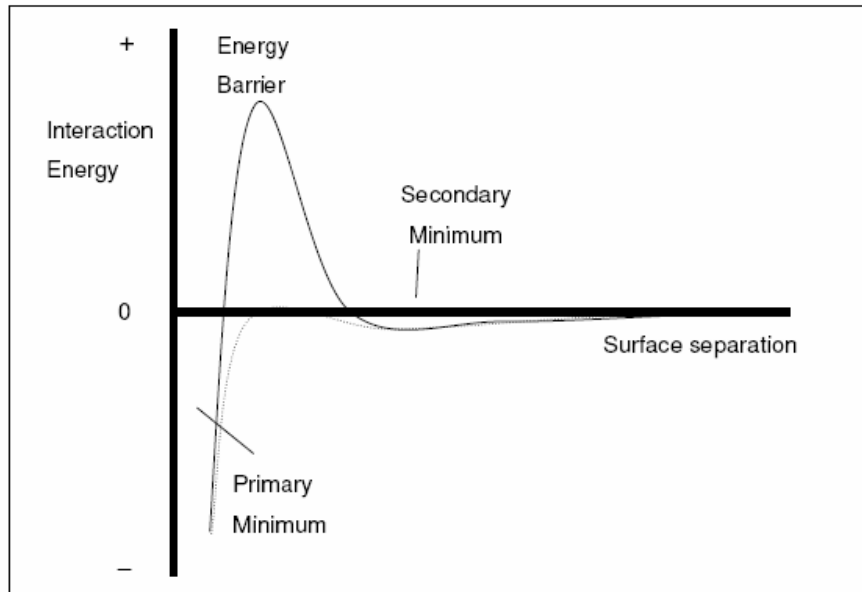
Figure 2.10 Interaction energy versus surface separation for two approaching colloids. Reprinted from Einarson et al. [8]. Copyright 1993 with permission from Elsevier.

There exist distances (primary and secondary minima) at which the forces of attraction exceed those of electrostatic repulsion (Figure 2.10). The vdW force decays as an inverse power of particle distance, whereas the electrostatic repulsion decays exponentially as $\exp(-\kappa H)$. If thermal agitation imparts sufficient energy for the particles to overcome the repulsive barrier, they will approach one another up to very close distances and the system will coagulate. However, if the maximum in the energy barrier is high enough, the system will remain stable as the particles cannot overcome the barrier. By increasing the concentration of an electrolyte in the solution, the electrical double layer compresses and reduces the electrostatic repulsion between the particles. Thus, the stability ratio, W (as defined below), decreases with increasing electrolyte concentration. The electrolyte concentration at which the energy barrier disappears, i.e. $V = 0$ and $dV/dH = 0$, is called the critical coagulation concentration (CCC).

2.3.4 Stability Ratio

2.3.4.1 Theoretical Determination from DLVO Theory

Colloidal particles collide randomly at a rate determined by their Brownian motion. The stability ratio, W, represents the ratio between the total number of collisions and the number of collisions that results in an aggregation process. W can be expressed as the fast coagulation rate k_f (as determined by diffusion, neglecting the potential barrier), divided by the actual aggregation rate k_s.

$$W = \frac{k_f}{k_s} \qquad 2.22$$

The stability ratio represents the effectiveness of the potential barrier in preventing particles from coagulating. From DLVO theory, Funchs[101] derived the W as

$$W = 2a \int_0^\infty \frac{\exp(V/kT)}{(2a+H)^2} dH \qquad 2.23$$

where H is the distance between the boundaries of two spheres, V is the net interaction energy (from DVLO theory), and a is the sphere radius. When $W = 1$, every collision forms an aggregate, and when $W > 1$, only some of the collisions form aggregates due to the presence of the energy barrier predicted by DLVO theory. Aggregation in the regime where an energy barrier is present is referred to as 'slow' aggregation. The stability factor is, in general, obtained by studying changes in the optical properties of suspensions (using turbidity[102-106] or light scattering[107, 108]) versus time and is a function of the electrolyte concentration.

The efficiency of the collisions or the total fraction of successful collisions is given by

$$W = \frac{1}{f_p + f_s} \qquad 2.24$$

where f_p is the fraction of particles which overcome the primary maximum and f_s is the fraction of particles which remain aggregated at the secondary minimum. Wang[109] proposed that the fraction of particles aggregated at the primary and secondary minimum is

$$f_p = \left(1 + \frac{\Delta V}{k_B T}\right) \exp\left(\frac{-\Delta V}{k_B T}\right)$$ 2.25

$$f_s = 1 - \left(1 - \frac{V_{min}}{k_B T}\right) \exp\left(\frac{V_{min}}{k_B T}\right)$$ 2.26

where ΔV is energy difference of secondary minimum and primary maximum, V_{min} is the secondary minimum. Einarson and Berg[8] proposed the rate constant of doublet formation can be calculated from the initial slope of the measured hydrodynamic radius with time measured by DLS using

$$k_s = \frac{1}{R_{h,1} \alpha N_o} \left[\frac{dR_h}{dt}\right]_{t=0}$$ 2.27

where $R_{h,1}$ is the initial hydrodynamic radius at the time zero, N_o is the initial particle number concentration and α is an optical factor that is a function of the initial particle radius, solvent refractive index and scattering angle.

2.3.5 Effects of Magnetic Fields

There are normally three contributions to the total energy: electrostatic, vdW and steric forces (osmotic and elastic). However, for magnetic fluids, the magnetic dipoles associated with the interacting particles must be taken into account.[110] According to Delgado et al.,[9] the magnetic energy contribution can be described as

$$V_M = -\frac{8\pi\mu_0 M^2 a^3}{9\left(\dfrac{H}{a}+2\right)^3}$$

2.28

where μ_0 is the magnetic permeability of vacuum, M is the magnetization of the particles, a is the particle radius, and H is the surface-to-surface distance between the particles. For magnetic fluids stabilized with nonionic polymers, the electrostatic contributions are negligible, so $V_R = 0$. Thus, for magnetic fluids, V can be described as

$$V = V_A + V_e + V_s + V_M$$

2.29

2.3.6 Magnetically Induced Flocculation

Due to the magnetic contribution to the total interparticle potential, magnetic fields may lead to flocculation. Generally, if steric stabilizers are present on the nanoparticles, permanent (irreversible) flocculation would not be expected. This is because the magnetic component is generally weaker than steric repulsive forces, and thus flocculation would involve contact between the steric stabilizing layers, but not between the magnetite surfaces. There is interest in magnetically induced flocculation because of the greater magnetic moment and thus mobility of the flocs under an applied magnetic field. Individual nanoparticles, in contrast, are too small to be easily directed under an applied gradient magnetic field.

Delgado et al. modeled poly(acrylic acid) coated magnetite nanoparticles using DLVO theory.[111] They suggested, when magnetic field was applied, the presence of a deeper secondary minimum (~ 4kT) in the total potential energy versus interparticle separation. This secondary minimum decreased with increasing pH beyond 7, due to the increasing

electrostatic repulsion from negatively charged carboxylate anions on the polymeric stabilizers.   Delgado et al. hypothesized the presence of loose flocculates in the presence of a magnetic field. Also, slower sedimentation rates were observed in the presence of a magnetic field. These slower sedimentation velocities were attributed to the loose flocculates causing chains of magnetite to form that could occupy all of the suspended volume.

Tsouris and Scott studied the effects of strong magnetic fields on uncoated maghemite nanoparticles (d = 0.2 um and 0.5 um) (Figure 2.11).[10] Superconducting magnets cooled with liquid helium were used to generate magnetic fields up to 6T, and particles were studied in dilute aqueous dispersions using dynamic light scattering at 90° and optical density solution (2-125 mg/L) at different pHs. It was observed that the application of a strong magnetic field resulted in flocculation of the paramagnetic nanoparticles. DLS measurements indicated a growth in particle size over time in the presence of strong magnetic fields.
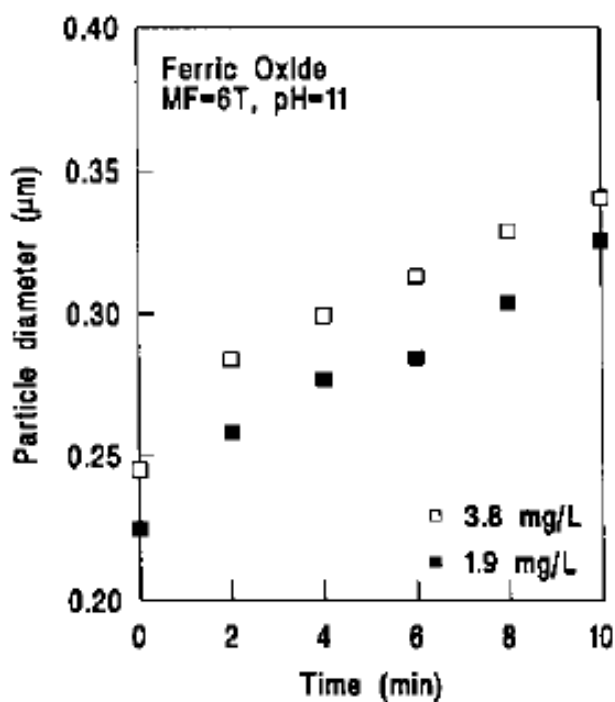
Figure 2.11 Particle size as a function of time measured using DLS on suspensions of ferric oxide. Reprinted from Tsouris and Scott[10]. Copyright 1995, with permission from Elsevier.

Chapter 3 Aqueous Dispersions of Magnetite Nanoparticles Complexed with Copolyether Dispersants: Experiments and Theory

Abstract

Magnetite (Fe$_3$O$_4$) nanoparticles have been synthesized and complexed with carboxylate-functional block copolymers, and then aqueous dispersions of the complexes were investigated as functions of their chemical and morphological structures. The block copolymer dispersants had either poly(ethylene oxide), poly(ethylene oxide-*co*-propylene oxide), or poly(ethylene oxide-*b*-propylene oxide) outer blocks, and all of them had a polyurethane center block that contained pendent carboxylate groups. The complexes were formed through interactions of the carboxylates with the surfaces of the magnetite nanoparticles. The magnetite cores of the magnetite-copolymer complexes were near 10 nm in diameter and the particles were superparamagnetic. Complexes with mass ratios of polymer to magnetite varying from 50:50 to 85:15 were studied. One of our objectives is to design complexes that form stable dispersions of discrete particles in water, yet that can be actuated (moved together) upon exposure to a uniform magnetic field. DLVO calculations that accounted for magnetic attractive interparticle forces as well as van der Waals, steric and electrostatic forces are presented. Compositions were identified wherein a shallow, attractive interparticle potential minimum appears once the magnetic term is applied. This suggests that it may be possible to tune the structures of superparamagnetic nanoparticle shells to allow discrete dispersions without a field, yet weak flocculation could be induced upon exposure to a field.

3.1 Introduction

Magnetic iron oxide nanoparticles such as magnetite or maghemite coated with polymers have potential for applications in drug delivery,[76, 84, 112] treatment of retinal detachment,[68, 113] as MRI contrast agents,[75, 114] and in bio-catalysis,[115] bio-separations,[116, 117] and high-gradient magnetic field separations.[118]   These colloidal dispersions, or ferrofluids, contain iron oxide nanoparticles of ~5-10 nm radius coated with polymers to impart desirable surface properties. If the nanoparticle complex is appropriately functionalized, it can be anchored onto a specific site, for instance on a cell,[119] or it can further complex with biological molecules such as antibodies.[120, 121] The high surface to volume ratio and good dispersibility of magnetic nanoparticles can also facilitate magnetic separations.[122]

Our group has previously reported the synthesis of a series of magnetite ferrofluids wherein the nanoparticles were prepared by chemical coprecipitation from iron chloride salts.[33]   Narrow particle size distributions and the absence of particle aggregation are desirable, since the behavior of aggregated particles deviates significantly from that of isolated primary particles.   The nanoparticles were coated with triblock copolymers containing poly(ethylene oxide) (PEO) end blocks, and then the complexes were dispersed in water.   Adsorption of these hydrophilic triblock copolymers occurred via carboxylate anchor groups pendent to a polyurethane center block, and this led to the formation of a brush layer that sterically stabilized the magnetite particles in water.

A major objective of the present work is to improve our understanding of how copolymer dispersants affect the capacity to disperse and loosely flocculate magnetite nanoparticles in aqueous and biological media upon application of external magnetic fields.   Clearly,

transporting clusters of magnetic nanoparticles using magnetic field gradients is more efficient than manipulating single nanoparticles, since the force imposed on a particle by a magnetic field gradient depends on the amount of magnetic component in the total particle (either a single particle or an aggregate of particles). It is envisioned that by tailoring the structures of dispersants for magnetic nanoparticles, the capacity for controlling aggregation together with improving magnetophoretic mobility may be gained. The PEO tail may be too hydrophilic to optimize nanoparticle flocculation in aqueous media. Thus, in order to introduce some hydrophobic character, we have introduced some propylene oxide units into the PEO dispersants. By varying the ratio of ethylene oxide (EO) to propylene oxide (PO) units and the copolymer architecture and block lengths, the hydrophobicity and relative tendency to flocculate can be investigated. This paper presents our initial approach for preparing such complexes, and describes the methods utilized to characterize the structures of the complexes.

Many methods for stabilizing magnetite nanoparticle dispersions have been employed to create diverse and useful materials. Magnetite nanoparticle dispersions have been stabilized by adsorption of small molecules such as oleic acid[34, 39] or phospholipids onto the nanoparticle surfaces.[123] Carboxylic acid functional homopolymers such as high molecular weight poly(acrylic acid)s have been studied as dispersion stabilizers for magnetite particles and dispersion stability measurements were conducted spectroscopically.[111] Deryaguin-Landau-Verwey-Overbeek (DLVO) theory and experimental measurements have been employed to investigate some of these dispersions, and the hydrophobic/hydrophilic character and steric interactions were found to be important for achieving stability. Hatton

et al. studied magnetite nanoparticles complexed with random copolymers of poly(styrenesulfonic acid), poly(acrylic acid) and poly(vinylsulfonic acid).[124] They observed that the random copolymers formed insufficiently thick coatings at low molecular weights, and formed bridges between particles and thus aggregation at higher molecular weights. The block copolymer stabilizers investigated herein with all the anchor groups located in close proximity in the central segment provide an ideal architecture for steric dispersants. Others have investigated non-functional blocks and carboxylic acid functional graft polymeric stabilizers. Lai et al. prepared γ-Fe_2O_3 nanoparticles, and stabilized their dispersions with Pluronic™ block copolyethers.[51] Moeser et al. used PEO and poly(propylene oxide) (PPO) grafted onto poly(acrylic acid) to stabilize dispersions of magnetite nanoparticles for high-gradient magnetic field separations from aqueous media.[77] They observed efficient separation of organic species with high partition coefficients. This was attributed to better solvation of the organic components by the hydrophobic copolymer segments relative to less solubility in the aqueous media.

Only a few studies of the dispersion and solid-state properties of magnetic nanoparticles that include the effects of magnetic fields on particle dispersion have been conducted. Tsouris and Scott demonstrated magnetic field-induced flocculation of polydisperse Fe_2O_3 particles with in-situ DLS measurements.[10] As expected, they found that increased particle size led to greater propensity for precipitation, with stronger magnetic fields being necessary to flocculate smaller particles. Furthermore, pH conditions near the isoelectric point led to faster flocculation. Others have studied the formation of chain-like aggregates of magnetic nanoparticles with applied magnetic fields in dilute conditions.[125] The absence of polymeric

stabilizers in these cases often produced irreversible flocculation. Another goal of our work is to design complexes that can be loosely flocculated with magnetic fields, but that can be redispersed with mild agitation due to steric interparticle repulsion.

The modified DLVO theory provides the framework for modeling particle pair interactions and predicting colloid stability. Theories for steric interactions between terminally attached chains on flat plates have proven successful in predicting surface forces as measured by the surface force apparatus.[126-128] Steric interaction potentials between spherical colloidal particles with polymer brushes can be derived from flat plate interaction models using the Deryaguin approximation when the ratio of brush thickness (L) to particle radius (R_c) is much less than one.[96, 127, 129] For example, this applies to sterically stabilized latex particles where the brush thickness only needs to be ~ 6 nm for particles with radii of ~ 50 nm.[130] However, for the present case where L/R_c ~ 1, the Deryaguin approximation does not apply and this necessitates a different approach for modeling steric interactions. In order to sterically stabilize metal oxide and metal nanoparticles in aqueous media where R_c ~ 5-10 nm, brushes with L/R_c ~ 1 are likely to be encountered since the Hamaker constant that characterizes attractive dispersion forces is on the order of 5×10^{-19} J (the non-retarded limit for magnetite in water).[97, 98, 131] Moreover, current methods for directly measuring steric interaction energies via the surface forces apparatus or atomic force microscopy are limited to systems where L/R_c << 1. Thus, direct measurements of forces between surfaces with brushes where L/R_c ~ 1 are not currently available. To address the modeling issue in the present case, we employ a model for steric interaction energies developed for star polymers.[97, 98]

In the present work, we have studied the influence of copolyether stabilizer microstructure and loading on the colloidal and solid-state properties of magnetite nanoparticle complexes. DLS, zeta potential and dispersion stability studies were used to characterize the solution microstructure of the polymer-coated nanoparticle dispersions. The compositions and solid-state properties of the polymer dispersants and the nanoparticle complexes were characterized via TGA, TEM and XPS, and SQUID and VSM were utilized to measure the magnetic properties of the complexes. Modeling of the colloidal stability of the nanoparticle complexes with DLVO theory[90, 91] was carried out to examine the potential for magnetic field-induced flocculation. DLVO theory allows investigation of the contributions of numerous interparticle forces such as electrostatic and van der Waals, as well as steric repulsions from anchored polymer chains on colloidal stability. Furthermore, the effect of magnetic fields on the interparticle potential can be evaluated.

3.2 Experimental

3.2.1 Materials

Tetrahydrofuran (THF, EMD Chemicals, 99.5%) was refluxed over sodium with benzophenone until the solution was deep purple and then fractionally distilled just prior to use. Potassium (98%), benzyl alcohol (BzOH, anhydrous, 99.8%), ethylene oxide (EO, 99.5%), and propylene oxide (PO, $\geq$ 99%) were purchased from Aldrich. Naphthalene (Aldrich 99%) was sublimed prior to use. Potassium naphthalene solution in THF was made by the method of Scott et al. with a concentration of 0.92 mol L^{-1}.[132] Glacial acetic acid (Aldrich) was diluted to a 2.5 M solution in THF. Dimethylformamide (DMF, EMD

Chemicals) was dried over CaH$_2$, fractionally vacuum distilled and stored under nitrogen at 25 °C. The benzyl alcohol initiated poly(ethylene oxide-*b*-propylene oxide) (BzO-PEO-*b*-PPO-OH) oligomer was dried overnight at 60 °C under reduced pressure prior to incorporation into the polyurethane block copolymer. Jeffamine™ M-2070, an EO/PO oligomer with a methoxy group on one end and an amine group on the other end (CH$_3$O-EO/PO-NH$_2$) was obtained from Huntsman Chemical Co. and dried at 60 °C under reduced pressure prior to incorporation into the polyurethane block copolymer. Isophorone diisocyanate (IPDI, Aldrich, 99.5%) was dried over CaH$_2$, fractionally distilled and stored under nitrogen. Bis(hydroxymethyl)propionic acid (BHMPA, Aldrich 98%) was dried under vacuum at 60 °C for 24 h prior to use. Dibutyltin dilaurate (DBTL, Aldrich 95%) catalyst was diluted to 10 mg mL^{-1} in THF. Palladium, 10 wt % on activated carbon, wet, Degussa type E101 NE/W (Aldrich) was used as received. A high-pressure Series 4561, 300-mL Parr reactor was utilized for the anionic polymerization of BzO-PEO-*b*-PPO-OH as well as for the hydrogenolysis of the benzyl ether end groups on the polyurethane copolymer.

3.2.2 Synthesis of Triblock Copolymer Dispersants (CH$_3$O-EO/PO-urethane-EO/PO-OCH$_3$) Comprised of a Central Polyurethane Segment Containing Pendent Carboxylic Groups

3.2.2.1 Synthesis of Benzyl Alcohol Initiated Poly(ethylene oxide-*b*-propylene oxide) (BzO-PEO-*b*-PPO-OH) Copolymer

A BzO-PEO-*b*-PPO-OH oligomer (37/63 wt/wt % EO/PO) was prepared with benzyl alcohol as the initiator. EO (10.0 g, 0.227 mol) was distilled from a lecture bottle into the

Parr pressure reactor that was cooled with an isopropanol-dry ice bath. THF (100 mL) was added to the reactor via syringe. An initiator solution consisting of benzyl alcohol (1.08 g, 10.0 mmol, the amount of initiator was calculated to target an oligomer with M_n = 2700 g mol^{-1}), THF (10 mL), and potassium naphthalene (10.9 mL of a 0.92 M solution, 10.0 mmol) was prepared in a 100-mL roundbottom flask. The initiator solution was added to the stirring reaction mixture via syringe. The cooling bath was removed and the reactor was allowed to warm to room temperature. The polymerization reaction was stirred overnight at room temperature, then purged with nitrogen for one hour to remove any residual EO. Then, PO (17.0 g, 0.294 mol) was added to the reactor via syringe, followed by 100 mL of THF. The polymerization mixture was heated to 60 °C and stirred for 72 h. The reactor was cooled to room temperature and purged with nitrogen for one hour. Acetic acid (10.0 mL of a 2.5 M solution in THF, 25 mmol) was added to terminate the reaction while it remained under an inert nitrogen atmosphere. The reactor was then opened and its contents were transferred to a 250-mL roundbottom flask. The solvent was removed under vacuum at room temperature, and the product was dissolved in 200 mL of dichloromethane. The product was washed twice with 100 mL each of deionized water. The solution was concentrated under vacuum at room temperature and precipitated in cold hexane to yield 27 g of polymer. Characterization via ^{1}H NMR showed a M_n of 2670 g mol^{-1} and 37/63 wt/wt % EO/PO. ^{1}H NMR (CDCl$_3$): 7.31 ppm (phenyl protons, 5H), 4.54 ppm (PhCH$_2$-O, 2H), 3.34-3.64 ppm (-CH$_2$- and –CH- on the PEO and PPO blocks), 1.09 ppm (-CH$_3$ on the PPO block).

3.2.2.2   Synthesis   of   a   Pentablock   Copolymer (BzO-PEO-*b*-PPO-urethane-PPO-*b*-PEO-OBz) Comprised of a Central Polyurethane Segment Containing Pendent Carboxylic Acid Groups, Flanked on Each Side by the BzO-PEO-*b*-PPO Copolymer

A polyurethane copolymer dispersion stabilizer with an average of three carboxylic acid groups in the central segment and 2670 g mol^{-1} BzO-PEO-*b*-PPO-OH tail blocks was synthesized via a similar method to that previously described.[33]   The first reaction step involved capping the monofunctional BzO-PEO-*b*-PPO-OH with IPDI.   The dried BzO-PEO-*b*-PPO-OH (4.95 g, 1.85 mmol) was transferred to a flame-dried, three-neck, 250-mL, roundbottom flask equipped with a magnetic stirrer and purged with nitrogen. IPDI (0.82 g, 3.7 mmol) was syringed into the flask, and then the flask was placed in an oil bath maintained at 70 °C under nitrogen.   The DBTL catalyst solution (0.05 mL, 0.5 mg DBTL) was added to the reaction flask via syringe.   The melt reaction was monitored by Fourier transform infrared spectroscopy (FTIR) by observing the decrease of the isocyanate absorption peak at 2260 cm^{-1}.   Once the BzO-PEO-*b*-PPO-OH was predominantly capped with the diisocyanate, BHMPA (0.37 g, 2.78 mmol) dissolved in DMF (10 mL) and another increment of DBTL catalyst solution (0.05 mL, 0.5 mg DBTL) was added to chain extend the block copolymer.   The reaction was continued until the disappearance of the isocyanate peak was confirmed via FTIR.   DMF was removed under reduced pressure at 50 °C.   The polymer was dissolved in 200 mL dichloromethane, and the dichloromethane solution was washed twice with 100 mL each of water.   The copolymer was precipitated into an excess of cold hexane yielding 5.5 g of polymer. ^{1}H NMR (CDCl$_3$): 7.31 ppm (phenyl protons, 10H),

4.54 ppm (Ph$\underline{CH}_2$-O, 4H), 3.34-3.64 ppm (-CH$_2$- and –CH- on the PEO and PPO blocks), 1.09 ppm (-CH$_3$ on the PPO block).

3.2.2.3 Deprotection of the Benzyl Endgroups of the Pentablock BzO-PEO-*b*-PPO-urethane-PPO-*b*-PEO-OBz Copolymer

BzO-PEO-*b*-PPO-urethane-PPO-*b*-PEO-OBz (9.2 g, ~2.8 meq benzyl), 30 mL of THF, and 0.3 g of catalyst (Palladium, 10 wt % on activated carbon) were charged into the Parr pressure reactor. The reactor was filled with 40 psi of hydrogen pressure, then the hydrogen was allowed to bubble out of the system at ambient pressure (3x). The reactor was pressurized to 65 psi with hydrogen and the reaction mixture was stirred at room temperature overnight. The reaction solution was then filtered through Celite 521. THF was removed under vacuum at room temperature yielding 8 g of hydroxyl terminated pentablock copolymer. ^{1}H NMR (CDCl$_3$): 3.34-3.64 ppm (-CH$_2$- and –CH- on the PEO and PPO blocks), 1.09 ppm (-CH$_3$ on the PPO block).

3.2.2.4 Synthesis of a Triblock Copolymer (CH$_3$O-EO/PO-urethane-EO/PO-OCH$_3$) Comprised of a Central Polyurethane Segment Containing Pendent Carboxylic Acid Groups, Flanked on Each Side by a Random CH$_3$O-EO/PO-NH$_2$ Oligomer (Jeffamine™ M-2070)

A polyurethane copolymer dispersion stabilizer with an average of three carboxylic acid groups in the central segment flanked by an 1,800 g mol^{-1} M$_n$ random CH$_3$O-EO/PO-NH$_2$ oligomer (Jeffamine™ M-2070, 3 mol EO/1 mol PO) was synthesized by polymerizing the

central polyurethane block first and then capping with the monoaminofunctional polyether oligomer.   A flame-dried, 250-mL, roundbottom flask equipped with a magnetic stir bar was charged with IPDI (0.89 g, 4.0 mmol), and BHMPA (0.40 g, 3.0 mmol) dissolved in DMF (10 mL) and purged with nitrogen.   The reaction was placed in an oil bath maintained at 70 °C under nitrogen.   DBTL catalyst solution (0.11 mL, 1.1 mg DBTL) was added to the reaction via syringe.   The reaction was monitored by FTIR by observing the decrease of the isocyanate absorption peak at 2260 cm^{-1}.   Once the intensity of the isocyanate absorption peak decreased by ~75%, Jeffamine™ M-2070 (3.6 g, 2.0 mmol) was added to the reaction flask.   The reaction was continued until the disappearance of the isocyanate peak was confirmed via FTIR.   After the reaction, most of the DMF was removed under reduced pressure at 50 °C.   The polymer was dissolved in 200 mL dichloromethane, and the dichloromethane solution was washed twice with 100 mL each of water.   The copolymer was precipitated by adding the solution into an excess of cold hexane yielding 5.2 g of polymer. ^{1}H NMR (CDCl$_3$): 3.34-3.64 ppm (-CH$_2$- and –CH- on the PEO/PPO units), 1.09 ppm (-CH$_3$ on the PEO/PPO units, IPDI CH, CH$_2$ and CH$_3$ protons).

3.2.3 Synthesis of Magnetite Nanoparticles and Polymer-magnetite Complexes.

Magnetite complexes were synthesized via a method similar to that previously described.[133]   Iron(III) chloride hexahydrate (1.00 g, 3.70 mmol) and iron(II) chloride tetrahydrate (0.368 g, 1.85 mmol) were charged to a three-neck, 250-mL flask fitted with a mechanical stirrer, pH electrode and nitrogen inlet and dissolved in 30 mL of Milli-Q water.   Deoxygenated, concentrated aqueous ammonium hydroxide was added with stirring until a

pH of 9.5 was reached (~10 mL). The reaction was stirred for 30 min and then the polymeric dispersant dissolved in dichloromethane (1.00 g stabilizer in 12 mL dichloromethane) was added to the reaction and the mixture was rapidly stirred. After 30 min of stirring, nitrogen was purged through the reaction until most of the dichloromethane was evaporated (over ~2 h). The aqueous dispersion of the copolymer-magnetite complex was centrifuged for 30 min at 3000 rpm (3x) to remove aggregates, and then dialyzed in a Spectra/Pore 6 membrane, MWCO 25000, for 5 days against Milli-Q water. The extraction solvent was refreshed twice a day to remove salts and any unbound polymer.

3.2.4 Characterization

^{1}H and quantitative ^{13}C NMR spectra were acquired on a Varian Unity 400 NMR spectrometer operating at 400 and 100.6 MHz, respectively. For quantitative ^{13}C NMR investigations of the polymer stabilizers, 0.63 g of polymer, 2.4 mL of CDCl$_3$ and 52 mg of chromium trisacetylacetonate (Cr(acac)$_3$) were analyzed with a 4.8-s relaxation delay and inverse gated decoupling.

Titrations to determine the concentration of carboxylic acids in the triblock polymers were conducted by dissolving the polymer (0.5 g) in 95 v/v % ethanol (25 mL), and titrating with 0.1 N KOH using phenolphthalein as an indicator. Each sample was titrated in triplicate and the reported data are the average of the titrated values.

Dynamic light scattering (DLS) measurements were conducted with a Malvern ALV/CGS-3 compact multi-angle light scattering spectrometer (Malvern Instruments Ltd, Malvern, UK) at a wavelength of 632.8 nm from a 22 mW, solid-state He-Ne laser at a

scattering angle of 90°.   An external re-circulating water bath was used to control the temperature at 25 ± 0.3 °C.   The temperature of the samples was equilibrated for at least 10 min before the measurements were taken.   Typically, 10 measurements of 30 seconds were acquired for each sample.   Comparative measurements were carried out on a Proterion DynaPro MS800 operated at 827 nm at a scattering angle of 90°.   The CGS-3 uses 1st to 3rd order cumulant fitting, with optional weighting and 17 forms of regularized fits for non-linear fitting.   The Dynapro data processing was performed with Wyatt's DYNAMICS software. The hydrodynamic radii and the size distributions were calculated with the regularization algorithm provided by this software.   The autocorrelation function was fit with an exponential fitting program (DTS) to extract the translational diffusion coefficient (D_T), and the Stokes-Einstein equation was used to convert diffusion coefficients to hydrodynamic radii (R_h).   For dilute suspensions of spheres, the Stokes-Einstein relationship applies and the diffusion coefficient can be related to the hydrodynamic radius R_h

$$D = \frac{k_b T}{6\pi\eta R_h}$$

3.1

Here k_b is the Boltzmann constant, T is the temperature, and η is the viscosity of the suspending liquid.   Intensity-averaged size distributions were converted to mass-averaged size distributions.   Quoted values of R_h are volume averages and are the averages of at least four measurements.   Samples were filtered through a 0.2 μm Teflon filter prior to the measurements.

Magnetite dispersion quality was investigated with a Philips 420T transmission electron microscope (TEM) and a JEOL 3000F field emission gun transmission electron microscope operating at 100 and 300 kV, respectively.   Aqueous dispersions of the polymer-magnetite

nanoparticle complexes were deposited on carbon-coated copper grids and allowed to air-dry.

Solid-state magnetic moments were recorded using a 7 Tesla Quantum Design MPMS SQUID magnetometer. Magnetization of magnetite and magnetite-copolymer complexes were measured from -70 to 70 kOe at 300 K. Magnetic properties of the polymer-coated magnetite nanoparticles were also measured in the solid state at room temperature using a Standard 7300 Series Lakeshore vibrating sample magnetometer (VSM). The magnetization of each complex was measured at room temperature over a range of applied fields from -8000 to +8000 Oe with a sensitivity of 0.1 emu.

Electrophoretic mobilities were measured at 25 $^{\circ}$C using a Zetasizer 3000HS apparatus (Malvern Instruments Ltd). Electrophoretic mobility (μ_e) was converted to a zeta potential (ξ) according to the Smoluchowski equation (Equation 3.2).[133]

$$\mu_e = \frac{\varepsilon_o \varepsilon_r}{\eta} \xi \qquad\qquad 3.2$$

where η, ε_o and ε_r are the medium viscosity, dielectric permittivity of vacuum, and relative dielectric permittivity, respectively. Equation 3.2 is valid when $\frac{a}{\kappa^{-1}} \gg 1$, where a is the particle radius and κ^{-1} is the Debye length.[134] For water at 25 °C, $\kappa^{-1} = \frac{0.304}{\sqrt{I}}$ and I is the effective ionic strength. The complexes were diluted in a 0.1 M NaCl solution prior to measurement, and five independent measurements were recorded to obtain a mean zeta potential.

Nitrogen sorption measurements were carried out on a Quantachrome NOVA 1200 high speed gas sorption analyzer. Cryogenic nitrogen sorption measurements were fitted using the Brunauer, Emmett and Teller (BET) model and specific surface areas were determined for

the magnetite nanoparticles.

X-ray photoelectron spectroscopy was carried out with a Perkin-Elmer model 5400 instrument fitted with a Mg K_α X-ray source (1253.8 eV) at a takeoff angle of 45°. The anode was operated at 250 W.

Thermogravimetric analysis was carried out on the magnetite nanoparticles, the copolymer dispersants, and the magnetite-polymer complexes using a TA Instruments TGA Q500. A temperature ramp rate of 10 ^{o}C min^{-1} was used under nitrogen. The samples were dried in a vacuum dried at 80 ^{o}C overnight prior to analysis.

Polymer-magnetite complex fluids were diluted in water and adjusted to pH 1.5-13 using aqueous HCl and NaOH. Stabilities of the dispersions under these conditions were evaluated by visual inspection.

3.3 Results and Discussion

One objective is to improve our understanding of how the hydrophilic/hydrophobic nature and architecture of copolymer dispersants adsorbed on magnetite nanoparticles affect the properties of their dispersions in aqueous media. This paper addresses the synthesis and characterization of a series of nanoparticle-copolymer complexes, and analyses of their dispersions in water, both experimentally and utilizing DLVO theory. The block copolymer dispersants had either PEO homopolymer or PEO/PPO copolyether outer blocks, and all of them had a polyurethane center block containing carboxylate anchor groups for binding to the surface of the magnetite. It was hypothesized that the PEO tail structure alone may be too hydrophilic to permit weak flocculation upon applying an external magnetic field. Thus,

some relatively hydrophobic PPO units were introduced into the nanoparticle brush layers with the goal of achieving better control over magnetic field-induced flocculation (i.e., actuation).

Our vision of these magnetite-copolymer complexes is that they comprise a magnetite core, a copolymer collapsed inner layer, and an extended PEO brush layer. The collapsed polymer inner layer that surrounds the magnetite sphere comprises the polyurethane anchor block. In the case of the PPO-*b*-PEO block copolymer tail, this inner layer likely also contains the PPO blocks due to their hydrophobic nature. In addition, the inner layer may also contain a portion of PEO due to geometric constraints associated with high concentrations of the dispersants on some of these nanoparticle surfaces. This aspect will be discussed herein.

3.3.1 Synthesis and Characterization of Magnetite Nanoparticle-copolymer Complexes

In our experimental efforts, we continuously strive to achieve well-defined nanoparticles and discrete dispersions. Experimental parameters that are particularly important for input into the DLVO calculations include the magnetite particle size, the number density of attached polymer chains, and the chemical compositions and lengths of the chains that form brush layers on the nanoparticles. Thus, to experimentally study a systematically varied series of dispersions, it is important to be able to control the adsorbed amounts of the polymer dispersants on the nanoparticle surfaces.

Magnetite nanoparticles were synthesized by aqueous co-precipitation of Fe(III) and Fe(II) chloride salts reacted with hydroxide.[33] This method is a facile means of obtaining

magnetite nanoparticles with only slight aggregation. The nanoparticles were then coated with a block copolymer dispersant containing carboxylate "anchor" groups in a central polyurethane block (Figure 3.1). The carboxylates in close proximity bind the central block of the copolymer to the iron oxide particle surfaces. The polyurethane anchor blocks were flanked by nonionic polyether "tail" blocks to prevent spontaneous flocculation of the nanoparticles in water through steric stabilization. Even though the central polyurethane block was in the anionic form, since the carboxylates were adsorbed onto the nanoparticle surface or encompassed within an inner polymer layer surrounding the magnetite, the mechanism of dispersion stabilization is primarily via steric repulsion.
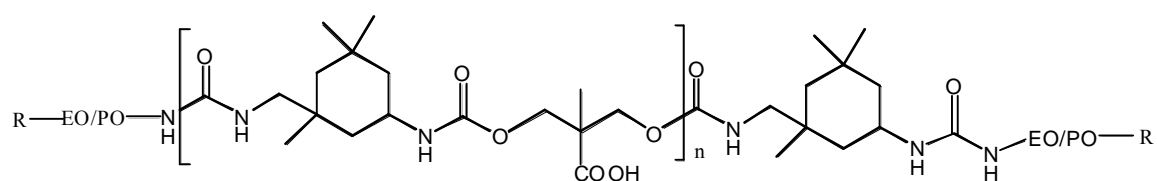
Figure 3.1 Block copolymer dispersion stabilizers with a central anchor block containing carboxylic acids flanked by end blocks as the stabilizing tails comprised of PEO and PPO units.

The tails of the dispersants were polyethers derived from EO and PO with varied architectures, compositions and end groups. The tail blocks of copolymer 1 were a commercial Jeffamine™ M-2070 and contained an average of 28 EO and 10 PO units. This copolymer had methoxy end groups. The Jeffamine™ M-2070 CH_3O-EO/PO-NH_2 polymer was analyzed via ^{13}C NMR to glean information regarding the sequencing of the EO and PO repeat units, following the peak assignments of Heatley et al.[135] The region from $\delta 73$-76

ppm representing the secondary and tertiary backbone carbons of the PO units suggests that the copolymer does not contain significant PO-PO-PO triads.   Thus, the copolymer tail has somewhat of a statistical nature rather than a blocky structure (Figure 3.2).   Heatley assigned resonances at δ75.26 and δ75.10 to the central methine carbons of *mm and mr (or rm)* PO-PO-PO triads, and these resonances are absent in the Jeffamine™ M-2070 spectrum. The tails of copolymer 2 were comprised of an average of 22 EO and 29 PO units and they had a diblock architecture with the outer segments being PEO.   The end groups of copolymer 2 were hydroxyl groups.   The tail blocks of copolymer 3 were PEO with methoxy end groups.   The molecular weights of the stabilizers ranged from nearly 5000 to 6500 g mol^{-1} based on NMR measurements (Table 3.1).
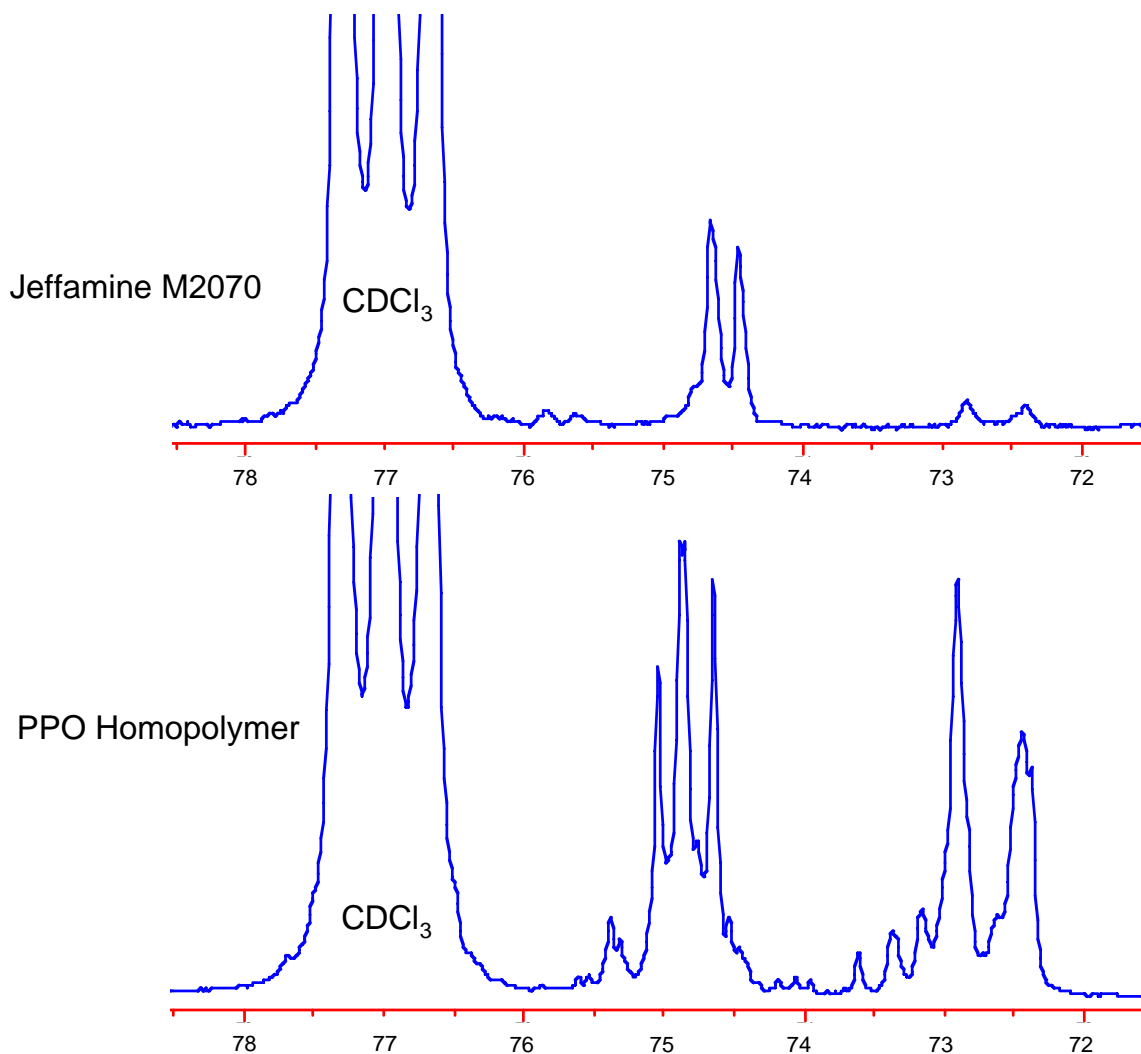
Figure 3.2 Quantitative ^{13}C NMR spectra of the Jeffamine™ M-2070 (amine terminated poly(ethylene oxide-*co*-propylene oxide)) tail block used to prepare copolymer 1 as compared to the same region for a poly(propylene oxide) homopolymer. The absence of peaks just upfield from $\delta=75$ ppm in the Jeffamine spectrum suggest that significant concentrations of PO-PO-PO triads are not present in the Jeffamine material. This suggests that the sequence distribution of this copolymer is somewhat random as opposed to blocky in nature.

Table 3.1 Chemical nature of the copolymer dispersion stabilizers

Copolymer	Total MW (g mol^{-1})	Tail MW (g mol^{-1})[1]	Ave # of COOH/chain[2]	Tail Microstructure	Ave # Repeat Units of EO/PO in the Tail
1	4850	1800	3.1	Statistical	28/10
2	6630	2670	3.0	Block	22/29
3	5160	1930	3.1	Homopolymer	44/0

[1] Derived from ^{1}H NMR in CDCl$_3$

[2] Derived from titration of the carboxylic acid groups

Magnetite-copolymer complexes were prepared with compositions containing from 15-50 weight percent of magnetite. Thus, complexes having a range of graft densities of polymeric stabilizers were produced. High-speed centrifugation and dialysis were utilized to remove aggregates and unbound polymers. The compositions of the complexes were verified using a combination of TGA weight loss and magnetization measurements (Table 3.2). Both techniques revealed that the complexes contained close to the targeted concentrations of polymer and magnetite. The magnetite concentration was calculated using magnetizations from VSM by comparing the magnetization of each complex with that of the bare magnetite nanoparticles of the same size (65 emu g^{-1} at 8000 Oe). The weight losses of the complexes during heating in the TGA furnace were also utilized to calculate the concentrations of polymer in the complexes. TGA analyses of the pure copolymers and bare magnetite were also carried out. The polymers completely pyrolyzed during the experiments and negligible weight loss was observed for pure magnetite (Figure 3.3). Nitrogen sorption BET measurements on the bare magnetite particles revealed a specific surface area (A_{sp}) of 95 m^2 g^{-1}. A calculation of magnetite radius by assuming a sphere with a surface area of 95 m^2 g^{-1} yields $3/(A_{sp}*\rho) = 6$ nm, where ρ is the magnetite density of 5.2 g cm^{-3}. The radius agrees fairly well with the radius of 5 nm obtained from TEM.

Table 3.2 Compositional data of the copolymer-magnetite complexes

Complex	Targeted Fe$_3$O$_4$ Conc. (wt %)	Fe$_3$O$_4$ Conc. from TGA[1] (wt %)	Magnetization[2] (emu g^{-1})	Fe$_3$O$_4$ Conc. from VSM (wt %)	Graft Density (σ) from TGA (chains nm^{-2})	Graft Density (σ) from VSM (chains nm^{-2})
1-35	30	35	20 (22)[3]	31	4.8	5.8
1-55	50	55	35	55	2.2	2.2
2-28	30	28	15	23	4.9	6.4
2-45	50	45	25	39	2.4	3.0
3-34	30	34	21	32	4.8	5.2

[1] Thermogravimetric analysis conditions**:** 30 - 700 $^{\mathrm{o}}$C, 10 $^{\mathrm{o}}$C min^{-1}, N$_2$

[2] Measured by VSM at 8000 Oe

[3] Magnetization measured by SQUID magnetometry
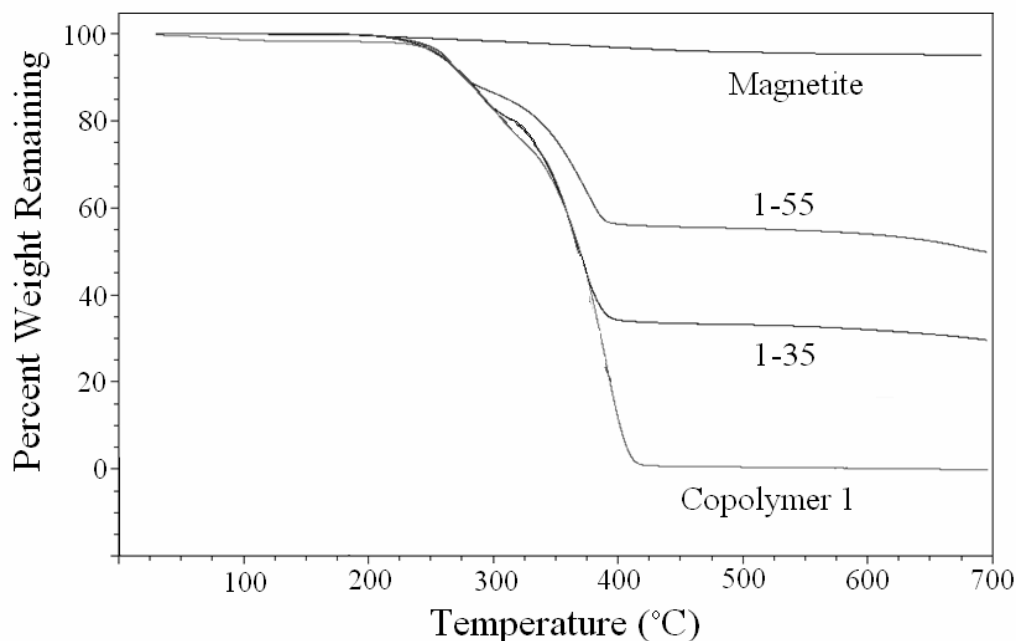
Figure 3.3 TGA analyses in N_2 of copolymer 1-magnetite complexes showing complete pyrolysis of the pure polymer and nearly complete weight retention of magnetite. The complexes had the expected weight losses based on the amount of polymer incorporated.

The graft densities of the polymers on the nanoparticle surfaces were calculated from the compositional and surface area data (Equation 3.3).

$$\sigma = 2 \left(\frac{m_{poly}}{m_{Fe_3O_4}} \right) \frac{N_A}{M_n A_{sp}}$$

3.3

In Equation 3.3, σ is the graft density expressed as the number of tail chains nm^{-2} (two tail chains per polymer), m_{poly}/m_{Fe3O4} is the mass ratio of polymer to magnetite, M_n is the number average molecular weight of the block copolymer, and N_A is Avogadro's number. The number of carboxylate groups available for adsorption per square nanometer of the nanoparticle surfaces was also calculated as $3\sigma/2$ since there were an average of three carboxylate groups per triblock copolymer and two chains extending from the surface per

molecule. The nomenclature adopted herein for the complexes is "copolymer number-wt % magnetite". For example, a complex designated as **2**-28 refers to a complex of copolymer 2 comprised of 28 wt % of magnetite and 72 wt % of copolymer 2.

TEM images of the complexes show that the primary particles have radii of ~ 4-5 nm (Figure 3.4). Both individual particles as well as larger clusters of particles are apparent from these images. Due to the strong electron density of the magnetite, the particles are clearly resolved in the micrographs.
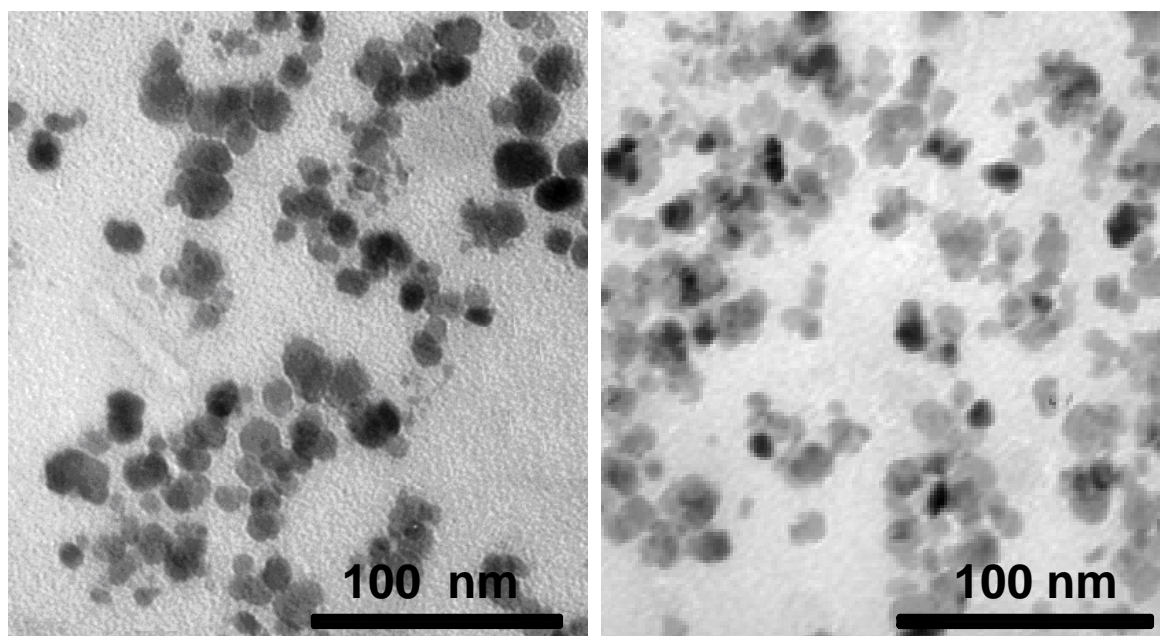
Figure 3.4 TEM micrographs of complexes **2**-28 (left) and **3**-34 (right).

XPS afforded elemental analyses of the surfaces of the nanoparticle complexes. The absence of iron on the surface confirmed full coverage by the polymeric stabilizer. The increased carbon and nitrogen signatures further supported the hypothesis of polymer coverage. The typical penetration depth of XPS of polymers at a take-off angle of 45$^\text{o}$ is ~3.5 nm, so this data suggests that the polymer surface layer is at least ~3.5 nm thick in the

solid state.   This thickness is close to the estimated end-to-end distances of the polyether tail blocks, ~ 3 nm for all of the copolymers.

The sizes of the nanoparticle complexes in water were examined by DLS.   The measurements were carried out at low concentrations, 0.1-1 mg mL^{-1}, to avoid multiple scattering.   An aqueous dispersion of the bare magnetite nanoparticles consisted of >90 wt % of particles with a hydrodynamic radius (R_h) of 4.2 nm (Figure 3.5a), which agreed well with the 5-nm radii derived from TEM.   A second DLS peak corresponding to some particle aggregates near 20 nm in R_h was also observed.   It is worthwhile to note that the intensity of the peak corresponding to the larger particles was high relative to that from the smaller particles since the scattering intensity is proportional to r^6.   Nonetheless, the smaller nanoparticles represented the majority of the sample by mass.
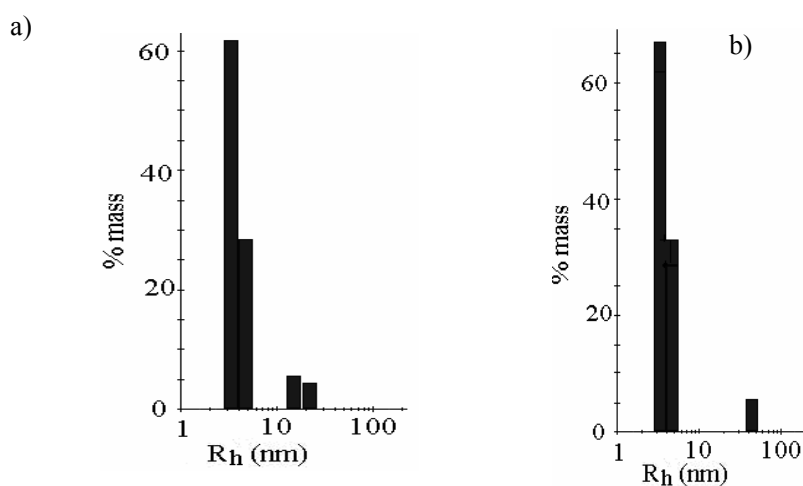
Figure 3.5 Hydrodynamic particle size distributions in water at 25 °C from DLS for a) bare magnetite nanoparticles (these particles were measured immediately after synthesis to avoid any aggregation that might occur with time) and b) complex **3**-34 at 0.4 wt %.

*Measured with the Proterion DynaPro MS800

The magnetite nanoparticle-copolymer complexes were mostly discrete nanoparticles with $R_h \sim$ 5-13 nm (Figure 3.5b and Table 3.3). DLS also revealed small amounts of aggregates, which were believed to arise from the magnetite precipitation process as observed with the uncoated bare magnetite nanoparticles. Zaitsev et al. synthesized magnetite nanoparticles via the chemical coprecipitation method and also observed sizes of the small species ranging from 3-5 nm and the size of the larger aggregate species ranging from 40-50 nm in DLS.[31] Ongoing work in our laboratories seeks to eliminate the formation of aggregates through novel synthesis and coating procedures. Copolymer 1 complexes with tails comprised of EO/PO units distributed randomly had smaller single particle dimensions than the copolymer 2 complexes that had blocky sequences in the tails. For the case of copolymer 2, this may be due to collapse of the PPO blocks into the inner polymer layer on the surface of the magnetite nanoparticles, with better extension of PEO segments into solution, resulting in a larger hydrodynamic radius.

Table 3.3 Sizes of the magnetite nanoparticle-copolymer complexes at 25 ^{o}C in water (0.1-0.5 wt %) measured by DLS at 90° using both the Malvern ALV/CGS-3 and the DynaPro MS800. The predicted dimensions of the complexes for aqueous dispersions of the magnetite-copolymer complexes are shown in the right-hand columns.

Complex	R_h (nm) CGS-3 (% mass)		R_h (nm) DynaPro (% mass)		Estimated Complex Dimensions		
	R_{h1}	R_{h2}	R_{h1}	R_{h2}	L_{inner}[1] (nm)	L_{EO}[2] (nm)	R_{eff}[3] (nm)
1-35	5 (75%)	35 (25%)	3 (96%)	28 (4%)	4.6	5.7	15.3
1-55	5 (71%)	40 (29%)	4 (88%)	35 (12%)	1.5	6.3	12.8
2-28	10 (70%)	45 (30%)	---		6.0	3.8	14.8
2-45	13 (80%)	43 (20%)	---		3.4	3.5	11.9
3-34	---		10 (78%)	37 (22%)	4.6	6.1	15.7

[1]For all of the complexes, the thickness of the inner polymer layer includes the anchor block. For complexes **1**-35 and **3**-34, the thickness of the inner polymer layer also includes a collapsed PEO component. For the complexes comprised of copolymer 2, the thickness of the inner polymer layer includes the anchor block plus the PPO component.

[2] L_{EO} refers to the calculated thickness of the PEO extended brush. For complexes **1**-35 and **3**-34, it does not include the collapsed portion of the PEO layer. For copolymer 1, L_{EO} was determined utilizing the DP of the total oligomer and assuming all of the units were EO.

[3] Derived from the sum of L_{inner} and L_{EO} along with the 5-nm core radius.

The effects of concentration, pH and time on the sizes of the copolymer 1-magnetite complexes in water were studied. The results showed only very small effects from changing the concentration of the complexes from 0.09 to 0.73 wt % or from changing pH from 4.5 to 7.0. The complexes also exhibited similar sizes when measured multiple times over the course of one month.

3.3.2 Prediction of the Magnetite-copolymer Nanoparticle Complex Dimensions Using the Core-shell-shell Model

As comparisons to the sizes derived from DLS, the sizes were predicted with a core-shell arrangement (Figure 3.6) using a density distribution (DD) model to estimate the inner polymer and brush layer thicknesses (Equation 3.4-3.6) on the magnetite, with the measured magnetite core radius of 5 nm (Table 3.3).[100] The DD model accounts for particle curvature by dividing the polymer domain into concentric shells and assuming a constant number of blobs equal to the number of adsorbed chains in each sub-layer. This model describes the blob size and segment volume fraction as a continuous function of distance from the surface and accounts for both excluded volume interaction between chains and brush extension in systems where the radius of curvature is comparable to the brush thickness.
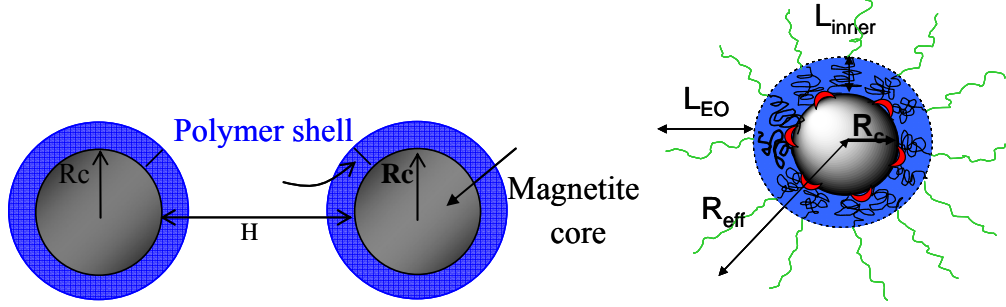
Figure 3.6 Schematic of two stabilized nanoparticles. The radius of the magnetite core utilized in the model was $R_c = 5$ nm derived from TEM micrographs, the core surface-to-surface distance is H, and the polymer layer thickness is $L = L_{inner} + L_{EO}$.

The volume fraction of statistical segments making up the PEO brush is given by:

$$\phi(r) = C(r/l)^{1/\nu}(l/r)^3 \qquad 3.4$$

where r is the radius from the center of the particle, ν is the Flory exponent (0.583 for PEO in water),[136] l is the statistical segment length of the corona chain (0.6 nm for PEO)[100]), and C is a coefficient defined by[100]

$$C = 3 * 4^{1/\nu} f^{(3\nu-1)/2\nu}/32\pi \qquad 3.5$$

In Equation 3.5, f is the number of corona chains per particle. To account for the inner polymer layer, we assume that the anchor block, and in the case of copolymer 2 the PPO blocks, form a dense, collapsed layer with thickness L_{inner} described by

$$L_{inner} = \left(\frac{3\sigma R_c^2 M_{shell}}{2\pi\rho_{shell}} + R_c^3\right)^{1/3} - R_c \qquad 3.6$$

For the two complexes with the highest polymer content, **1**-35 and **3**-34, the PEO statistical segment volume fraction as calculated in equation 3.4 at the edge of the inner layer (at $r = R_c + L_{inner}$) was larger than one, indicating that short portions of the PEO chains near the anchor

block were essentially in a dense, essentially unsolvated state. In these cases, equation (4) was solved to find the value of "r" ($> R_c + L_{inner}$) needed to bring the PEO volume fraction down to one. This additional PEO layer thickness was added to that of the anchor block layer to obtain the overall value of L_{inner}. The thickness of the PEO brush, L_{EO}, was then calculated from

$$L_{EO} = \left[N_{EO} l^{1/\nu} \frac{8f^{(1-\nu)/2\nu}}{3\nu 4^{1/\nu}} + (R_c + L_{inner})^{1/\nu} \right]^{\nu} - (R_c + L_{inner}) \qquad 3.7$$

The effective radius (R_{eff}) was calculated as the sum of the magnetite core, the PPO/urethane, and the PEO shell thickness

$$R_{eff} = R_c + L_{inner} + L_{EO} \qquad 3.8$$

For nanoparticles coated with copolymer 2 having PPO-*b*-PEO sequences with PEO outer blocks, the polymer shell was considered to have a collapsed PPO inner shell because of the hydrophobicity of PPO and its insolubility in water. The PPO layer thickness calculations were made assuming the PPO was densely packed as in the theta state. We also accounted for the urethane anchor segment as part of the PPO layer since it binds on the surface of the magnetite. The outer PEO shells should extend well in water as brushes to stabilize the particles. For nanoparticles coated with copolymer 1, it was assumed that the tails were comprised of only EO units, so the expression for the PPO shell thickness, L_{PO}, was zero. It was reasoned that an upper bound on the complex size could be calculated by assuming all of the units were EO. Thus, the brush thickness predicted by this approach

should be somewhat larger than that observed experimentally for copolymer 1 complex that contained some PO in the statistically sequenced tails. The graft densities used in these equations were obtained from the amounts of copolymer in the complexes derived from TGA, the molecular weights of the copolymers, and the nanoparticle surface area from the nitrogen sorption data (Table 3.2). It was assumed that not all of the carboxylate groups were bound to the magnetite surface due to the steric limit of approximately five carboxylates per square nanometer.

Analysis of the DLS data for the smaller size fraction (the fraction showing the highest % abundance by mass) in Table 3.3 indicates that the shell thickness formed from the statistical EO/PO copolymer 1 tail is extremely small. This suggests that the hydrophobicity imparted by the fairly low concentration of PO in the tail strongly favors placement of the tail in the inner polymer layer relative to extension of these polymers in water. Both copolymers 1 and 3 also have relatively hydrophobic methoxy termini, but it is not yet possible to discern what effects these end groups exert on brush extension. Since the brush thickness predictions for the copolymer 1 complexes did not take the PO units into account, it is not surprising that the experimental and predicted sizes do not agree.

In contrast, the experimental and predicted sizes of the complexes with copolymers 2 and 3 showed closer agreement. Thus, it is reasoned that predictions of the properties of aqueous dispersions of the copolymer 2 and 3 complexes using the extended DLVO theory, particularly of the steric potential term which relies heavily on the brush layer thickness, may afford reasonable predictions of colloidal stability.

3.3.3 Modeling Interactions Between Magnetite Nanoparticle-polymer Complexes to Predict Compositions that could be Actuated with the Application of a Magnetic Field

DLVO theory provides a useful tool for modeling the interparticle potential energies of the magnetite nanoparticle-polymer complexes in aqueous dispersions. The extended DLVO theory has been employed to model the aggregation of micron-size magnetic particles that were stabilized in water with an ionic surfactant.[137, 138] Interparticle potentials including van der Waals (V_a), electrostatic (V_e), steric (V_s), and magnetic (V_m) interactions were combined in the models to predict the total potentials (V_t).[134, 139] The van der Waals component was calculated as a function of the particle core-core separation distance (H), utilizing the magnetite core radius (R_c), and the effective Hamaker constant, A_{eff}, which includes retardation effects (Equation 3.9).[138]

$$V_a = -\frac{1}{6} A_{eff} \left(\frac{2R_c^2}{H(4R_c + H)} + \frac{2R_c^2}{(2R_c + H)^2} + \ln\left(\frac{H(4R_c + H)}{(2R_c + H)^2} \right) \right) \qquad 3.9$$

The effective Hamaker constant, A_{eff}, was calculated as[139]

$$A_{eff} = \frac{3}{4} kT \left(\frac{\bar{\varepsilon}(0) - \varepsilon(0)}{\bar{\varepsilon}(0) + \varepsilon(0)} \right)^2 + \frac{3\hbar\omega}{16\sqrt{2}} \frac{\left(\bar{n}_o^2 - n_o^2 \right)^2}{\left(\bar{n}_o^2 + n_o^2 \right)^{3/2}} F(h) \qquad 3.10$$

where k is the Boltzmann constant (1.38×10^{-23} J K^{-1}), T is the temperature (298 K), $\varepsilon(0)$ (80) and $\bar{\varepsilon}(0)$ (20,000) are the dielectric constants for the medium (water) and the substrate (magnetite),[131] n_o (1.333) and $\bar{n}_0$ (1.970) are the low frequency refractive indices of the medium (water) and substrate (magnetite), $\hbar$ is Planck's constant (6.63×10^{-34} Js), and ω is the frequency of the dominant relaxation in the UV (1.88×10^{16} rad s^{-1}). For these values, $A_{eff} = (3.035 \times 10^{-21}$ J$) + (5.435 \times 10^{-19}$ J$)(F(h))$.

F(h) accounts for retardation effects, and equals one at the non-retarded limit:

$$F(h) \approx \left(1 + \left(\frac{\pi h}{4\sqrt{2}}\right)^{3/2}\right)^{-2/3}$$

3.11

The dimensionless surface-to-surface separation, h, is related to the dimensional surface-to-surface separation, H, and the speed of light, c (3 x 10^8 m s^{-1}), by

$$h = n_o\left(n_o^{-2} + n_o^2\right)^{1/2} \frac{H\omega}{c}$$

3.12

For these values, h = (1.987 x 10^8 m^{-1}) * H where H is in units of meters.

While more detailed calculations of A_{eff} can take into account the presence of organic layers on the particle surface,[140-142] the present calculations for A_{eff} and V_a are considered to be sufficiently accurate due to the dominant effect of the steric potential term and the magnitude of the attractive magnetic interaction.

Electrostatic interactions cause stabilizing, repulsive interparticle forces due to the repulsion of like charges. For aqueous systems, the pair interaction energy due to electrostatic repulsion, V_e, was described with a constant potential expression useful for particle surface potentials ≤ 25 mV,

$$V_e = 2\pi R_c \varepsilon \varepsilon_o \psi_o^2 \ln(1 + e^{-\kappa H})$$

3.13

where ε is the dielectric constant of the medium (water), ε_o is the permittivity of free space, and ψ_o is the surface potential. Equation 3.13 is valid when $\frac{a}{\kappa^{-1}} \gg 1$. The surface potential ψ_o was approximated by measured values of the zeta potential. Zeta potential measurements were conducted on the 0.84 wt% **1**-35 complex in dilute solutions of 0.1 M aqueous NaCl (where $\kappa^{-1} \sim 1$ nm) at pH values of 4.5 (0 mV), 5.8 (-1.6 mV), and 7.1 (-1.3 mV). For bare magnetite, the isoelectric point is near pH 6.8.[143] The low zeta potential values of the complexes are consistent with extensive neutralization of the surface charges on the magnetite by the carboxylate groups and an outward shift of the slip plane due to the nonionic

PEO brush.[133]   The contributions of the electrostatic repulsive potential to the total pair interaction potential for the coated magnetite nanoparticles can thus be considered essentially negligible.

The primary means for achieving stable magnetite dispersions is derived from the steric brush layer around the nanoparticles formed by the copolyether dispersants.   Thus, the steric term in the interparticle potential energies is the major factor governing the behavior of these dispersions in water.   For the present complexes, the steric potentials V_s were calculated using the model by Likos et al. that is based on interactions between star polymer molecules.[97, 98]   This model is consistent with the Density Distribution model employed for predicting brush dimensions in that both account for chain-chain interactions and curvature effects using the blob model of Daoud and Cotton.[99]   Moreover, this model can account for pair interactions ranging from soft- to hard-sphere like interactions as the number and length of corona chains are varied.   We adapted the model essentially by replacing the star polymer core with the magnetite particle plus the inner polymer layer.   The interparticle potential V_s is given by

$$V_s(r) = 5/18 f^{1.5} \frac{1}{1+\sqrt{f}/2} \frac{\sigma}{r} \exp[\frac{-\sqrt{f}(r-\sigma)}{2\sigma}]kT \qquad \text{for } r \geq \sigma$$

$$V_s(r) = 5/18 f^{1.5} [-\ln(\frac{\sigma}{r}) + \frac{1}{1+\sqrt{f}/2}]kT \qquad \text{for } r \leq \sigma$$

$$3.14$$

The length scale σ has been shown by Likos[97] to be equal to $1.3*R_g$ where, in our case, R_g is the radius of gyration of the magnetite-polymer complex.   We calculated R_g using[100]

$$\langle R_g^2 \rangle = \int_0^\infty n(r)r^4 dr / \int_0^\infty n(r)r^2 dr \qquad 3.15$$

where n(r) is defined in terms of the refractive indices of the core (n_c), inner layer (n_s), and solvent (n_0) and is given by

$$n(r) = n_c - n_o \qquad\qquad r < R_c$$

$$n(r) = n_{inner} - n_o \qquad R_c < r < (R_c + L_{inner})$$

$$n(r) = (n_s - n_o)C(l/r)^3 (r/l)^{1/\nu} \quad (R_c + L_{inner}) < r < R_{eff}$$

$$n(r) = 0 \qquad\qquad\qquad R_{eff} < r. \qquad\qquad 3.16$$

The contributions from magnetic interactions between superparamagnetic particles in an applied magnetic field were estimated at 10,000 Oe from knowledge of the magnetization of the particles derived from the SQUID measurements (M = 4.47 x10^5 A/m, that is 86.6 emu/g), the magnetic permeability of vacuum (μ_0 = 1.26x10^{-6} Tm A^{-1}), interparticle distances between the surfaces of the cores (H), and the magnetite core radii (R_c = 5 nm) (Equation 3.17).[9] Magnetic hysteresis measurements of the neat (solid) complexes utilizing a SQUID device demonstrated that the nanoparticles were superparamagnetic. The lack of magnetic hysteresis is a characteristic of superparamagnetic particles since the magnetic moment is free to rotate and relax rapidly without concomitant movement of the particle. Due to the superparamagnetic nature of the nanoparticles, it was assumed that the magnetic attractive potentials in zero applied fields were negligible. Thus, the difference in magnetic attractions with and without a field, and its effect on colloidal stability were estimated.

$$V_M = -\frac{8\pi\mu_0 R_c^3 M^2}{9\left(\dfrac{H}{R_c} + 2\right)^3} \qquad\qquad 3.17$$

A plot of the interparticle potentials with vs. without the magnetic term predicts the behavior of a representative dispersion of the **2**-45 magnetite-copolymer complex in water (Figure 3.7).

The total interaction energy is dominated by steric repulsion.   In the absence of a magnetic field, the onset of steric repulsion occurs rather abruptly at a separation of about 8 nm and leads to a primary maximum $>>10kT$ (not shown).   The electrostatic and van der Waals interactions make negligible contributions to the total interaction energy.   Upon application of a magnetic field with a strength of 10,000 Oe (nearly saturated), a secondary minimum with a depth of $\sim -0.5kT$ appears near a separation distance of about 8 nm.
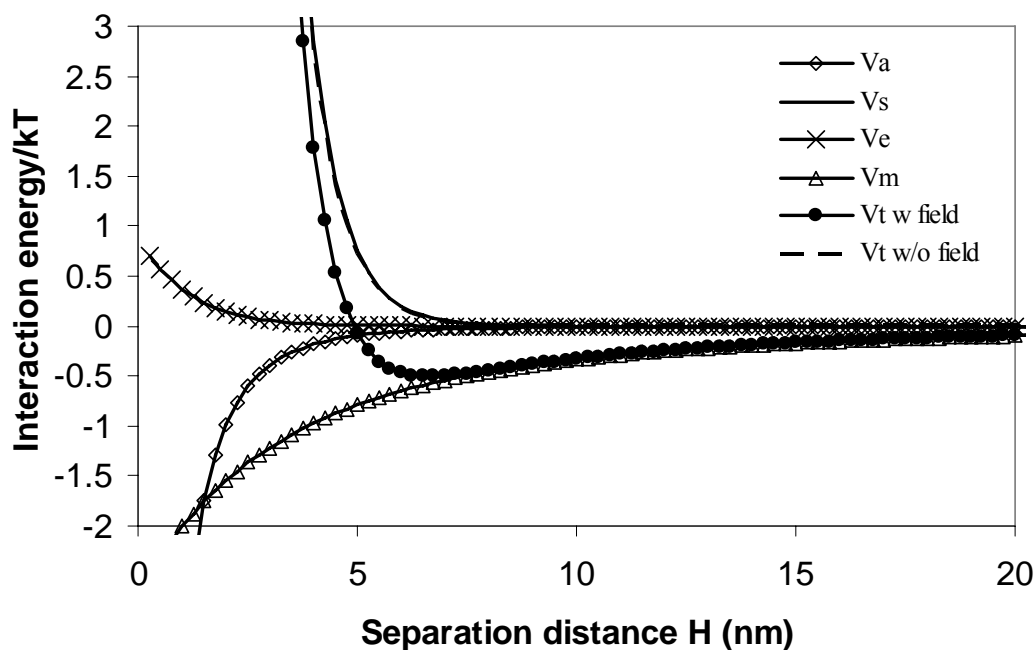
Figure 3.7 Component and total DLVO potentials for magnetite nanoparticles comprised of complex **2**-45 (Table 3.3).   Ionic strength = 0.1 M.

The total potentials for the magnetite nanoparticle complexes illustrate the effect of changing the brush thickness due to changing the complex composition (Figure 3.8).   In

comparison to the **2**-45 complexes, the **2**-28 and the **3**-34 complexes, both containing

significantly more polymer, exhibit the onset of steric repulsion at particle separations of

about 12 nm. When a 10,000 Oe magnetic field is applied, a weak secondary minimum

occurs with a depth of about -0.3kT. Since a secondary minimum depth of about -2kT is

required for weak, reversible flocculation,[139] the model predicts that these complexes will not

flocculate in the presence of a strong magnetic field. However, it does demonstrate the

design methodology needed to tailor the polymer layers to achieve actuation through loose

(reversible) flocculation.
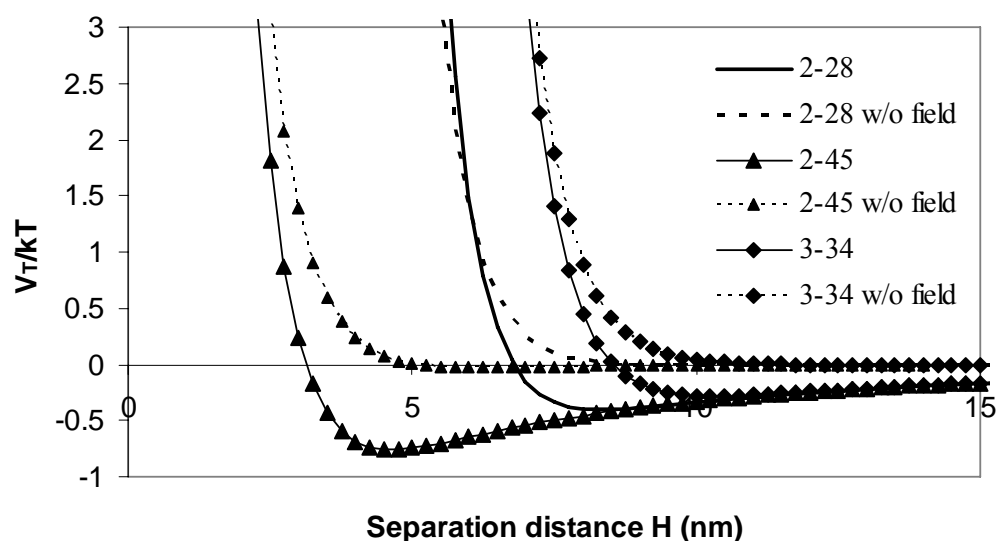
Figure 3.8 Total potentials calculated from DLVO theory for the 5-nm radius magnetite

nanoparticles with the predicted brush thickness from Table 3.3. Solid lines represent

application of a 10,000 Oe magnetic field.

The DLVO calculations provide insight into the effects of brush thickness and external

magnetic fields on the stability of the magnetite-polymer complexes dispersed in water under various conditions. Different brush thicknesses correspond to various polymer chain molecular weights and polymer graft densities. The parameters used in the calculations correspond to the actual magnetite core size, graft densities and shell thicknesses. The predictions suggest that it may be possible to tune the nanoparticle shells to obtain loosely flocculated aggregates in the presence of a field, and that such aggregates may be redispersible upon mild agitation. The depth of the secondary minimum increased in magnitude with decreased shell thickness. This suggests that shortening the polyether tail blocks and reducing the density of attached corona chains would increase the tendency and strength of flocculation in the presence of a magnetic field. In order to achieve controlled flocculation upon application of an external magnetic field, relatively thin polymer shells may be needed with a thickness less than approximately 5 nm and corona chain graft densities less than 3 chains/nm^2. Also, if a compositional change affected the brush thickness due to hydrophobic interactions, this would also potentially affect the ability to flocculate.

3.4 Conclusions

This paper represents our initial efforts toward designing magnetite-copolymer particles that can be dispersed in water, yet can be flocculated (actuated) by exposing the dispersions to a uniform magnetic field. Copolymeric steric dispersants that had either a homopolymer PEO tail or a block PPO-*b*-PEO tail with outer PEO segments could be adsorbed onto magnetite nanoparticle surfaces, and DLS measurements showed the prevalence of discrete

nanoparticles with tails that extended well into the aqueous medium. Brush layer thicknesses calculated using a density distribution model were in reasonable agreement with the experimental sizes. The extended DLVO theory was employed to predict the interparticle potentials by considering the van der Waals, electrostatic, steric and magnetic interparticle forces. In the absence of an applied magnetic field (conditions where the magnetic attractions for the superparamagnetic nanoparticles were assumed to be negligible), steric repulsive forces accounted for most of the repulsive stabilizing forces, and the dispersions were predicted to be stable. By tailoring the thicknesses of the polymer stabilizing shells, we were able to identify a range of compositions where a shallow secondary minimum with a depth of -0.3 to -0.5kT should occur at several nanometers of separation distance when a field of 10,000 Oe is applied. These results suggest that it will be possible to tune the density and sheath layer thickness of a polymer shell on superparamagnetic nanoparticles sufficiently to obtain discrete dispersions without a field, yet these materials could be flocculated and thus actuated with an external magnetic field. Ongoing research will test this hypothesis experimentally. Furthermore, we will pursue compositions that can be stabilized in biological buffer solutions that have relatively high ionic strengths.

3.5 Acknowledgments

Chapter 4 Magnetically Controllable Flocculation of Magnetite Nanoparticle Dispersions Complexed with Copolyether Dispersants

Abstract

Well-defined, narrow size dispersity magnetite (Fe$_3$O$_4$) nanoparticles were synthesized via the thermolysis of the Fe(acac)$_3$ precursor in the presence of benzyl alcohol. The magnetite nanoparticles were coated with triblock and pentablock copolymers possessing poly(ethylene oxide) and poly(propylene oxide-*b*-ethylene oxide) tailblocks and a carboxylate-containing anchor block. Suspensions of the nanoparticle complexes were investigated in phosphate buffered solutions, an analog to biological fluids. The nanoparticle complexes were found to exhibit longer term stability in PBS buffer solutions than magnetite made using an aqueous coprecipitation method. The nanoparticle complexes were characterized using TGA, XPS, VSM, DLS and TEM, to examine their compositions as well as their dispersion quality. Stability measurements in phosphate buffered saline (PBS) demonstrated longer term stability for the copolymer complexes without PPO in the outer blocks. The stability of the dispersions was analyzed using the classical DLVO theory of colloidal stability extended to account for steric and magnetic interactions between particles. Diagrams of potential energy versus interparticle distance indicate the predominant effect of steric and magnetic interactions on the particle stability. DLVO calculations on the nanoparticle complexes predicted the presence of a secondary energy minimum in the presence of an applied magnetic field, which was attributed to the attractive magnetic interaction. Exposure of the pentablock copolymer-magnetite complexes to a 1500 Oe

magnetic field with concomitant DLS measurements suggested that flocculation could be induced with an applied magnetic field. These results suggest the ability to tune the structures of superparamagnetic nanoparticle shells to allow discrete dispersions without a magnetic field, yet weak flocculation upon exposure to a magnetic field. Further research will be required to understand these effects.

4.1 Introduction

Nanosized magnetic iron oxide nanoparticles such as magnetite coated with hydrophilic water soluble polymers have received increasing attention due to their wide ranging applications in drug delivery,[76, 84, 112] treatment of retinal detachment,[68, 113] as magnetic resonance imaging (MRI) contrast agents,[75, 114] in bio-catalysis,[115] bio-separations,[116, 117] and in high-gradient magnetic field separations.[118] Magnetite is the most attractive candidate magnetic material for use in the human body due to its biocompatibility and low toxicity. Colloidal dispersions of magnetite, called ferrofluids, contain iron oxide nanoparticles of ~5 nm radius coated with polymers to impart desirable surface properties and solubility characteristics. Copolymers with a variety of molecular weights, compositions, structures, and end-groups have been applied as surface steric stabilizers. Additionally, the conformation of the polymer coating and graft density are also important factors from the perspective of physicochemical properties. Furthermore, if the copolymer is appropriately functionalized, it is possible to attach drugs using linkers that can be released at a desired site after being directed via an external magnetic field.[144] Copolymer composition may also be chosen to achieve selective interaction with cells,[119] or antibodies.[120, 121]

Our group has previously reported the synthesis of a series of magnetite ferrofluids wherein the nanoparticles were prepared via chemical coprecipitation from iron chloride salts.[33] Magnetite nanoparticles synthesized using these methods possess both size and shape dispersity, and often contain irregular aggregates inherently present in the samples, which are difficult or impossible to separate. Recently, Sun et al. synthesized magnetite nanoparticles using the high-temperature thermolysis of organometallic precursors such as Fe(acac)$_3$ in the presence of oleic acid and other ligands, to produce well-defined magnetite nanoparticles with narrow size distributions.[1] Narrow particle size distributions and the absence of particle aggregates are desirable, since the behavior of aggregated particles deviates significantly from that of isolated primary particles. Furthermore, Pinna et al. developed an analogous high-temperature thermolysis synthetic method which involved an alcohol ligand, benzyl alcohol, which is more easily displaced than oleic acid. [42]

Many methods for stabilizing magnetite nanoparticle dispersions have been employed to create diverse and useful materials.   Magnetite nanoparticle dispersions have been stabilized by adsorption of small molecules such as oleic acid[1] or carboxylic acid functional homopolymers[111] or random copolymers[124].   Previously, our group has reported the use of block copolymer stabilizers for magnetite nanoparticle dispersion synthesis.[33] These block copolymer stabilizers, which are also utilized in the present work, provide ideal architectures for steric dispersants due to the separate functions of the central and outer blocks. The central urethane block possesses all of the carboxylic acid anchor groups, ensuring strong attachment to the magnetite surface, while the polyether tail blocks extend into solution to provide steric stabilization. The block copolymer eliminates problems such as interparticle bridging or weak

adsorption typically experienced with random copolymers.

Because of the important and diverse biomedical applications of magnetic nanoparticles, we desire to create complexes which are stable in aqueous physiological conditions. Sun et al. have previously developed magnetite nanoparticle complexes which are stable in aqueous buffer solutions and mimic physiological conditions.[78] However, these nanoparticle complexes were not stable in acidic conditions and furthermore no studies of these complexes were performed relating to the effects of magnetic fields. Few examples exist of studies regarding the dispersion and solid-state properties of magnetic nanoparticles that include the effects of magnetic fields on particle dispersion and stability. Magnetic field-induced flocculation of polydisperse microsized latex particles with embedded Fe_2O_3 was accomplished by Tsouris and Scott, who monitored the changes with in-situ DLS measurements.[10] Other researchers detected chain-like clusters in oleic acid coated magnetite fluids in dilute solution conditions utilizing cross magnetic fields.[125] One goal of our work is to create complexes that can be weakly flocculated under applied magnetic fields, and then can be re-dispersed with mild agitation due to steric interparticle repulsion caused by the adsorbed block copolymer stabilizers. The block copolymer stabilizer may be designed to allow reversible flocculation through the introduction of hydrophobic character, from propylene oxide units. Since flocculation in a magnetic field improves particle transport, through increased particle sizes, the capacity for controlling aggregation together with improving magnetophoretic mobility is achievable. However, aggregation and coagulation to form large particle clusters in-vivo is undesirable since large aggregates could obstruct small blood vessels, possibly resulting in death. The superparamagnetism and steric

stabilization of the nanoparticles ensured that no large scale aggregation or coagulation of the particles would occur during and after treatment of a patient with a magnetic field.

DLVO theory allows an analysis of potential contributions to the stability of colloidal particles. This theory may be extended to include magnetic interactions, which are necessary to create a secondary minimum in the potential versus interparticle separation curves. Controlling the depth of the secondary minimum ensures magnetically induced flocculation. The depth is tunable via changes in molecular weight, compositions, and molecular structure which affect the steric repulsive potential relative to attractive van der Waals and magnetic forces.

In the present work, we have studied the influence of copolyether stabilizer architecture and composition on the colloidal and solid-state properties of well-defined, narrow size dispersity magnetite nanoparticle complexes both in the presence and absence of magnetic field. Magnetite nanoparticles were coated with triblock or pentablock copolymers containing poly(ethylene oxide) (PEO) or poly(ethylene oxide-*b*-propylene oxide) (PEO-*b*-PPO) end-blocks, allowing the complexes to be dispersed in PBS buffer solution. The selected PEO or PEO-*b*-PPO was utilized because of their biocompatibility in aqueous suspensions and the ability to vary hydrophilicity/hydrophobicity. The complexes were studied with a number of solution and solid state techniques. Also, the interparticle potentials were modeled including the magnetic, van der Waals, steric and electrostatic potentials using extended DLVO theory of colloidal stability, allowing a prediction of the effects of magnetic field strength, graft density and molecular weight. The effect of polymer composition and magnetic field on both the observed stability and the calculated interparticle energy of

interaction will be discussed.

4.2 Experimental

4.2.1 Materials

Tetrahydrofuran (THF, EMD Chemicals, 99.5%) was refluxed over sodium with benzophenone until the solution was deep purple and then fractionally distilled just prior to use. Potassium (98%), benzyl alcohol (BzOH, anhydrous, 99.8%), ethylene oxide (EO, 99.5%), and propylene oxide (PO, $\geq$ 99%) were purchased from Aldrich. Naphthalene (Aldrich, 99%) was sublimed prior to use. Potassium naphthalene solution in THF was made by the method of Scott et al. with a concentration of 0.92 mol L^{-1}.[132] Glacial acetic acid (Aldrich) was diluted to a 2.5 M solution in THF. N,N-Dimethylformamide (DMF, EMD Chemicals) was dried over CaH_2, fractionally vacuum distilled and stored under nitrogen at 25 °C. The benzyl alcohol initiated poly(ethylene oxide-b-propylene oxide) (BzO-PEO-b-PPO-OH) oligomer was dried overnight at 60 °C under reduced pressure prior to incorporation into the polyurethane block copolymer. Jeffamine™ M-2070, an EO/PO oligomer with a methoxy group on one end and an amine group on the other end (CH_3O-EO/PO-NH_2) was obtained from Huntsman Chemical Co. and dried at 60 °C under reduced pressure prior to incorporation into the polyurethane block copolymer. Isophorone diisocyanate (IPDI, Aldrich, 99.5%) was dried over CaH_2, fractionally distilled and stored under nitrogen. Bis(hydroxymethyl)propionic acid (BHMPA, Aldrich 98%) was dried under vacuum at 60 °C for 24 h prior to use. Dibutyltin dilaurate (DBTL, Aldrich 95%) catalyst was diluted to 10 mg mL^{-1} in THF. Palladium, 10 wt % on activated carbon, wet, Degussa

type E101 NE/W (Aldrich) was used as received.   A high-pressure Series 4561, 300-mL Parr

reactor was utilized for the anionic polymerization of BzO-PEO-*b*-PPO-OH as well as for the

hydrogenolysis of the benzyl ether end groups on the polyurethane copolymer. Phosphate-

buffered saline (PBS), 1X solutioin without calcium and magnesium was purchased from

Cellgro™ Mediatech, Inc.

4.2.2 Synthesis of Triblock Copolymer Dispersants (HO-EO/PO-urethane-EO/PO-OH)
Comprised of a Central Polyurethane Segment Containing Pendent Carboxylate
Groups

4.2.2.1 Synthesis of Benzyl Alcohol Initiated Poly(ethylene oxide-*b*-propylene oxide)
(BzO-PEO-*b*-PPO-OH) Copolymer

A BzO-PEO-*b*-PPO-OH oligomer (37/63 wt/wt % EO/PO) was prepared with benzyl

alcohol as the initiator.   EO (10.0 g, 0.227 mol) was distilled from a lecture bottle into the

Parr pressure reactor that was cooled with an isopropanol-dry ice bath.   THF (100 mL) was

added to the reactor via syringe.   An initiator solution consisting of benzyl alcohol (1.08 g,

10.0 mmol, the amount of initiator was calculated to target an oligomer with M_n = 2700 g

mol^{-1}), THF (10 mL), and potassium naphthalene (10.9 mL of a 0.92 M solution, 10.0 mmol)

was prepared in a 100-mL round-bottomed flask.   The initiator solution was added to the

stirring reaction mixture via syringe.   The cooling bath was removed and the reactor was

allowed to warm to room temperature.   The polymerization reaction was stirred overnight at

room temperature, then purged with nitrogen for one hour to remove any residual EO.   Then,

PO (17.0 g, 0.294 mol) was added to the reactor via syringe, followed by 100 mL of THF.

The polymerization mixture was heated to 60 °C and stirred for 72 h.   The reactor was

cooled to room temperature and purged with nitrogen for one hour.   Acetic acid (10.0 mL of

a 2.5 M solution in THF, 25 mmol) was added to terminate the reaction while it remained

under an inert nitrogen atmosphere.   The reactor was then opened and its contents were

transferred to a 250-mL roundbottom flask.   The solvent was removed under vacuum at

room temperature, and the product was dissolved in 200 mL of dichloromethane.   The

product was washed twice with 100 mL each of deionized water.   The solution was

concentrated under vacuum at room temperature and precipitated in cold hexane to yield 27 g

of polymer.   Characterization via ^{1}H NMR showed a M_n of 2670 g mol^{-1} and 37/63 wt/wt %

EO/PO. ^{1}H NMR (CDCl$_3$): 7.31 ppm (phenyl protons, 5H), 4.54 ppm (Ph$\underline{CH_2}$-O, 2H),

3.34-3.64 ppm (-CH$_2$- and –CH- on the PEO and PPO blocks), 1.09 ppm (-CH$_3$ on the PPO

block).

4.2.2.2   Synthesis   of   a   Pentablock   Copolymer

(BzO-PEO-*b*-PPO-urethane-PPO-*b*-PEO-OBz) Comprised of a Central Polyurethane

Segment Containing Pendent Carboxylic Acid Groups, Flanked on Each Side by the

BzO-PEO-b-PPO Copolymer

A polyurethane copolymer dispersion stabilizer with an average of three carboxylic acid

groups in the central segment and 2670 g mol^{-1} BzO-PEO-*b*-PPO-OH tail blocks was

synthesized via a similar method to that previously described.[133]   The first reaction step

involved capping the monofunctional BzO-PEO-*b*-PPO-OH with IPDI.   The dried

BzO-PEO-*b*-PPO-OH (4.95 g, 1.85 mmol) was transferred to a flame-dried, three-neck,

250-mL, roundbottom flask equipped with a magnetic stirrer and purged with nitrogen. IPDI (0.82 g, 3.7 mmol) was syringed into the flask, and then the flask was placed in an oil bath maintained at 70 °C under nitrogen. The DBTL catalyst solution (0.05 mL, 0.5 mg DBTL) was added to the reaction flask via syringe. The melt reaction was monitored by Fourier transform infrared spectroscopy (FTIR) by observing the decrease of the isocyanate absorption peak at 2260 cm^{-1}. Once the BzO-PEO-*b*-PPO-OH was predominantly capped with the diisocyanate, BHMPA (0.37 g, 2.78 mmol) dissolved in DMF (10 mL) and another increment of DBTL catalyst solution (0.05 mL, 0.5 mg DBTL) was added to chain extend the block copolymer. The reaction was continued until the disappearance of the isocyanate peak was confirmed via FTIR. DMF was removed under reduced pressure at 50 °C. The polymer was dissolved in 200 mL dichloromethane, and the dichloromethane solution was washed twice with 100 mL each of water. The copolymer was precipitated into an excess of cold hexane yielding 5.5 g of polymer. ^{1}H NMR (CDCl$_3$): 7.31 ppm (phenyl protons, 10H), 4.54 ppm (PhCH$_2$-O, 4H), 3.34-3.64 ppm (-CH$_2$- and –CH- on the PEO and PPO blocks), 1.09 ppm (-CH$_3$ on the PPO block).

4.2.2.3   Deprotection   of   the   Benzyl   Endgroups   of   the   Pentablock BzO-PEO-*b*-PPO-urethane-PPO-*b*-PEO-OBz Copolymer

BzO-PEO-*b*-PPO-urethane-PPO-*b*-PEO-OBz (9.2 g, ~2.8 meq benzyl), 30 mL of THF, and 0.3 g of catalyst (Palladium, 10 wt % on activated carbon) were charged into the Parr pressure reactor. The reactor was filled with 40 psi of hydrogen pressure, then the hydrogen was allowed to bubble out of the system at ambient pressure (3x). The reactor was

pressurized to 65 psi with hydrogen and the reaction mixture was stirred at room temperature overnight. The reaction solution was then filtered through Celite 521. THF was removed under vacuum at room temperature yielding 8 g of hydroxyl terminated pentablock copolymer. ^{1}H NMR (CDCl$_3$): 3.34-3.64 ppm (-CH$_2$- and –CH- on the PEO and PPO blocks), 1.09 ppm (-CH$_3$ on the PPO block).

4.2.3 Synthesis of primary magnetite nanoparticles using benzyl alcohol

Magnetite nanoparticle complexes were synthesized via a method similar to that previously described by Pinna et al.[42] Iron (III) acetylacetonate (2.12 g, 6mmol) and deoxygenated benzyl alcohol (40 mL) were combined in a 250 mL 3- neck round bottom flask equipped with condenser and mechanical stirrer. The reaction mixture was heated to 200 ^{o}C at the heating rate of 4-5 ^{o}C/min and kept at that temperature for 4 hours under the N$_2$. During this process, the initial dark-red color of the solution gradually changed to black. The solution was then cooled down to room temperature, and centrifuged to collect the particles. The particles were washed 3 times with acetone (3 x 20 mL) and redispersed in 30 mL chloroform that contained 0.05 mL oleic acid to obtain colloidal stability. Chloroform was then evaporated and the dried particles were washed with acetone to remove the excess oleic acid and completely fried in vacuum at room temperature. The final products were fine black magnetite powder. The monodisperse Fe$_3$O$_4$ nanoparticles are coated with a layer of benzyl alcohol and very small amount oleic acid and are soluble in hexane and chloroform and other nonpolar or weakly polar organic solvents.

4.2.4 Synthesis of magnetite-copolymer complexes

To modify the surface of the Fe_3O_4 nanoparticles, 167 mg triblock copolymer and 50 mg magnetite power were redispersed in 10 mL chloroform and mixed together. The mixture was sonicated at 90W (VWR^{TM} 75T model) for 2 h and stirred at room temperature for 2 d, which was chosen to allow complete ligand exchange of carboxylic acid of polymers with benzyl alcohol or oleic acid on the magnetite surface. Then the mixture in chloroform was precipitated in hexanes (3:1 v/v, hexanes/$CHCl_3$) twice to remove excess polymer and benzyl alcohol or oleic acid ligands. A magnet was used to collect the precipitates and the particles were dried in vacuum at room temperature. The final black powders are readily dispersed in H_2O or PBS (137 mM NaCl, 2.7 mM KCl, and 10 mM Na_2HPO_4/KH_2PO_4, pH =7.4) with sonication.

4.2.5 Characterization

^{1}H NMR spectra were acquired on a Varian Unity 400 NMR spectrometer operating at 400 MHz, respectively.

Titrations to determine the concentration of carboxylic acids in the triblock polymers were conducted by dissolving the polymer (0.5 g) in 95 v/v % ethanol (25 mL), and titrating with 0.1 N KOH using phenolphthalein as an indicator. Each sample was titrated in triplicate and the reported data are the average of the titrated values.

Dynamic light scattering (DLS) measurements were conducted with a Malvern ALV/CGS-3 compact multi-angle light scattering spectrometer (Malvern Instruments Ltd, Malvern, UK) at a wavelength of 632.8 nm from a 22 mW, solid-state He-Ne laser at a scattering angle of 90° at 25 ± 0.3 °C. The temperature of the samples was equilibrated for

at least 10 min before the measurements were taken. Typically, 10 measurements of 30 seconds were acquired for each sample. The CGS-3 uses 1st to 3rd order cumulant fitting, with optional weighting and 17 forms of regularized fits for non-linear fitting. Flocculation experiments were carried out using Proterion DynaPro MS800 operated at 827 nm and at a scattering angle of 90°. The Dynapro data processing was performed with Wyatt[TM] DYNAMICS software. The hydrodynamic radii and the size distributions were calculated with the regularization algorithm provided by this software. Intensity-averaged size distributions were converted to volume-averaged size distributions. Quoted values of R_h are volume averages and are the averages of at least four measurements. Samples were sonicated for 5 min and then filtered through a 0.2 μm Teflon filter prior to the measurements.

Magnetite dispersion quality was investigated with a Philips 420T transmission electron microscope (TEM) and a JEOL 3000F field emission gun transmission electron microscope operating at 100 and 300 kV, respectively. Aqueous dispersions of the polymer-magnetite nanoparticle complexes were deposited on carbon-coated copper grids and allowed to air-dry.

Solid-state magnetic moments were recorded using a 7 Tesla Quantum Design MPMS SQUID magnetometer. Magnetization of magnetite and magnetite-copolymer complexes were measured from -70 to 70 kOe at 300 K. Magnetic properties of the polymer-coated magnetite nanoparticles were also measured in the solid state at room temperature using a Standard 7300 Series Lakeshore vibrating sample magnetometer (VSM). The magnetization of each complex was measured at room temperature over a range of applied fields from -8000 to +8000 Oe with a sensitivity of 0.1 emu.

X-ray photoelectron spectroscopy was carried out with a Perkin-Elmer model 5400 instrument fitted with a Mg K_α X-ray source (1253.8 eV) at a takeoff angle of 45°. The anode was operated at 250 W.

Thermogravimetric analysis was carried out on the magnetite nanoparticles, the copolymer dispersants, and the magnetite-polymer complexes using a TA Instruments TGA Q500. A temperature ramp rate of 10 $^\circ$C min^{-1} was used under nitrogen. The samples were dried in a vacuum dried at 80 $^\circ$C overnight prior to analysis.

Stabilities of the dispersions were evaluated by visual inspection.

4.2.6 Controlled Flocculation of Magnetite-copolymer Complexes with Weak, Uniform Magnetic Fields

Magnetic field induced flocculation was carried out in a DC Solenoid (Walker LDJ Scientific) which was equipped with a recirculating chiller and power supply control PSC-4. The mapping of the magnetic field was performed with an MG-10D gaussmeter (Walker LDJ Scientific) showing the maximum field strength was 1500 Gauss. Samples were prepared according to procedures described for DLS. The samples were first measured with DLS, and then introduced to the magnetic field for a specific time interval, following by subsequent measurement in DLS (< 5 min) and reintroduction to the magnetic field. The flocculation results are reported in terms of cumulative exposure time to the magnetic field. DLS measurements outside of the magnetic field over ~ 5 min spans revealed that flocculation did not occur outside of the magnetic field.

4.3 Results and Discussions

A primary objective of our work is to synthesize magnetite nanoparticle dispersions which are stable in aqueous buffer systems that mimic biological fluids. Once biologically stable magnetic nanoparticle dispersions are developed, numerous biological applications of these systems may be pursued. These include the use of magnetic nanoparticles for protein separation, drug delivery applications and magnetic heating of biological fluids, also called magnetic hyperthermia. Thus, it is critical to characterize nanoparticle stability in buffered aqueous solutions. Biological media contain dissolved salts, which classically pose challenges for stabilizing colloidal dispersions due to the screening of electrostatic interparticle repulsive forces. Steric repulsion between polymeric stabilizers anchored on the nanoparticle surfaces is an attractive mechanism for maintaining dispersion through increasing repulsive forces.

In order for these nanoparticle dispersions to be directed to specific locations in the body, external gradient magnetic fields must be employed. The ability to externally direct the nanoparticle fluids increases with the force applied from an external magnetic field, which increases with nanoparticle size and magnetic moment. However, passage through tissue, once the particles reach the desired destination, is improved for decreased nanoparticle size. Thus, a mechanism for creating reversible flocculation is desirable. With the application of an external magnetic field, the nanoparticles would temporarily aggregate and the magnetic moments would align. This would lead to increased magnetic force on the aggregate compared to the smaller individual particles and increased ability to direct the particles.

To achieve reversible flocculation, the stability of the nanoparticles in aqueous buffers

must be tuned to respond to the weak attractive forces that exist in the presence of a magnetic field. In order to tune the stability, we turned to altering the hydrophilic/hydrophobic balance of the copolymer dispersants adsorbed on magnetite nanoparticles. The incorporation of PPO into the polyether tail-blocks increases the hydrophobicity of the tail-blocks and increases the potential for the polymers to flocculate given additional stimulus from an external magnetic field. Thus, we have studied a series of copolymer dispersants containing both pure PEO tail-blocks as well as PEO-PPO block polyether tail-blocks.

This paper addresses the synthesis and characterization of a series of nanoparticle-copolymer complexes, and analyses of their dispersions in water, both experimentally and utilizing DLVO theory. The block copolymer dispersants possessed either PEO homopolymer or PEO/PPO copolyether outer blocks, and each contained a polyurethane center block with carboxylate anchor groups for binding to the surface of the magnetite. Our vision of these magnetite-copolymer complexes is that they comprise a magnetite core, a copolymer collapsed inner layer, and an extended PEO brush layer. The collapsed polymer inner layer that surrounds the magnetite sphere comprises the polyurethane anchor block.   In the case of the PPO-*b*-PEO block copolymer tail, this inner layer likely also contains the PPO segment due to its hydrophobic nature.

4.3.1 Synthesis of Primary Magnetite Nanoparticles

The nanoparticles were synthesized using a high temperature thermolysis of organometallic precursors. In contrast to traditional aqueous coprecipitation methods, the high temperature thermolysis offers a facile method for the synthesis of nanoparticles with

very narrow size and shape distributions. Additionally, these synthesis methods eliminate the formation of aggregates of magnetite nanoparticles, which are frequently present in significant quantities in magnetite nanoparticles synthesized using aqueous coprecipitation methods. The high temperature thermolysis methods also allow the incorporation of other metals such as platinum into mixed metal nanoparticles.
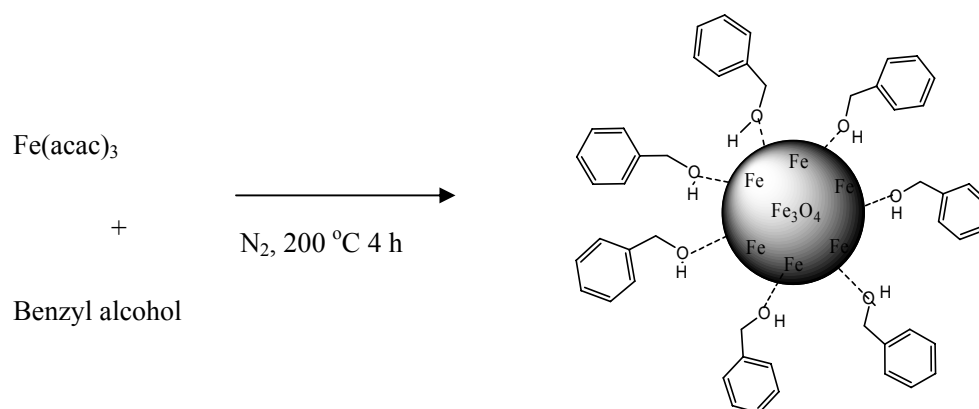
Figure 4.1 Synthesis of magnetite nanoparticles containing benzyl alcohol stabilizing ligands.

Early high-temperature thermolysis methods developed by Sun et al. required the use of carboxylic acid containing ligands such as oleic acid and oleylamine.[1] The presence of these ligands resulted in solubility of the complexes in organic solvents such as hexane and chloroform and insolubility in water or biological buffers. Solubility in water can be achieved through the exchange of the carboxylic acid-containing hydrophobic ligands with quaternary ammonium salt containing ligands. However, these ligands offer only electrostatic interparticle repulsion without steric repulsion. Initially, we began the synthesis of magnetite nanoparticles using this synthetic method.   In our case, we utilized centrally functionalized carboxylic acid containing triblock and pentablock copolymers possessing polyether

tailblocks. In order to form complexes that are water soluble and possessed steric repulsion, the oleic acid ligands must be exchanged with these polymeric block copolymer stabilizers. In our experience, it has proven difficult to obtain complete displacement of the oleic acid ligands with polymeric ligands. This is likely due to the fact that the oleic acid ligands produce a hydrophobic surface which prevents the approach of the polymeric stabilizer. Thus, magnetite nanoparticle complexes synthesized using Sun's high temperature thermolysis method displayed instability in aqueous media.

Recently, high temperature thermolysis methods developed by Pinna et al. have utilized less-strongly coordinating ligands such as benzyl alcohol (Figure 4.1).[42] These methods also yield well-defined particles with narrow size distributions. The nanoparticles synthesized using this method are soluble in organic solvents such as chloroform and hexane and also lack significant quantities of nanoparticle aggregates. The purification methods for these nanoparticles involved first precipitating them in ethanol, which removes excess ligand and secondly redispersing them in hexane and centrifuging to remove any aggregates present. Most importantly, the benzyl alcohol ligands on these nanoparticles are easily displaced by stronger carboxylic acid containing ligands such as the block copolymer stabilizers described in this work.

4.3.2 Synthesis of Magnetite Nanoparticle-Copolymer Complexes

In our experimental efforts, we strive to achieve well-defined nanoparticles and discrete dispersions. The nanoparticles were coated with a triblock copolymer dispersant containing carboxylate "anchor" groups in the central polyurethane block (Figure 4.2). In order to

achieve well-defined nanoparticle dispersions, we have developed an effective method for attachment of the block copolymers. The primary magnetite nanoparticles were coated with carboxylic acid centrally functionalized triblock and pentablock copolymers by sonicating the nanoparticles and copolymers in a common solvent, chloroform for 4 h followed by stirring for 48 h. Sonication has proven an integral step in ligand exchange, in order to input the energy needed to displace existing surface ligands. The attachment of the copolymer dispersants to the magnetite nanoparticles leads to significant solubility changes for the nanoparticles. After functionalization, the particles are precipitated in hexane, which would dissolve any displaced benzyl alcohol or oleic acid ligands. Furthermore, the hexane should remove any potentially unfunctionalized nanoparticles, which were not observed by visual inspection. The precipitation was followed by centrifugation and collection of the magnetite nanoparticles using a magnet. The collected nanoparticle complexes were then re-dispersed in chloroform and precipitated a second time in hexane. The nanoparticle complexes were then dried with nitrogen to remove chloroform and hexane. The nanoparticle complexes were finally dispersed in PBS buffer solution with sonication for 2 h.
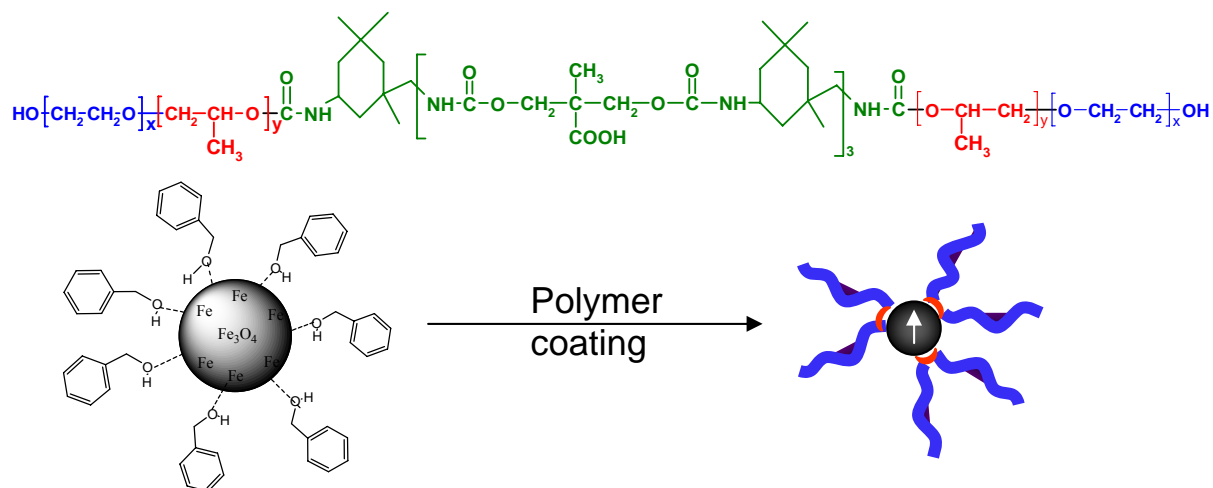
Figure 4.2 Coating of magnetite nanoparticles with block copolymer stabilizers to form aqueous soluble complexes from organic soluble precursors.

A series of polymeric dispersants possessing differing PEO or PEO-*b*-PPO polyether tailblocks were utilized to stabilize the nanoparticle complexes (Table 4.1). The differing polyether tailblock composition was integral to controlling the stability of the complexes in aqueous media. The introduction of PPO to the polyether tailblocks led to the development of greater hydrophobic character which decreased the stability of the complex in aqueous media. A second important parameter of study was the polyether tailblock molecular weight, which affected the interparticle steric repulsion. Higher polyether tailblock molecular weight would prevent close approach of the magnetite nanoparticles, leading to lower potential magnetic interaction since magnetic attractions scale as a function of interparticle distance. Thus, the molecular weight of the tailblock was a critical factor to design of complexes.

Table 4.1 Chemical composition of the copolymer dispersion stabilizers.

Polymeric Stabilizer	Total tail Mn $(g \ mol^{-1})$	EO-PO Mn $(g \ mol^{-1})$[1]	Tail Mw/Mn	Ave # of COOH/chain[2]	Ave # Repeat Units of EO/PO
2700EO	2700	2700-0	1.05	3.0	61/0
5300EO	5300	5300-0	1.05	3.1	120/0
1500EO-500PO	2000	1500	1.09	3.1	34/9
3300EO-900PO	4200	3300	1.07	3.0	75/15

[1] Derived from ^{1}H NMR in $CDCl_3$

[2] Derived from titration of the carboxylic acid groups

4.3.3 Characterization of Magnetite Nanoparticle Copolymer Complexes

Magnetite-copolymer complexes were prepared with compositions targeting 30 weight percent of magnetite. These complexes were analyzed using thermogravimetric analysis (TGA) in order to determine the actual polymer content of the samples. TGA results indicated a slightly higher magnetite content, close to 40-45 wt%, suggesting the successful removal of the uncoated free polymer during the purification steps. TGA analyses of the pure copolymers and bare magnetite revealed 100 wt% loss in the case of the polymer. Thus, the polymers completely pyrolyzed during the experiments and negligible weight loss was observed for pure magnetite (Figure 4.3).
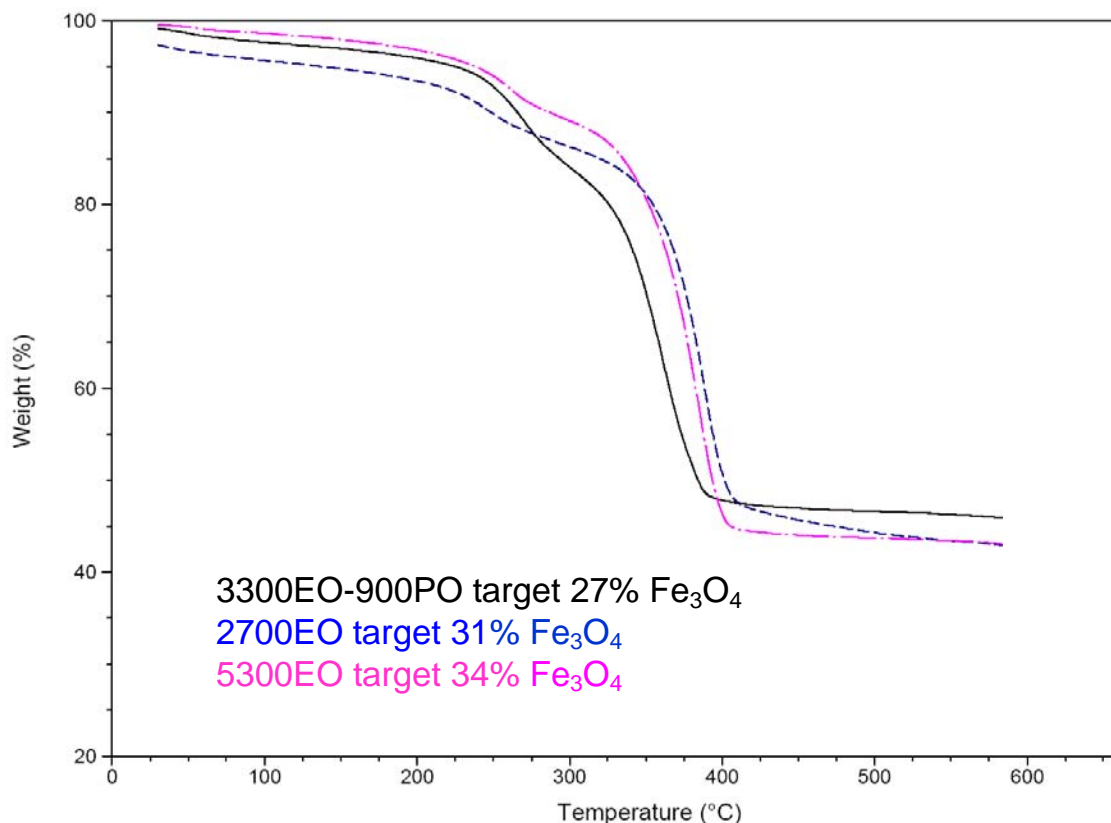
Figure 4.3 Thermogravimetric analysis of magnetite nanoparticle complexes, for determining the weight fraction of polymer present.

The graft densities of the polymers on the nanoparticle surfaces were calculated from the compositional and surface area data (Equation 4.1).

$$\Gamma = 2\left(\frac{m_{poly}}{m_{Fe_3O_4}}\right)\frac{N_A}{M_n A_{sp}}$$ 4.1

In equation 4.1, Γ is the graft density expressed as the number of tail chains nm^{-2} (two tail chains per polymer), m_{poly}/m_{Fe3O4} is the mass ratio of polymer to magnetite, M_n is the number average molecular weight of the block copolymer, and N_A is Avogadro's number. The number of carboxylate groups available for adsorption per square nanometer of the nanoparticle surfaces was also calculated as $3\Gamma/2$ since there were an average of three carboxylate groups per triblock copolymer and two chains extending from the surface per

108

molecule.   The nomenclature adopted herein for the complexes is the composition of the polyether tail (e.g. 1500EO-500PO).

Table 4.2 Compositional data of the copolymer-magnetite complexes

Complexes	Magnetite wt%[1]	Γ (chain/nm^2)	f (chain/particle)
2700EO	46	2.2	710
5300EO	42	1.5	460
1500EO-500PO	45	3.0	930
3300EO-900PO	47	1.5	470

[1] Thermogravimetric analysis conditions: 30 - 700 ^{o}C, 10 ^{o}C min^{-1}, N$_2$

Transmission electron micrographs of the nanoparticle complexes revealed that the magnetic nanoparticles synthesized using the benzyl alcohol method formed discrete complexes when coated with carboxylic acid functionalized block copolymers as shown in Figure 4.4. Size distribution data was collected from the TEM micrograph of these particles which is shown in Figure 4.5.   The peak particle diameter from the fitting was 6.1$\pm$2.3 nm.
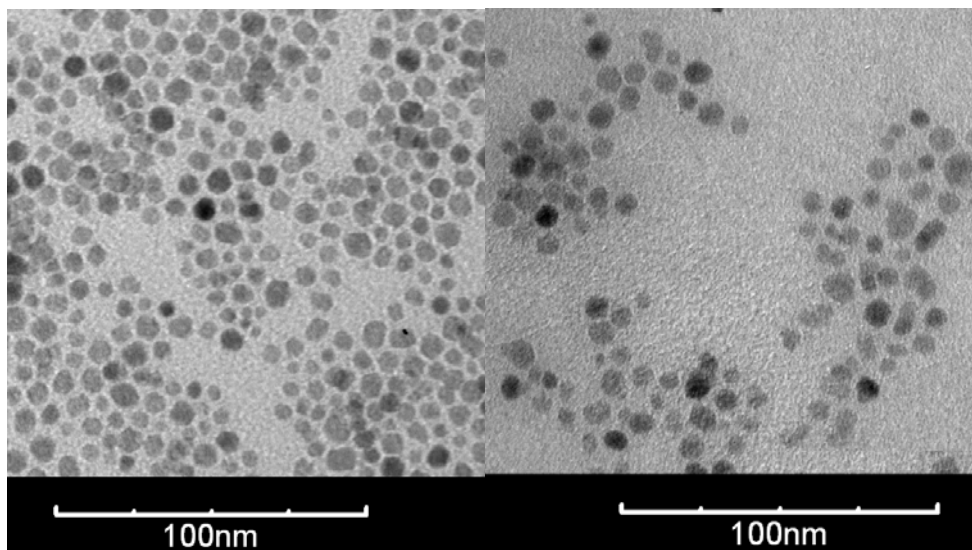
Figure 4.4 TEM micrographs of complexes benzyl alcohol magnetite (left) and 3300EO-900PO complex (right).
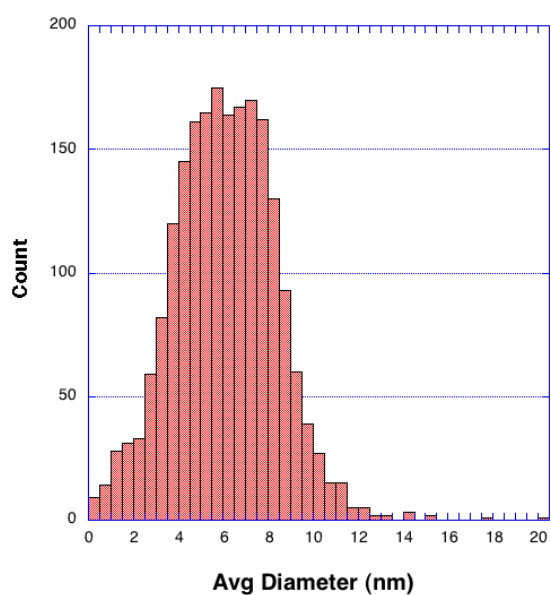
Figure 4.5 Particle size distribution for magnetite nanoparticles synthesized using benzyl alcohol ligands. Mean particle diameter is 6.1 nm with a standard deviation: 2.3 nm.

X-ray photoelectron spectroscopy (XPS) proved a useful technique for characterizing the surface of the magnetite nanoparticle complexes. XPS allows the determination of the elemental composition of the surface, typically to a depth of 3.5 nm at a take-off angle of 45° which was used in the experiments. XPS revealed nearly complete coverage of the surface with the copolymer stabilizers due to low levels of iron detected. The fact that some iron was detected suggested that the polymer layer depth may be less than 3.5 nm. The increased carbon and nitrogen signatures, compared to the precursor magnetite nanoparticles, further supported the hypothesis of polymer coverage.

Table 4.3 XPS Characterization of magnetite nanoparticle complexes.

Element	Atomic Surface Concentration (%)		
	2700EO	300EO-900PO	5300EO
C	82	78	74
O	17	20	23
Fe	0	1	2
N	1	1	1
Cl	0	0	0

Fourier transform infrared spectroscopy (FTIR) also proved useful for confirming the presence of the block copolymer stabilizer on the nanoparticle surfaces. The presence of C-H stretches ($\sim$2900 cm^{-1}), carbonyl stretches ($\sim$1750 cm^{-1}), and C-O stretches ($\sim$1100 cm^{-1})

confirmed the presence of the block copolymer on the surfaces of the magnetite (Figure 4.6).
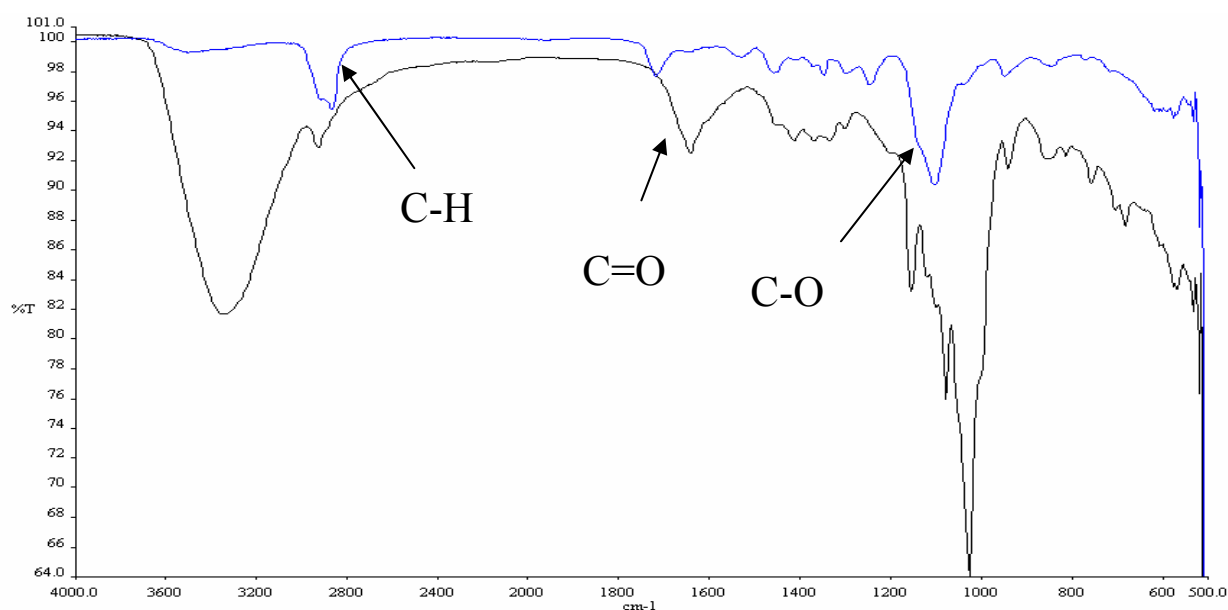
Figure 4.6 Magnetite nanoparticles synthesized using the benzyl alcohol method modified with 3300 EO-900 PO copolymer.

4.3.4 Characterization of the Dispersion Properties of the Magnetic Nanoparticle Complexes

The magnetite nanoparticle complexes were characterized using DLS, in order to study the influence of different solvent conditions and polymeric stabilizers on the colloidal properties. Samples were sonicated for 5 min. DLS measurements were carried out at low concentrations, 0.1-1 mg mL^{-1}, to avoid multiple scattering and the DLS results are shown in Table 4.4. The results indicated that the hydrodynamic radii of the complexes ranged from 16 to 22 nm in pure water and PBS buffer solution. These values are in the range expected given the size of the magnetite core and the thickness of the polymer brush layer, as described in the following sections. A second observation worth noting is that the complexes containing

PEO exhibited similar R_h values compared to complexes containing both PEO and PPO. This indicated that the PPO block did not strongly impact the tendency of the particles to aggregate in aqueous media in the absence of a magnetic field, despite the hydrophobicity and insolubility in water. This was attributed to the fact that the PPO blocks were placed adjacent to the central carboxylic acid functionalized urethane block, and were hidden by the outer PEO blocks which extended into solution. Thus, the PPO blocks formed an inner hydrophobic layer in the particles.

Dynamic light scattering (DLS) measurements on the dispersed Fe_3O_4 nanoparticles indicated that before surface modification, the nanoparticles had an average hydrodynamic diameter of 10.4 nm in hexane (Figure 4.7A) which was slightly larger than the 6.1-nm diameter derived from TEM since particles are solvated and dynamic. After ligand exchange, the average hydrodynamic diameter of the particles in PBS from DLS measurements was 21 nm with 3300EO-900PO (Figure 4.7B), 22 nm with 5300EO (Figure 4.7C) and 18 nm with 2700EO (Figure 4.7D).
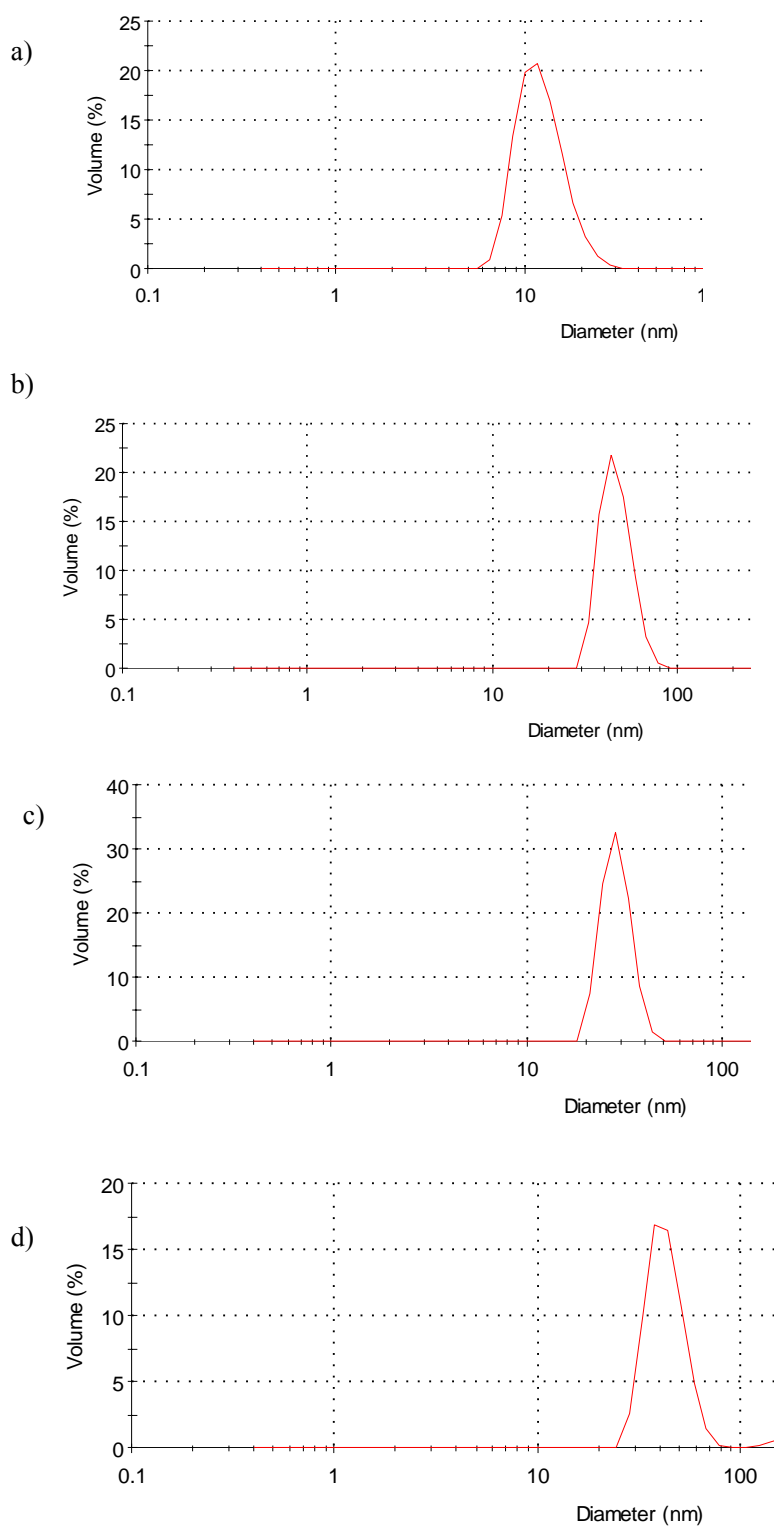
Figure 4.7 DLS of (A) Fe$_3$O$_4$ nanoparticles coated with benzyl alcohol in hexane dispersion R_h = 5.4 nm and (B) nanoparticles coated with 3300EO-900PO in PBS dispersion R_h=21 nm (C) 5300EO in PBS R_h = 22 nm (D) 2700EO in PBS R_h = 18 nm.

Table 4.4 Summary of DLS results for magnetite nanoparticle complexes synthesized using the benzyl alcohol method. Samples were tested shortly after preparation. 0.1-1.0 wt%

Complexes	R_h in water (nm)[1]	R_h in PBS (nm)[1]	R_h in PBS (nm)[2]	R_h in PBS (nm)[3]	Stability in PBS
2700EO	20	18	17	20	Days
5300EO	22	22	20	24	Days
1500EO-500PO	16	14	13	15	<1 d
3300EO-900PO	21	21	20	23	<1 d
1300EO-800PO	15	14	13	16	Hours

[1] Volume averaged

[2] Number averaged

[3] Intensity averaged

Beyond the complex size in solution, a second measure of the tendency of particles to aggregate is the complex stability. In Table 4.4 are listed the typical duration of time that nanoparticle complexes with a concentration of 0.5 mg/ml remained stable in PBS buffer from visual inspection. It is clear that the stability of the PPO containing samples was significantly lower than the pure PEO containing polymers in PBS buffer solutions. This was correlated to the DLS results in PBS buffer only for sample 1100EO-900PO, which exhibited much larger clusters than other PPO containing block copolymer (R_h = 38 nm in PBS).

Interestingly, this sample also possessed the highest weight fraction of PPO in the tailblocks of the copolymer stabilizer. In terms of stability in solution, the other PPO containing samples also began to visibly flocculate before any of the pure PEO tailblock complexes. The block polyether complexes, 1500EO-500PO, 1300EO-800PO and 1100EO-900PO with the same total tail blocks molecular weight followed a trend of decreasing stability with increasing PO content. In comparing 1500EO-500PO and 3300EO-900PO, both complexes had the same weight ratio of EO to PO but the higher overall molecular weight of the 3300EO-900PO sample resulted in greater stability due to increased steric repulsive interactions. Interestingly, the 3300EO-900PO complex via DLS showed stability of only three hours in PBS.

4.3.5 Prediction of the Magnetite-copolymer Nanoparticle Complex Dimensions Using the Core-shell-shell Model

The density distribution (DD) model was utilized to calculate the particle dimensions which were compared to the particle size measured using DLS. The sizes were predicted with a core-shell-shell (double shell) model (Figure 4.8) to estimate the inner polymer and brush layer thicknesses (Eq. 4-6) on the magnetite, with the measured magnetite core radius of 5 nm (Table 4.5). The DD model accounts for particle curvature by dividing the polymer domain into concentric shells and assuming a constant number of blobs equal to the number of adsorbed chains in each sub-layer. This model describes the blob size and segment volume fraction as a continuous function of distance from the surface and accounts for both excluded volume interactions between chains and brush extension in systems where the radius of curvature is comparable to the brush thickness.
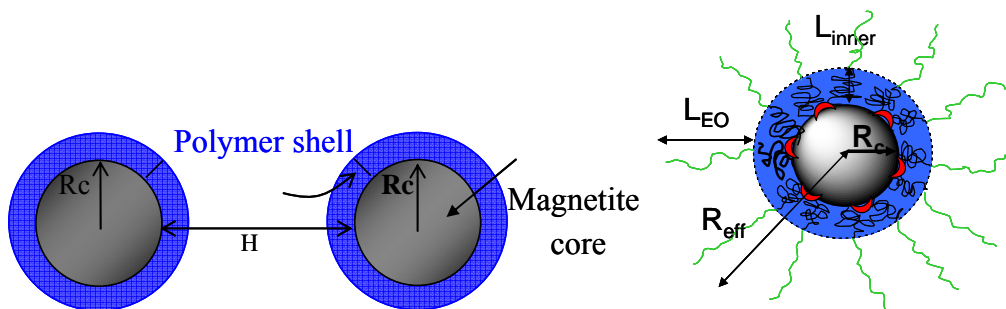
Figure 4.8 Schematic of two stabilized nanoparticles. The radius of the magnetite core utilized in the model was R_c = 5 nm derived from DLS R_h of bare magnetite, the core surface-to-surface distance is H, and the polymer layer thickness is $L = L_{inner} + L_{EO}$.

For nanoparticles coated with copolymers having PPO-*b*-PEO sequences with PEO outer blocks, the polymer shell was considered to have a collapsed PPO inner shell because of the hydrophobicity of PPO and its insolubility in water. The PPO layer thickness calculations were made assuming the PPO was densely packed as in the theta state. We also accounted for the urethane anchor segment as part of the PPO layer since it binds on the surface of the magnetite. The outer PEO shell should extend well in water as brushes to stabilize the particles. For nanoparticles coated with copolymer containing PEO tails, it was assumed that the tails were comprised of only EO units, so the expression for the PPO shell thickness, L_{PO}, was zero while the urethane anchor block still led to a nonzero shell thickness. The graft densities used in these equations were obtained from the amounts of copolymer in the complexes derived from TGA, the molecular weights of the copolymers, and the nanoparticle surface area calculated from the R_h of bare magnetite particles in hexane. It was assumed that not all of the carboxylate groups were bound to the magnetite surface due to the steric limit of approximately five carboxylates per square nanometer.

In order to determine whether all of the PEO extended as brushes into solution, the volume fraction of statistical segments making up the PEO brush is calculated by:

$$\phi(r) = C(r/l)^{1/\nu}(l/r)^3 \qquad 4.2$$

where r is the radius from the center of the particle, ν is the Flory exponent (0.583 for PEO in water),[136] l is the statistical segment length of the corona chain (0.6 nm for PEO)[139]), and C is a coefficient defined by:[100]

$$C = 3 * 4^{1/\nu} f^{(3\nu-1)/2\nu}/32\pi \qquad 4.3$$

In equation 4.3, f is graft density on the magnetite, the number of tail chains per particle. To account for the inner polymer layer, we assume that the anchor block, PPO/urethane form a dense, collapsed layer with thickness L_{inner} described by:

$$L_{inner} = \left(\frac{3\sigma R_c^2 M_{shell}}{2\pi\rho_{shell}} + R_c^3 \right)^{1/3} - R_c \qquad 4.4$$

The PEO statistical segment volume fraction as calculated in equation 4.2 at the edge of the inner layer (at $r = R_c + L_{inner}$) was equal to or less than one, indicating that all the PEO chains extended and formed the brushes to provide stabilization of the particles. The thickness of the PEO brush, L_{EO}, was then calculated from

$$L_{EO} = \left[N_{EO} l^{1/\nu} \frac{8 f^{(1-\nu)/2\nu}}{3\nu 4^{1/\nu}} + (R_c + L_{inner})^{1/\nu} \right]^\nu - (R_c + L_{inner}) \qquad 4.5$$

The effective radius (R_{eff}) was calculated as the sum of the magnetite core, the PPO/urethane, and the PEO shell thickness

$$R_{eff} = R_c + L_{inner} + L_{EO} \qquad 4.6$$

R_g is the radius of gyration of the magnetite-polymer complex. L_{inner} is defined as the sum of thicknesses of polymer layers from the urethane anchor block and the poly(propylene

oxide) blocks. We calculated R_g using

$$\langle R_g{}^2 \rangle = \int_0^\infty n(r)r^4 dr \Big/ \int_0^\infty n(r)r^2 dr \qquad 4.7$$

where n(r) is defined in terms of the refractive indices of the core (n_c), inner layer (n_s), and

solvent (n_o) and is given by

$$n(r) = n_c - n_o \qquad\qquad r < R_c$$

$$n(r) = n_{inner} - n_o \qquad\qquad R_c < r < (R_c + L_{inner})$$

$$n(r) = (n_s - n_o)C(l/r)^3(r/l)^{1/\nu} \quad (R_c + L_{inner}) < r < R_{eff}$$

$$n(r) = 0 \qquad\qquad\qquad R_{eff} < r. \qquad 4.8$$

The length scale σ has been shown by Likos[97, 98] to be equal to 1.3R_g. It will used

later for the calculations of steric potential.

Table 4.5 Sizes of the magnetite nanoparticle-copolymer complexes at 25 ^{o}C in water (0.1-0.5 wt %) measured by DLS at 90° using the Malvern ALV/CGS-3. The predicted dimensions of the complexes for aqueous dispersions of the magnetite-copolymer complexes are shown in the right-hand columns. R_h from DLS is fairly close to the calculation from the core-shell model.

Complexes	f (chain/particle)	L_{an} (nm)	L_{po} (nm)	L_{inner} (nm)	Φ	L_{EO}[a] (nm)	R_{eff} (nm)	σ (nm)	R_h[b] (nm)
2700EO	710	1.5	0	1.5	1.0	8.9	15.5	9.1	14
5300EO	460	1.1	0	1.1	0.8	13.6	19.6	11.6	18
1500EO-500PO	930	1.9	0.7	2.6	1.0	5.7	13.3	8.0	14
3300EO-900PO	470	1.1	0.7	1.8	0.7	9.2	16.0	9.0	16

[1] L_{EO} refers to the calculated thickness of the PEO extended brush.

[2] Derived from the sum of L_{inner} and L_{EO} along with the 5-nm core radius.

4.3.6 Magnetic Field Induced Flocculation via Solenoid Study on Nanoparticle Copolymer Complexes with DLS

The magnetic flocculation of the 3300EO-900PO complex was studied by exposing the sample to a 1500 Gauss magnetic field within a solenoid and carrying out DLS measurements at regular time intervals. At this magnetic field, the magnetization of the particles is 64 emu/g. Prior to the experiments, the magnetic field inside the solenoid was determined to be uniform in a roughly 5 cm section near the center via magnetic field mapping measurements using a gaussmeter. The hydrodynamic radius of the sample was observed to increase with

exposure to the magnetic field from 20 to 35 nm over a period of 20 min of exposure (Figure 4.9).   As a control, the sample was measured periodically in the absence of a magnetic field, which resulted in a nearly constant hydrodynamic radius ~20 to 24 nm over the course of nearly 3 hours.   Thus, the presence of the magnetic field resulted in increased hydrodynamic radius of the particle, indicating the formation of aggregates of increasing size with time. The ability to aggregate in the presence of a magnetic field is important to biological applications where localization of the particles in the body can be more easily achieved for larger aggregates than for individual particles.

Figure 4.9 DLS measured volume average R_h of the nanoparticles in PBS with and without 1500 Oe magnetic field. Time is the accumulative exposure to the magnetic field.

Analogous magnetic flocculation experiments were conducted on the 3300EO-900PO complex in DI water and compared to reproduced experiments in PBS (Figure 4.10). The application of an external magnetic field (1500 Oe) to the samples in DI water resulted in nearly constant R_h and scattering intensity. Again, in the presence of PBS, the R_h increased from 18 to 32 nm and the scattering intensity increased from 2.2×10^6 cnt/s to 4.4×10^6 cnt/s, due to the formation of larger sized aggregates (scattering intensity is proportional to R_h^6). The ability to magnetically flocculate the complex in PBS buffer was clearly related to the reduced stability in PBS, which was noted earlier. The higher ionic strength of the PBS solution compared to DI water resulted in screening of electrostatic interactions and further may influence the stability of the complex by altering the solution dimensions of the steric stabilizer layer. However, without the magnetic field, the presence of PBS did not cause significant aggregate formation over the course of the experiment (~ 1 h). Thus, the application of an external weak magnetic field was sufficient to induce flocculation with the already lowered stability of the magnetite complexes in PBS. Interestingly, after the particles were exposed in the field for 30 min, with gentle shaking, the intensity dropped from 4.4×10^6 cnt/s to 2.3×10^6 cnt/s, indicating the formation of loose flocculi due to the weak magnetic field. This was a fortuitous result, since PBS mimics the composition of physiological systems, and thus magnetically induced flocculation is predicted to be possible in the body as well.
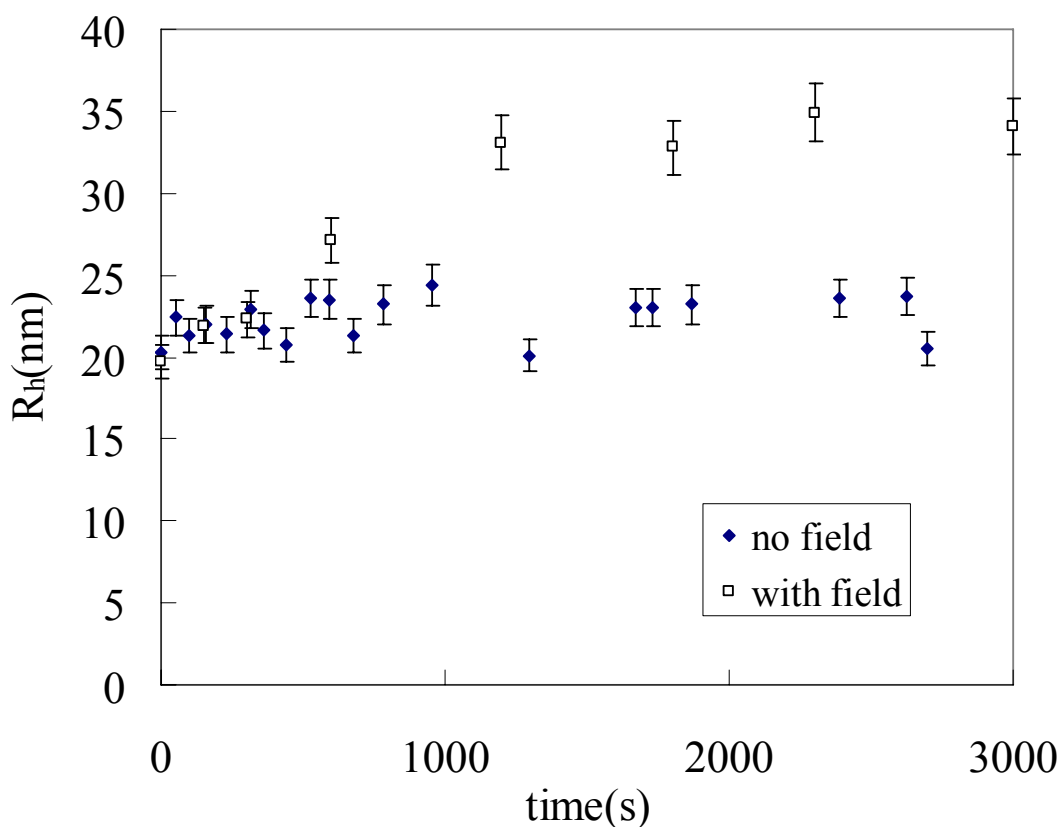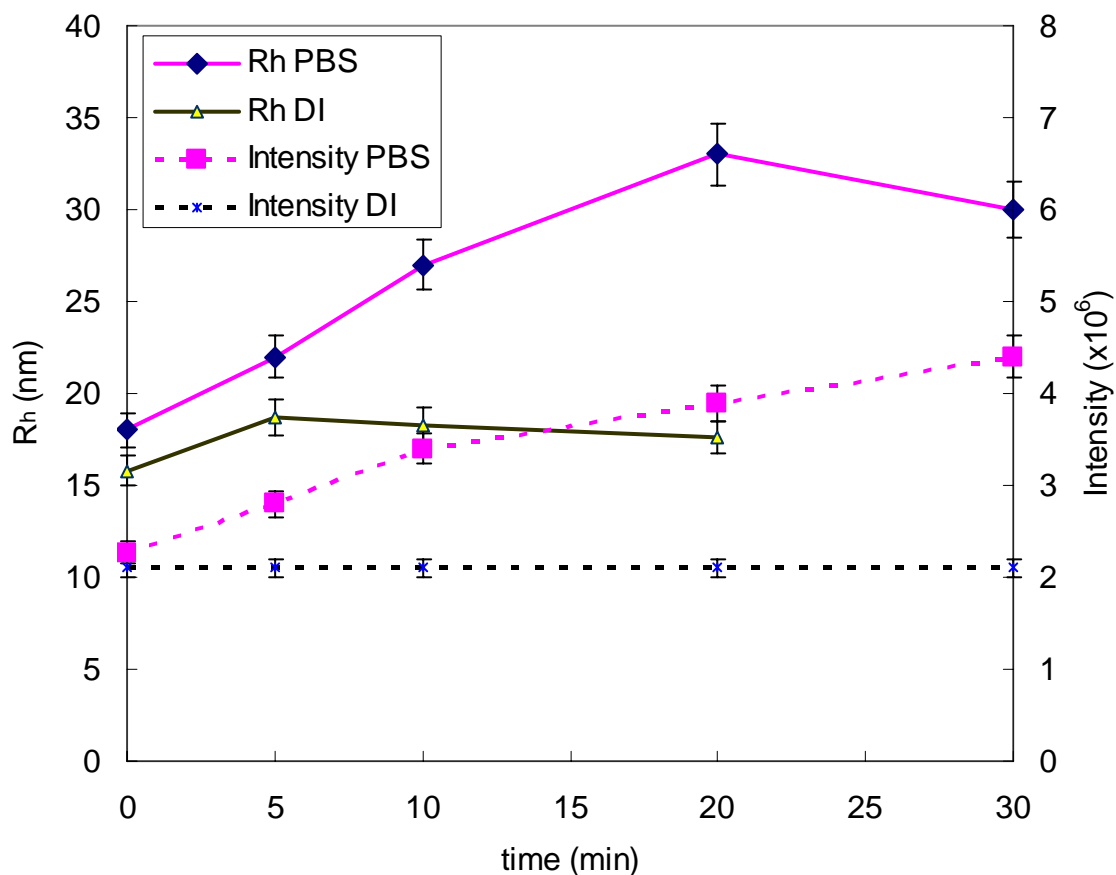
Figure 4.10 DLS measured volume average R_h of the nanoparticles in PBS with and without 1500 Oe magnetic field. Time is the accumulative exposure to the magnetic field.

4.3.7 Modeling Interactions Between Magnetite Nanoparticle-polymer Complexes to Predict Compositions that Could be Actuated with the Application of a Magnetic Field

DLVO theory provides a useful tool for modeling the interparticle potential energies of the magnetite nanoparticle-polymer complexes in aqueous dispersions. The extended DLVO theory has been employed to model the aggregation of micron-size magnetic particles that were stabilized in water with an ionic surfactant.[139] Interparticle potentials including van der Waals (V_a), electrostatic (V_e), steric (V_s), and magnetic (V_m) interactions were combined in the models to predict the total potentials (V_t).[140-142] The van der Waals component was

calculated as a function of the particle core surface-surface separation distance (H), utilizing the magnetite core radius (R_c), and the effective Hamaker constant, A_{eff}, which includes retardation effects (Equation 4.9).[139] Calculation of the effective Hamaker constant is provided in a supplementary note to this paper.

$$V_a = -\frac{1}{6} A_{eff} \left(\frac{2R_c^2}{H(4R_c + H)} + \frac{2R_c^2}{(2R_c + H)^2} + \ln\left(\frac{H(4R_c + H)}{(2R_c + H)^2} \right) \right)$$
  4.9

While more detailed calculations of A_{eff} can take into account the presence of organic layers on the particle surface,[140-142] the present calculations for A_{eff} and V_a are sufficiently accurate due to the dominant effect of the steric potential term and the magnitude of the attractive magnetic interaction.

Electrostatic interactions cause stabilizing, repulsive interparticle forces due to the repulsion of like charges. For aqueous systems, the pair interaction energy due to electrostatic repulsion, V_e, was described with a constant potential expression useful for particle surface potentials ≤ 25 mV ,

$$V_e = 2\pi R_c \varepsilon \varepsilon_o \psi_o^2 \ln(1 + e^{-\kappa H})$$
  4.10

where ε is the dielectric constant of the medium (water), ε_o is the permittivity of free space, and ψ_o is the surface potential. Equation 10 is valid when $\frac{a}{\kappa^{-1}} \gg 1$. The surface potential ψ_o was approximated by measured values of the zeta potential. For bare magnetite, the isoelectric point is near pH 6.8.[143] Previous studies with similar complexes showed zeta potentials in the range of 0 to -1.3 mV and so it was assumed that the zeta potential for the complexes in the present paper were similar. The low zeta potential values of the complexes are consistent with extensive neutralization of the surface charges on the magnetite by the

carboxylate groups and an outward shift of the slip plane due to the nonionic PEO brush.[133] The contributions of the electrostatic repulsive potential to the total pair interaction potential for the coated magnetite nanoparticles can thus be considered essentially negligible.

A short-range repulsive interaction should be introduced to account for the role of the adsorbed polymer layer in avoiding particle aggregation. The primary means for achieving stable magnetite dispersions is derived from the steric brush layer around the nanoparticles formed by the copolyether dispersants. Thus, the steric term in the interparticle potential energies is the major factor governing the behavior of these dispersions in water. For the present complexes, the steric potentials V_s were calculated using the model by Likos et al. that is based on interactions between star polymer molecules.[97, 98] This model is consistent with the Density Distribution model employed for predicting brush dimensions in that both account for chain-chain interactions and curvature effects using the blob model of Daoud and Cotton.[99] Moreover, this model can account for pair interactions ranging from soft- to hard-sphere like interactions as the number and length of corona chains are varied. We adapted the model essentially by replacing the star polymer core with the magnetite particle plus the inner polymer layer. The interparticle potential V_s is given by

$$V_s(r) = 5/18 f^{1.5} \frac{1}{1+\sqrt{f}/2} \frac{\sigma}{r} \exp[\frac{-\sqrt{f}(r-\sigma)}{2\sigma}]kT \qquad \text{for } r \geq \sigma$$

$$V_s(r) = 5/18 f^{1.5} [-\ln(\frac{\sigma}{r}) + \frac{1}{1+\sqrt{f}/2}]kT \qquad \text{for } r \leq \sigma \qquad 4.11$$

Where r is core-core distance and $\sigma = 1.3 R_g$.

The contributions from magnetic interactions between superparamagnetic particles in an applied magnetic field were estimated at 10,000 Gauss from knowledge of the magnetization

of the particles derived from the SQUID measurements (M = 4.47 x10^5 A/m, that is 86.6

emu/g), the magnetic permeability of vacuum (μ_0 = 1.26x10^{-6} Tm A^{-1}), interparticle distances

between the surfaces of the cores (H), and the magnetite core radii (R_c = 5 nm) (Equation

4.12).[9]   Magnetic hysteresis measurements of the neat (solid) complexes utilizing a SQUID

device demonstrated that the nanoparticles were superparamagnetic.   The lack of magnetic

hysteresis is a characteristic of superparamagnetic particles since the magnetic moment is free

to rotate and relax rapidly without concomitant movement of the particle.   Due to the

superparamagnetic nature of the nanoparticles, it was assumed that the magnetic attractive

potentials in zero applied field were negligible.   Thus, the difference in magnetic attractions

with and without a field, and its effect on colloidal stability were estimated using Eq. 4.12,

where the value of the magnetization (M), changes from 86 emu/g at saturation (~10,000 Oe)

to 64 emu/g at 1500 Oe.

$$V_M = -\frac{8\pi\mu_0 R_c{}^3 M^2}{9\left(\dfrac{H}{R_c}+2\right)^3} \qquad\qquad 4.12$$

A plot of the interparticle potentials with and without the magnetic term predicts the behavior

of a representative dispersion of the 3300EO-900PO complex in water (Figure 4.11).   The

total interaction energy is dominated by steric repulsion.   In the absence of a magnetic field,

the onset of steric repulsion occurs rather abruptly at a separation of about 8 nm and leads to

a primary maximum >>10 *kT* (not shown).   The electrostatic and van der Waals interactions

make negligible contributions to the total interaction energy.   Upon application of a

magnetic field with a strength of 10,000 Oe (nearly saturated), a secondary minimum with a

depth of ~ -0.25*kT* appears near a separation distance of about 10 nm.
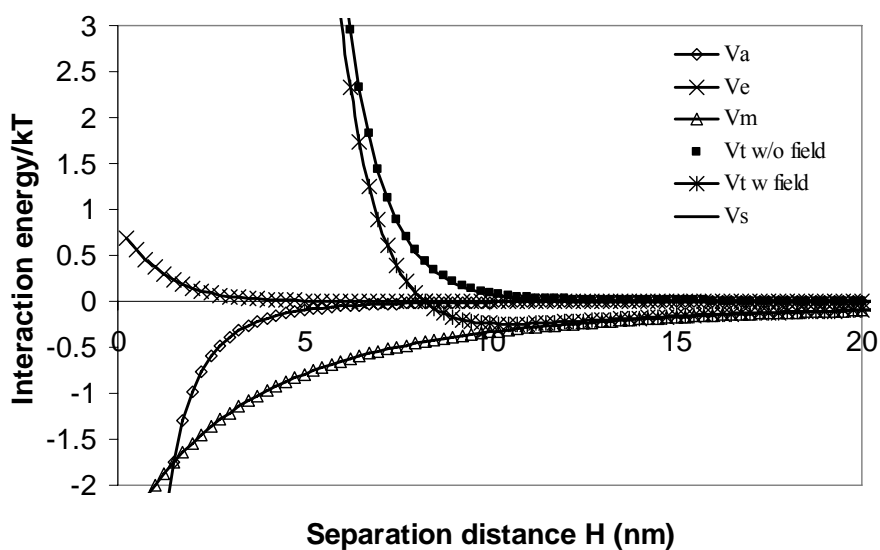
Figure 4.11 Component and total potentials of magnetite 3300EO-900PO complex with and without a magnetic field of 10k Oe.

The total potentials for the magnetite nanoparticle complexes illustrate the effect of changing the brush thickness and graft density f due to changing the complex composition (Figure 4.12). 3300EO-900PO and 2700EO complexes showed similar onset of the steric potential. In comparison, the 1500EO-500PO and 5300EO complexes, both containing similar amount of polymer, exhibit the onset of steric repulsion at particle separations of about 5 nm and 15 nm. When a 10,000 Oe magnetic field is applied, a weak secondary minimum occurs with a depth of less than -1 kT. Since a secondary minimum depth of about -2 kT is required for weak, reversible flocculation, the model predicts that these complexes will not flocculate in the presence of a strong magnetic field. However, it does demonstrate the design methodology needed to tailor the polymer layers to achieve actuation

through loose (reversible) flocculation.

Figure 4.12 Total potentials calculated from DLVO theory for the 5-nm radius magnetite nanoparticles with the predicted brush thickness from Table 4.5. Solid lines represent application of a 10k Oe magnetic field.

For PEO in water the Flory exponent is 0.583 because water is a good solvent for PEO. As we know, adding the salt will decrease the solvation of PEO in water because the ions will compete with polymer chains for available water molecules. So the Flory exponent will decrease as well. Our experimental study used PBS which contains dissolved salts. We calculated the potential energy with $\nu = 0.5$ in θ condition for comparison with $\nu = 0.583$. The calculated total potential with and without magnetic field for all the complexes is shown in Figure 4.13. Compared to Figure 4.12, the depth of secondary minimum is similar but the

separation occurred at shorter distance since the PEO brushes are shorter when $\nu = 0.5$. This effect will be more conspicuous for higher PEO MW. For example, the 5300EO complex secondary minimum shifted from 15 to 12 nm while that for the 1500EO-500PO complex shifted from 6 to 5 nm.

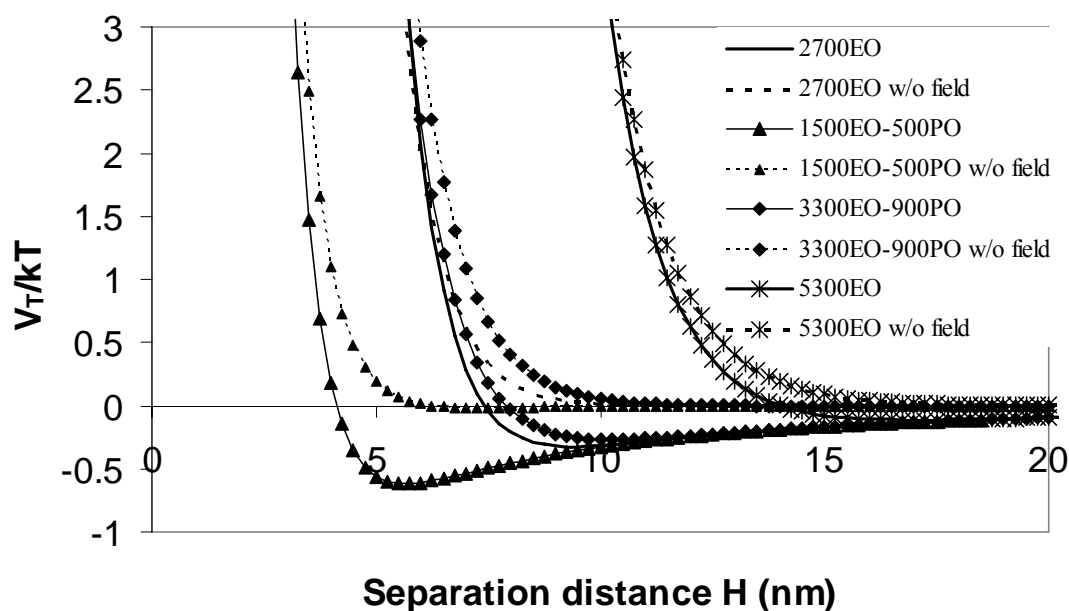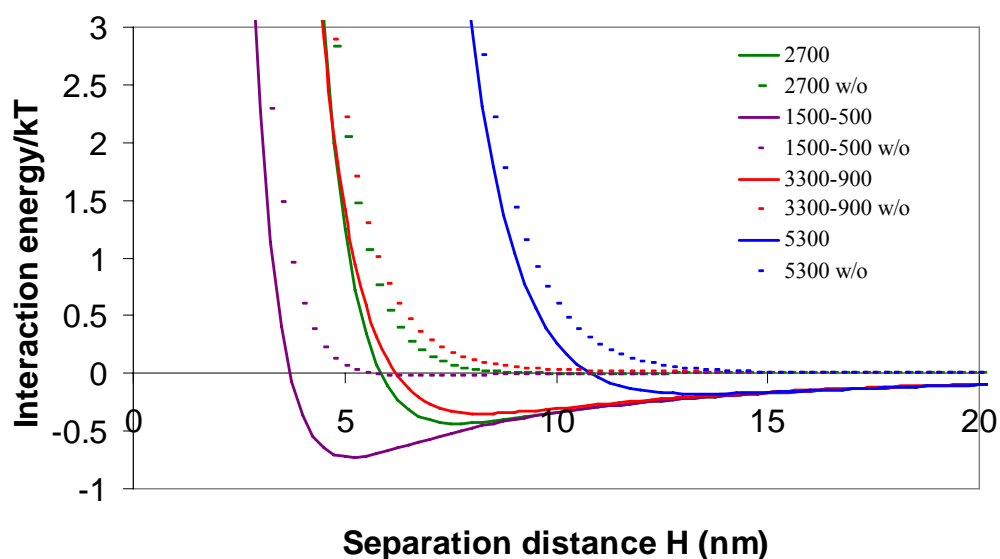**Figure 4.13** Total potentials calculated from DLVO theory for the 5-nm radius magnetite nanoparticles with the predicted brush thickness as Flory exponent = 0.5. Solid lines represent application of a 10k Oe magnetic field.

The total potentials with magnetic field for the complexes 3300EO-900PO illustrated the effect of varying the brush thickness and graft density, f (Fig. 4.14). With decreased graft density, the onset of the steric repulsion occurred at shorter interparticle separation. When f = 162 chains/particle, a primary maximum was observable. With even lower values of f, there was insufficient steric stabilization and the particles fell into a primary minimum. The results indicated it was possible to achieve the magnetically induced flocculation through lowering

the graft density. However, a minimum graft density existed below which irreversible aggregation would occur.
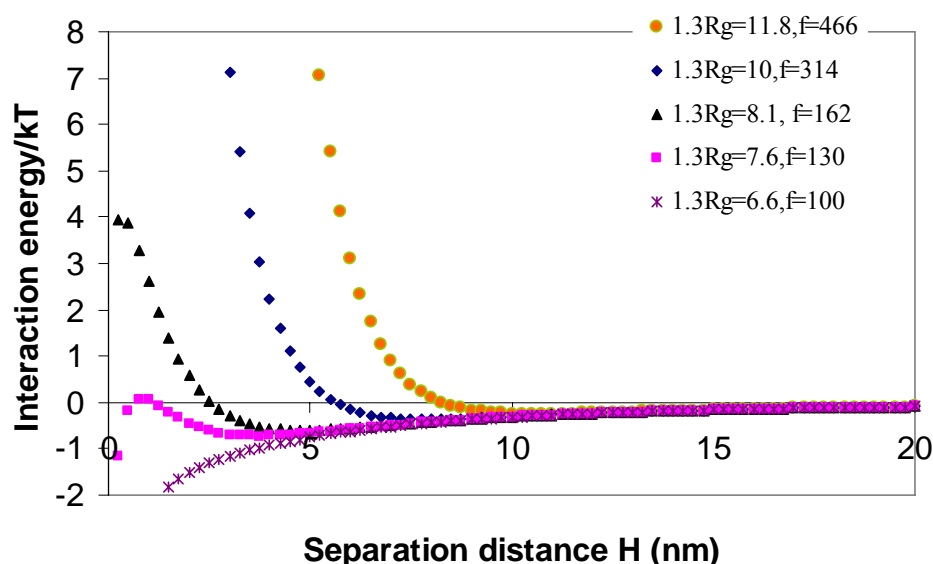
Figure 4.14 Total interparticle potentials with magnetic field (10K Oe) for 3300EO-900PO complex with various theoretical graft densities (f). The R_g values were calculated using Vagberg's model.

For the effect of varying magnetic field strengths, DLVO calculations were utilized to calculate the total interparticle potential of the 3300EO-900PO complex for field strengths of 1500 and 10000 Oe, as shown in Figure 4.15. As expected, the stronger the magnetic field, the deeper the secondary minimum that was predicted. For a magnetic field strength of 10000 Oe, which represented the field strength required to achieve saturation magnetization of the magnetite nanoparticles, the secondary minimum was predicted to be 0.25 kT. For the lower

field strength of 1500 Oe, which corresponded to the strength of the magnetic field used in the magnetically induced flocculation experiments, a value of the secondary minimum of 0.15 kT was obtained. Clearly, greater field strengths favor flocculation, however, it is desirable to achieve flocculation in weaker fields, since these are more easily generated in biomedical applications.
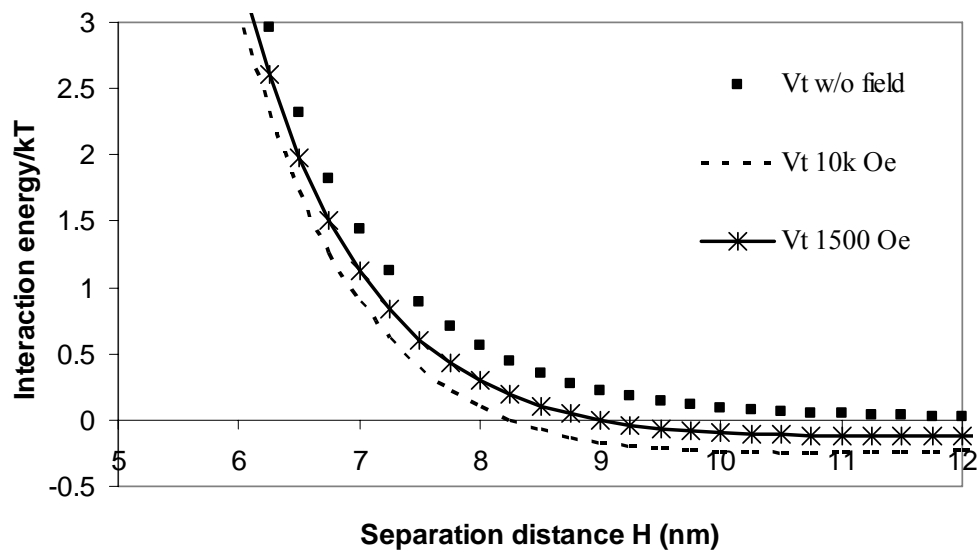
Figure 4.15 Effect of magnetic field strength on the total interparticle potentials.

4.3.8 Stability Ratio and Determination of V_{min} from Flocculation Data

Colloidal particles collide randomly at a rate dictated by their Brownian motion. The stability ratio, *W*, represents the ratio between the total number of collisions and the number of collision that results in an aggregation process and can be expressed as the fast coagulation rate k_f (as determined by diffusion, neglecting the potential barrier), divided by the actual aggregation rate k_s (slow aggregation rate).

$$W = \frac{k_f}{k_s} \qquad\qquad 4.13$$

When $W = 1$, every collision forms an aggregate, and when $W > 1$, only some of the collisions form aggregates due to the presence of the energy barrier predicted by DLVO theory. Aggregation in the regime where an energy barrier is present is referred to as 'slow' aggregation. The stability ratio represents the effectiveness of the potential barrier in preventing particles from coagulation. The inverse of the W provides a measure of effectiveness of collisions leading to aggregation. The stability ratio can be obtained experimentally from the ratio of k_f and k_s. The fast rate constant can be described by Smoluchowski's diffusion-limited rate constant of double formation,

$$k_f = \frac{8 k_B T}{3\mu} \qquad\qquad 4.14$$

Where k_B is Boltzmann's constant, T is temperature and μ is the solvent viscosity. The value of k_s can be obtained using DLS from an expression developed by Virden and Berg[145], where the initial change in R_h with time is measured. The relation is

$$k_s = \frac{1}{R_{h,1}\alpha N_o}\left[\frac{dR_h}{dt}\right]_{t=0} \qquad\qquad 4.15$$

Where $R_{h,1}$ is the initial R_h at time zero, N_o is the initial particle number concentration and α is an optical factor that is a function of R_h, scattering angle and wavelength of the light in the medium. A value of 0.7 was used for α. Wang described f_s ($= 1/W$) as[109]

$$f_s = 1 - \left(1 - \frac{V_{min}}{kT}\right)\exp\left(\frac{V_{min}}{kT}\right) \qquad\qquad 4.16$$

The presence of steric potential generally eliminates aggregation into deep primary minimum and only loose reversible aggregation at large separation distance is observed at the shallow

secondary minimum.

The results of fitting the magnetically induced flocculation data to the above model is shown in Table 4.6. The magnetically induced flocculation of the 3300EO-900PO complex in the presence of a 1500 Gauss magnetic field produced a rate of change in hydrodynamic radius of 0.015 nm/s with standard deviation σ_m of 0.00126. Using the above models, this resulted in a stability ratio of $W = 90400$. This corresponded to secondary minimum of 0.00469 kT, which was significantly lower than that predicted for this complex from DLVO theory (0.15 kT). The difference between the predicted and experimentally determined value of the secondary minimum was attributed to inaccuracy in the electrostatic component potential (V_e). The values of the zeta potential used in the calculation of V_e were from taken from magnetite produced using the coprecipitation method. These are likely to be smaller than the zeta potential of the current magnetite. If this is the case, the repulsive electrostatic forces calculated for our complex will be greater than those predicted, resulting in greater stability and a shallower secondary minimum. This hypothesis is also consistent with the result of lower stability in the presence of PBS.

The magnetic flocculation experiments which were conducted on the same complex in PBS without the magnetic field produced a much higher (and thus more stable) stability ratio of 3.013×10^6. For this stability ratio, a secondary minimum of 0.000814 kT is calculated, which is nearly negligible, as expected from DLVO predictions. Finally, the flocculation experiment was also conducted in DI water, which resulted in an intermediate flocculation rate. However, for this data, the variance of the slope (σ_m) is greater than the value of dR_h/dt, suggesting that the fluctuations in R_h were too high to get a consistent slope. Nevertheless,

the stability ratio for this experiment was determined to be 2.537×10^5, which is intermediate between the PBS buffer experiment in the presence of the magnetic field and in the absence of the magnetic field. The secondary minimum was calculated as 0.00281 kT, which is about half of the value for the sample in the PBS buffer with the magnetic field.

Table 4.6 Results of fitting magnetically induced flocculation data with stability ratio models. The DLS data from the first 10 minutes of exposure was used to calculate dR_h/dt.

Conditions	dR_h/dt (nm/s)	σ_m*	f_s	W	V_{min}/kT
PBS w/Field	0.015	0.00126	1.106E-5	90400	0.00469
PBS w/o field	0.0004	0.000144	3.319E-7	3012800	0.000814
DI w/Field	0.00095	0.00176	3.942E-6	253700	0.00281

*Variance of the slope corresponding to dR_h/dt

4.4 Conclusions

In this work we have demonstrated that it is feasible to obtain stable polymer coated magnetite dispersions consist of well-defined, narrow size distribution magnetite nanoparticles dispersed in aqueous media and PBS. Magnetite nanoparticles were synthesized using a procedure involving benzyl alcohol ligands. These nanoparticles were coated with block copolyether stabilizers containing carboxylic acid central functionality. The well dispersibility of water and PBS confirmed the adsorption of the polymer on the magnetite, forming polymer shell. The magnetite nanoparticle complexes were found to exhibit greater

stability in aqueous buffers that mimic biological fluids, when compared to nanoparticle complexes synthesized using coprecipitation methods. The benzyl alcohol method was thought to be advantageous due to the greater ease of displacing alcohol ligands compared to carboxylic acid containing ligands. The nanoparticle complexes were studied using XPS, TGA, TEM and DLS. The stability of the complexes depended on the combined effects of polymer composition and external magnetic field.   The overall stability of the systems can be explained considering colloidal interactions as van der Waals, electrostatic, steric and magnetic forces induced by the magnetic field applied using the extended DLVO theory. In the absence of an applied magnetic field (conditions where the magnetic attractions for the superparamagnetic nanoparticles were assumed to be negligible), steric repulsive forces accounted for most of the repulsive stabilizing forces, and the dispersions were predicted to be stable.   The effects of graft density, the molecular weight of the stabilizing polymers, the presence of dissolved salt and various magnetic field strengths were modeled using DLVO calculations. The depth of the secondary minimum increased in magnitude with decreased shell thickness and graft density, suggesting increased tendency to flocculate in the presence of a magnetic field. Magnetically induced flocculation measurements were conducted in PBS using DLS, indicating that magnetically induced flocculation was possible.   Stability ratios calculated from the magnetically induced flocculation results were compared with predictions from DLVO and suggested that the complexes possessed greater stability than previously presumed.

In summary, the stabilization of magnetite nanoparticle dispersion in physiological condition is possible by means of a careful selection of polymer stabilizer that was capable of

forming adsorbed layers that facilitate a strong steric repulsion between the particles. The desirable magnetorheological response of the fluid with a weak external magnetic field can be achieved.

4.5 Acknowledgments

Chapter 5 Conclusions

Magnetite (Fe_3O_4) nanoparticles were synthesized using both aqueous solution coprecipitation and high temperature thermolysis of organometallic precursors. The magnetite nanoparticles were complexed with centrally functionalized carboxylate-containing block copolymers, and aqueous dispersions of the complexes were investigated as functions of their chemical and morphological structures. The block copolymer dispersants possessed either poly(ethylene oxide), poly(ethylene oxide-*co*-propylene oxide), or poly(ethylene oxide-*b*-propylene oxide) outer blocks, and all contained a polyurethane center block with pendant carboxylic acid functional groups. The magnetite cores of the magnetite-copolymer complexes were near 10 nm in diameter and the particles were superparamagnetic. The nanoparticle complexes were designed to be dispersible in phosphate buffered saline, an analog to biological fluids, and to exhibit reversible flocculation induced by a magnetic field.

The nanoparticle complexes were characterized with a range of solution- and solid-state techniques including TGA, XPS, TEM, VSM, DLS and zeta potential measurements. Narrower particle size dispersity was obtained in the case of the particles synthesized through the thermolysis technique. Furthermore, the nanoparticle complexes synthesized using the thermolysis route were found to exhibit longer term stability in PBS buffer solutions than magnetite made using the previous coprecipitation method. The increased stability in aqueous buffers, which is important for biomedical applications, was attributed to complete coverage of the narrower size distribution magnetite. Stability measurements in phosphate buffered saline (PBS) demonstrated longer term stability for the triblock copolymer

complexes with pure PEO outer blocks.

DLVO calculation methods which sum the contributions from van der Waals, steric, electrostatic forces and magnetic attractive were utilized to examine the interparticle potentials in the presence and absence of external magnetic fields. Compositions were identified wherein a shallow, attractive interparticle potential minimum appears once the magnetic term is applied. This suggested the possibility of tuning the structures of superparamagnetic nanoparticle shells to allow discrete dispersions without a field, yet weak flocculation could be induced upon exposure to a field, which has important implications for potential biomedical applications where movement of particles with an external magnetic field is desirable. Exposure of the pentablock copolymer complexes with narrow size-dispersity magnetite from the high temperature thermolysis method in PBS to a 1500 Oe magnetic field with concomitant DLS measurements indicated the flocculation of the magnetic nanoparticles through the increased hydrodynamic radius and scattering intensity. These results confirmed the ability to tune the structures of superparamagnetic nanoparticle shells to permit discrete dispersion in the absence of a magnetic field, yet weak flocculation upon exposure to a magnetic field.

Bibliography

1. Sun, S. Z., H. *J. Am. Chem. Soc.* **2002, 124, 8204-8205.**

2. Wakamatsu, H.; Yamamoto, K.; Nakao, A.; Aoyagi, T. *J Magnetism Magnetic Mater* **2006, 302, 327-33.**

3. Matsuno, R.; Yamamoto, K.; Otsuka, H.; Takahara, A. *Macromolecules* **2004, 37, 2203-9.**

4. Lin, Y.-S.; Wu, S.-H.; Hung, Y.; Chou, Y.-H.; Chang, C.; Lin, M.-L.; Tsai, C.-P.; Mou, C.-Y. *Chem Mater* **2006, 18, 5170-2.**

5. Holzapfel, V.; Lorenz, M.; Weiss, C. K.; Schrezenmeier, H.; Landfester, K.; Mailander, V. *J. Phys. Condens. Matter* **2006, 18, S2581-94.**

6. Vincent, B.; Edwards, J.; Emmett, S.; Jones, A. *Colloids Surf.* **1986, 18.**

7. Hiemenz, P., *Principles of Colloid and Surface Chemistry*. **Marcel Dekker: New York, 1986.**

8. Einarson, M. B.; Berg, J. *J. Colloid Interface Sci.* **1993, 155, 165.**

9. Plaza, R. C.; Vincent, J. d.; Gomez-Lopera, S.; Delgado, A. V. *J. Coll. Interf. Sci.* **2001, 306-13.**

10. Tsouris, C.; Scott, T. C. *J. Colloid Interf. Sci.* **1995, 71, 319-330.**

11. Evan, D. R. Univ. of South Australia.

12. Panyam, J.; Lof, J.; O'Leary, E.; Labhasetwar, V. *J Drug Target* **2002, 10, 515–523.**

13. Hobbs, K.; Monsky, W.; Yuan, F.; Roberts, W.; Griffith, L.; Torchilin P, J. R. *Proc Natl Acad Sci USA* **1998, 95, 4607–4612.**

14. Coulembier, O.; Degee, P.; Guerin, P.; Dubois, P. *Langmuir* **2003, 19, 8661-6.**

15. Schuch, H.; Klingler, J.; Rossmanith, P.; Frechen, T.; Gerst, M.; Feldthusen, J.; Muller, A. H. E. *Macromolecules* **2000, 33, 1734-40.**

16. Moradian-Oldak, J.; Leung, W.; Fincham, A. G. *J. Struct. Bio.* **1998, 122, 320-327.**

17. Park, H. H.; Yoon, J. E.; Kim, Y. C.; Yun, L.; Lee, S. C. *Macromolecules* **2004, 37.**

18. Chen, C., *Magnetism and Metallurgy of Soft Magnetic Materials. .* **Dover Publications: New York, 1986; p 4.**

19. Sorensen, C. M., In *Nanoscale Materials in Chemistry*, Klabunde, K. J., Ed. John Wiley and Sons, Inc.: New York 2001.

20. Bean, C. P.; Livingston, J. D. *J. Appl. Phys.* **1959, 30, 120S.**

21. Kodama, R. H.; Berkowitz, A. E. *Phys. Rev. B* **1999, 59, 6321.**

22. Berkowitz, A. E.; Schuele, W. J.; Flanders, P. J. *J. Appl. Phys.* **1968, 39, 1261.**

23. Chantrell, R.; Popplewell, J.; Charles, S. *IEEE Trans Mag* **1978, 14, 975-7.**

24. Gubin, S. P. *Colloids Surf. A: Phys. Chem. Eng. Aspects* **2002, 202, 155.**

25. Hess, P. P., P., . *J. Appl. Polym Sci.* **1966, 10, 1915.**

26. Berkovski, B. B., V., , *Magnetic Fluids and Applications Handbook.* **Begell: New York, 1996; p 1.**

27. Gubin, S. P.; Spichkin, Y. I.; Koksharov, Y. A.; Yurkov, G. Y.; Kozinkin, A. V.; T.I., N.; Korobov, M. S.; Tishin, A. M. *Journal of Magnetism and Magnetic Materials* **2003, 265, 234–242.**

28. Rutnakornpituk, M.; Thompson, M. S.; Harris, L. A.; Farmer, K. E.; Esker, A. R.;

Riffle, J. S.; Connolly, J.; St. Pierre, T. G. *Polymer* 2002, 43, 2337-48.

29. Vadala, M. L.; Rutnakornpituk, M.; Zalich, M. A.; St Pierre, T. G.; Riffle, J. S. *Polymer* 2004, 45, 7449-61.

30. Elmore, W. C. *Physical Reviews* 1938, 54, 309.

31. Zaitsev, V.; Filimonov, D.; Presnyakov, I.; Gambino, R.; Chu, B. *J Coll Int Sci* 1999, 212, 49-57.

32. Liu, Y.; Wang, A.; Claus, R. O. *Appl. Phys. Lett.* 1997, 71, 2265-7.

33. Harris, L. A.; Goff, J. D.; Carmichael, A. Y.; Riffle, J. S.; Harburn, J. J.; St. Pierre, T. G.; Saunders, M. *Chemistry of Materials* 2003, 15, 1367-1377.

34. Kholmetskii, A.; Vorobyova, S.; Lesnikovich, A.; Mushinskii, V.; Sobal, N. *Materials Letters* 2005, 59, 1993-6.

35. Zhao, S. Y.; Lee, D. K.; Kim, C. W.; Cha, H. G.; Kim, Y. H.; Kang, Y. S. *Bull. Korean Chem. Soc.* 2006, 27, (2).

36. Sun, S.; Anders, S.; Thomson, T.; Baglin, J. E. E.; Toney, M. F.; Hendrik, F.; Hamann, C. B. M.; Terris, B. D. *J. Phys. Chem. B* 2003, 107, 5419-5425.

37. Zeng, H.; Rice, P. M.; Wang, S. X.; Sun, S. *J. Am. Chem. Soc.* 2004, 126, 11458.

38. Sun, S.; Murray, C. B.; Weller, D.; FolksL.; Moser, A. *Science* 2000, 287, 1989.

39. Sun, S.; Zeng, H.; Robinson, D. B.; Raoux, S.; Rice, P. M.; Wang, S. X.; Li, G. *Journal of the American Chemical Society* 2004, 126, 273-279.

40. Woo, K.; Hong, J.; Choi, S.; Lee, H. W.; Ahn, J. P.; Kim, C. S.; Lee, S. W. *Chem. Mater.* 2004, 16, 2814-8.

41. Peng, S.; Wang, C.; Xie, J.; Shouheng, S. *J Am Chem Soc* 2006, 128, 10676-7.

42. Pinna, N.; Grancharov, S.; Beato, P.; Bonville, P.; Antonietti, M.; Niederberger, M. *Chemistry of Materials* 2005, 17, 3044-3049.

43. Zhang, Y.; Huang, Z.; Tang, F.; Ren, J. *Thin Solid Films* 2006, 515, 2555-61.

44. Yu, D.; Sun, X.; Zou, J.; Wang, Z.; Wang, F.; Tang, K. *J. Phys. Chem. B* 2006, 110, 21667-21671.

45. Cho, S.-J.; Idrobo, J.-C.; Olamit, J.; Liu, K.; Browning, N.; Kauzlarich, S. *Chem Mater* 2005, 17, 3181-6.

46. Tebble, R. S. C., D. J. , *Magnetic Materials*. Wiley-Interscience: London, 1969.

47. Sun, S.; Zeng, H. *J Am Chem Soc* 2002, 124, 8204-5.

48. Cornell, R. M.; Schertmann, U., *The Iron Oxides: Structure, Properties, Reactions, Occurrence and Uses,*. VCH Publishers: Weinheim, 1996.

49. Kobayashi, M.; Matsuno, R.; Otsuka, H.; Takahara, A. *Sci Tech Adv Mater* 2006, 7, 617-28.

50. Shamim, N.; Hong, L.; Hidajat, K.; Uddin, M. *J Coll Int Sci* 2006, 304, 1-8.

51. Lai, J.; Shafi, K. V. P. M.; Ulman, A.; Loos, K.; Lee, Y.; Vogt, T.; Lee, W.; Ong, N. P. *J. Chem. Phys. B Letters* 2005, 109, 15-18.

52. Tie, S.-L.; Lin, Y.-Q.; Lee, H.-C.; Bae, Y.-S.; Lee, C.-H. *Coll and Surf A* 2006, 273, 75-83.

53. Zureick, A. H. S., B. ;Munley, E. . *Structural Engineering Review* 1995, 7, 257.

54. Dababnch, M. S. A., N. Y. . *IEEE Transactions on Magnetics* 1995, 31, (6), 4178.

55. Hou, Y.; Kondoh, H.; Shimojo, M.; Sako, E. O.; Ozaki, M.; Kogure, T.; Ohta, T. *J. Phys. Chem. B* 2005, 109, 4845-4852.

56. Korolev, V.; Ramazanova, A.; Yashkova, V.; Balmasova, O.; Blinov, A. *Colloid J* 2004, 66, 700-704.

57. Yang, J.; S-B, P.; Yoon, H.-G.; Huh, Y.-M.; Haam, S. *Int J Pharm* 2006, 324, 185-90.

58. Qiao, R.; Zhang, X.; Qiu, R.; Li, Y.; Kang, Y. *J Phys Chem C* 2007, ASAP.

59. Horak, D.; Chekina, N. *J Apply Polym Sci* 2006, 102, 4348-57.

60. Ma, Z.; Guan, Y.; Liu, X.; Liu, H. *Polym Adv Tech* 2005, 16, 554-8.

61. Lindlar, B.; Boldt, M.; Eiden-Assmann, S.; Maret, G. *Adv Mater* 2002, 14, 1656-8.

62. Mornet, S.; Vasseur, S.; Grasset, F.; Duguet, E. *J. Mater. Chem.* 2004, 14, 2161–75.

63. Katz, E. S.-H.-I., L.;Basnar, B.; Felner, I. ; Willner, I. . *Langmuir* 2004, 20, 9714-19.

64. Cheng, F. Y.; Su, C. H.; Yang, Y. S.; Yeh, C. S.; Tsai, C. Y.; Wu, C. L.; Wu, M. T.; Shieh, D. B. *Biomaterials* 2004, 26, (7), 729.

65. Mornet, S.; Vasseur, S.; Grasset, F.; Veverka, P.; Goglio, G.; Demourgues, A.; Portier, J.; Pollert c, E.; Duguet, E. *Prog. Solid State Chem* 2006, 34, 237.

66. Lind, K.; Kresse, M.; Debus, N. P.; Muller, R. H. *J Drug Target* 2002, 10, 221.

67. Mornet, S.; Vasseur, S.; Grasset, F.; Veverka, P.; Goglio, G.; Demourgues, A.; Portier, J.; Pollert, E.; Duguet, E. *Prog Sol State Chem* 2006, 34, 237-47.

68. Dailey, J. P.; Phillips, J. P.; Li, C.; Riffle, J. S. *Journal of Magnetism and Magnetic Materials* 1999, 194, 140-148.

69. Xu, C.; Xu, K.; Gu, H.; Zhong, X.; Guo, Z.; Zheng, R.; Zhang, X.; Xu, B. *Journal of the American Chemical Society* 2004, 126, 3392-3.

70. Shimomura, M.; Abe, T.; Sato, Y.; Oshima, K.; Yamauchi, T.; Miyauchi, S. *Polymer* 2003, 44, 3877-82.

71. Gomez-Lopera, S. A.; Plaza, R. C.; Delgado, A. V. *J. Coll. Interf. Sci.* 2001, 240, 40–47.

72. Riley, T.; Stolnik, S.; Heald, C. R.; Xiong, C. D.; Garnett, M. C.; Illum, L.; Davis, S. S. *Langmuir* 2001, 17, 3168-3174.

73. Gupta, A. K.; M., G. *Biomaterials* 2005, 26, 1565–1573.

74. Rossi, L. M.; Quach, A. D.; Rosenzweig, Z. *Anal. Bioanal. Chem.* 2004, 380, 606–613.

75. Cheng, F. Y.; Shieh, D. B.; Yeh, C. S. *Biomaterials* 2005, 26, 729-738.

76. Asmatulu, R.; Zalich, M. A.; Claus, R. O.; Riffle, J. S. *Journal of Magnetism and Magnetic Materials* 2005, 292, 108-119.

77. Moeser, G. D.; Roach, K. A.; Green, W. H.; Laibinis, P. E.; Hatton, T. A. *Ind. Eng. Chem. Res.* 2002, 41, (19), 4739-4749.

78. Xie, J.; Xu, C.; Xu, Z.; Hou, Y.; Young, K.; Wang, S.; Pourmond, N.; Sun, S. *Chem. Mater.* 2006, 18, 5401-5403.

79. Muller, K.; Skepper, J.; Posfai, M.; Trivedi, R.; Howarth, S.; Corot, C.; Lancelot, E.; Thompson, P.; Brown, A.; Gillard, J. *Biomaterials* 2007, Effect of ultrasmall superparamagnetic iron oxide nanoparticles (Ferumoxtran-10) on human monocyte-macrophages in vitro, 1629-42.

80. Selim, K.; Ha, Y.-S.; Kim, S.-J.; Chang, Y.; Kim, T.-J.; Lee, G.-H.; Kang, I.-K. *Biomaterials* 2007, 28, 710-6.

81. Buchanan, K.; Zhu, X.; Meldrum, A.; Freeman, M. *Nano Letters* 2005, 5, 383-7.

82. Lei, Y.; Chim, W.-K. *Chem Mater* **2005**, 17, 580-5.

83. An, L.; Li, W.; Nie, Y.; Xie, B.; Li, Z.; Zhang, J.; Yang, B. *J Coll Int Sci* **2005**, 288, 503-7.

84. Tan, S. T.; Wendorff, J. H.; Pietzonka, C.; Jia, Z. H.; Wang, G. Q. *ChemPhysChem* **2005**, 6, 1461-1465.

85. Andrade, S.; Rabelo, D.; Garg, V.; Oliveira, A.; Morais, P. *J Magnetism Magnetic Mater* **2005**, 289, 25-7.

86. Abdelghani-Jacquin, C.; Dichtl, M.; Jakobsmeier, L.; Hiller, W.; Sachmann, E. *Langmuir* **2001**, 17, 2129-2136.

87. Buzmakov, V. M.; Pshenichnikov, A. F. *J. Coll. Interf. Sci.* **1996**, 182, 63–70.

88. Meriguet, G.; Jardat, M.; Turq, P. *J. Chem. Phys.* **2004**, 121, 6078-6085.

89. Chae, B.; Lane, A.; Wiest, J. *J Rheol* **2001**, 45, 1193-1203.

90. Deryaguin, B. V.; Landau, L. D. *Acta Physicochim. (USSR)* **1941**, 14, 633-652.

91. Verwey, E. J. W.; Overbeek, J. T. G., *Theory of Stability of Lyophobic Colloids*. Elsevier: Amsterdam, 1948.

92. Lifshitz, E. M. *Soviet Phys. JETP 2* **1956**, 73.

93. Wennerstrom, H. *Colloid and Surfaces A* **2003**, 228, 189-95.

94. Hidalgo-Alvarez, R. *Adv. Colloid Interface Sci.* **1996**, 67, 1-118.

95. Vlassopoulos, D. *Journal of Polymer Science: Pt. B: Polymer Physics* **2004**, 42, 2931-2941.

96. Gast, A. P. *Langmuir* **1996**, 12, (17), 4060-4067.

97. Likos, C. N. *Soft Matter* **2006**, 2, 478-498.

98. Likos, C. N.; Lowen, H.; Watzlawek, M.; Abbas, B.; Jucknischke, O.; Allgaier, J.; Richter, D. *Physical Review Letters* **1998**, 80, (20), 4450-4453.

99. Daoud, M.; Cotton, J. P. *Journal de Physique (Paris)* **1982**, 43, (3), 531-538.

100. Vagberg, L. J. M.; Cogan, K. A.; Gast, A. P. *Macromolecules* **1991**, 24, 1670-1677.

101. Funchs, N., Z. *Phys. Rev. B* **1934**, 89, 736.

102. Ortega-Vinuesa, J. L.; Martin-Rodriguez, A.; Hidalgo-Alvarez, R. *J. Coll. Interf. Sci.* **1996**, 184, 259-67.

103. Romero-Cano, M. S.; Martin-Rodriguez, A.; de las Nieves, F. J. *Langmuir* **2001**, 17, 3505-11.

104. Romero-Cano, M. S.; Martin-Rodriguez, A.; de las Nieves, F. J. *J. Coll. Interf. Sci.* **2000**, 227, 322.

105. Maroto, J.; de las Nieves, F. J. *J. Coll. Interf. Surf., A.* **1998**, 132, 153.

106. Romero-Cano, M. S.; Martin-Rodriguez, A.; de las Nieves, F. J. *J. Coll. Interf. Sci.* **2000**, 227, 329.

107. Holthoff, H.; Egelhaaf, S. U.; Borkovec, M.; Schurtenberger, P.; Sticher, H. *Langmuir* **1996**, 12, 5541.

108. Ottewill, R. H.; Sirs, J. *A., P. S. G. Bulletin,* **1957**, 10, 262.

109. Wang, Q. *J Coll Int Sci* **1991**, 145, 99-107.

110. Rosensweig, R. E., *Ferrohydrodynamics*. Cambridge Univ. Press: Cambridge, UK., 1985.

111. Viota, J. L.; de Vincente, J.; Duran, J. D. G.; Delgado, A. V. *J. Colloid Interf.*

Sci. 2005, 284, 527-541.

112. Gruettner, C.; Teller, J.; Westphal, F.; Ivkov, R. Magnetic nanoparticle compositions, and methods related thereto. 2005.

113. Dailey, J. P.; Riffle, J. S. Magnetized Scleral Buckle with Polymerizing Magnetic Polymers. 2005.

114. Lawaczeck, R.; Menzel, M.; Pietsch, H. *Appl. Organomet. Chem.* 2004, 18, 506-513.

115. Yang, H. H.; Zhang, S. Q.; Chen, X. L.; Zhuang, Z. X.; Xu, J. G.; Wang, X. R. *Anal. Chem.* 2004, 76, 1316-1321.

116. Bruce, I. J.; Sen, T. *Langmuir* 2005, 21, 7029-7035.

117. Chandler, D. J.; Herren, M. A. Manufacture of heat-expandable microcapsules. WO 2001078087, 2001.

118. Moeser, G. D.; Roach, K. A.; Green, W. H.; Hatton, T. A.; Laibinis, P. E. *AIChE Journal* 2004, 50, 2835-2848.

119. Schwalbe, M.; Joerke, C.; Buske, N.; Hoeffken, K.; Pachmann, K.; Clement, J. H. *Journal of Magnetism and Magnetic Materials* 2005, 293, (1), 433-437.

120. Liu, X.; Guan, Y.; Yang, Y.; Ma, Z.; Wu, X.; Liu, H. J. *Applied Polymer Science* 2004, 94, 2205-2211.

121. Tan, W.; Wang, K.; He, X.; Zhao, X. J.; Drake, T.; Wang, L.; Bagwe, R. P. *Medicinal Res. Rev.* 2004, 24, 621-638.

122. Hutten, A.; Sudfeld, D.; Ennen, I.; Reiss, G.; Hachmann, W.; Heinzmann, U.; Wojczykowski, K.; Jutzi, P.; Saikaly, W.; Thomas, G. J. *Biotechnology* 2004, 112, (1-2), 47-63.

123. Bucak, S.; Jones, D. A.; Laibinis, P. E.; Hatton, T. A. *Biotechnol. Prog.* 2003, 19, 477-484.

124. Ditsch, A.; Laibinis, P. E.; Wang, D. I. C.; Hatton, T. A. *Langmuir* 2005, 21, 6006-6018.

125. Pschenichnikov, A. F.; Fedorenko, A. A. *Journal of Magnetism and Magnetic Materials* 2005, 292, 332-344.

126. Ansarifar, M. A.; Luckham, P. F. *Polymer* 1988, 29, 329-335.

127. Ploehn, H. J.; Russel, W. B. *Advances in Chemical Engineering* 1990, 15, 137-228.

128. Taunton, H. J.; Toprakcioglu, C.; Fetters, L. J.; Klein, J. *Nature (London)* 1988, 332, 712-714.

129. Lin, E. K.; Gast, A. P. *Macromolecules* 1996, 29, 390-397.

130. Farinha, J. P. S.; d'Oliveira, J. M.; Martinho, J. M. G.; Xu, R.; Winnik, M. A. *Langmuir* 1998, 14, (9), 2291-2296.

131. Sverjensky, D. A.; Sahai, N. *Geochim. Cosmochim. Acta* 1998, 62, (23/24), 3703-3716.

132. Scott, N. D.; Walker, J. F.; Hansley, V. L. *Journal of the American Chemical Society* 1936, 58, 2442-2444.

133. Hunter, R. J., *Zeta Potential in Colloid Science: Principles and Applications*. Academic Press: London, 1981.

134. Israelachvili, J. N., *Intermolecular and Surface Forces*. Academic Press: London,

1991.

135.   **Zaitsev, V. S.; Filimonov, D. S.; Presnyakov, I. A.; Gambino, R. J.; Chu, B.** *Journal of Colloid and Interface Science* **1999, 212, 49-57.**

136.   **Devanand, K.; Selser, J. C.** *Macromolecules* **1991, 24, (22), 5943-5947.**

137.   **Chin, C.-J.; Yiacoumi, S.; Tsouris, C.** *Colloids and Surfaces A: Physicochemical and Engineering Aspects* **2002, 204, 63-72.**

138.   **Promislow, J. H. E.; Gast, A. P.; Fermigier, M.** *J. Chem. Phys.* **1995, 102, 5492-5498.**

139.   **Russel, W. B.; Saville, D. A.; Schowalter, W. R.,** *Colloid Dispersions*. **Cambridge University Press: Cambridge, 1987.**

140.   **Bevan, M. A.; Petris, S. N.; Chan, D. Y. C.** *Langmuir* **2002, 18, (21), 7845-7852.**

141.   **Croll, S.** *Progress in Organic Coatings* **2002, 44, 131-146.**

142.   **Tadmor, R.; Klein, J.** *Journal of Colloid and Interface Science* **2002, 247, 321-326.**

143.   **Regazzoni, A. E.; Blesa, M. A.; Maroto, A. J. G.** *J. Colloid Interf. Sci.* **1983, 91, (2), 560-570.**

144.   **Alexiou, C.** *Cancer Res* **2000, 60, 6641-8.**

145.   **Virden, J. W., Berg, J. C.** *J Coll Int Sci* **1992, 149.**

VITAE

Qian Zhang grew up in Maanshan, Anhui, China. She received her bachelor and master's degrees in Chemical Engineering with highest honors from East China University of Science and Technology, Shanghai, China. Motivated by an interest in polymer and colloid science after graduation she joined chemistry department of Virginia Polytechnic Institute and State University in Blacksburg, Virginia in August 2003. She worked under the joint supervision of Dr. Judy S. Riffle (Department of Chemistry) and Dr. Richey M. Davis (Department of Chemical Engineering). Her research focused on the synthesis, characterization and modeling of water soluble magnetite-copolymer complexes. She successfully defended on April 3, 2007. After graduation she will join Hewlett-Packard in San Diego, CA to continue efforts in research and development.